THOSE QUEER AMPHIBIOUS ANIMALS: DIGGING INTO THE FOSSIL RECORD OF OTARIOID PINNIPEDS TO INVESTIGATE THEIR EARLY DIVERSIFICATION, LOCOMOTOR EVOLUTION, AND CONSERVATION BIOGEOGRAPHY

by

M. KELLUM TATE-JONES

A DISSERTATION

Presented to the Department of Earth Sciences
and the Division of Graduate Studies of the
University of Oregon in partial fulfillment of the
requirements
for the degree of
Doctor of Philosophy

June 2023

DISSERTATION APPROVAL PAGE

Student: M. Kellum Tate-Jones

Title: Those Queer Amphibious Animals: Digging into the Fossil Record of Otarioid Pinnipeds to Investigate Their Early Diversification, Locomotor Evolution, and Conservation Biogeography

This dissertation has been accepted and approved in partial fulfillment of the requirements for the Doctor of Philosophy degree in the Department of Earth Sciences by:

Edward B. Davis	Chairperson/Advisor
Samantha S. B. Hopkins	Core Member
Valerie J. Sahakian	Core Member
Stephen R. Frost	Institutional Representative

and

Krista Chronister	Vice Provost for Graduate Studies

Original approval signatures are on file with the University of Oregon Division of Graduate Studies.

Degree awarded June 2023

DISSERTATION ABSTRACT

M. Kellum Tate-Jones

Doctor of Philosophy

Department of Earth Sciences

June 2023

Title: Those Queer Amphibious Animals: Digging into the Fossil Record of Otarioid Pinnipeds to Investigate Their Early Diversification, Locomotor Evolution, and Conservation Biogeography

Seals, sea lions, walruses, and their extinct relatives and ancestors have played a critical role in marine ecosystems for over 25 million years. Known collectively as pinnipeds, these secondarily aquatic animals are unique among modern marine mammals for their obligatorily amphibious lifestyle and display remarkable ecological diversity, employing a range of strategies for aquatic locomotion and occupying coastal and pelagic habitats from the tropics to the poles. In addition to their extant representatives, their fossil record contains over a hundred named pinniped species, although the majority of these species are relatively derived members of the Phocidae (true seals), Otariidae (eared seals, including sea lions and fur seals), and Odobenidae (walruses). In my first chapter, I contributed to our understanding of early pinniped evolution by describing the new species *Eodesmus condoni* and performing a phylogenetic analysis to determine its placement within Pinnipedia. My analysis resolved *E. condoni* as the most basal species yet described of the extinct pinniped family Desmatophocidae. I then explored the evolution of aquatic locomotion in otarioid pinnipeds (otariids, odobenids, and desmatophocids) by using three-dimensional geometric morphometric analyses to first investigate the relationship between humerus morphology and swimming modes and then

to predict the swimming mode used by fossil otarioid taxa. My results supported the plesiomorphy of hindlimb-dominated propulsion in all pinnipeds as well as the Otarioidea, with forelimb propulsion evolving three separate times: in the lineages of desmatophocid *Allodesmus kernensis*, odobenid *Pontolis barroni*, and an ancestor of modern Otariidae, likely through exaptation of humeral structures that first evolved for pinniped terrestrial locomotion. Finally, I use ecological niche modeling to compare the range of environmental conditions inhabited by the sole surviving walrus *Odobenus rosmarus* during the Pleistocene to the conditions in which it currently resides. This study reveals that during the Pleistocene, the regions where *O. rosmarus* lived encompassed warmer conditions than its current range. Contrary to predominant narrative about walrus response to climate change, these findings suggest that *O. rosmarus* may indeed be able to survive in the seasonally ice-free conditions that will characterize the Arctic in the coming decades.

This dissertation includes previously published and unpublished coauthored material.

CURRICULUM VITAE

NAME OF AUTHOR: M. Kellum Tate-Jones

GRADUATE AND UNDERGRADUATE SCHOOLS ATTENDED:

University of Oregon, Eugene
University of Arkansas at Little Rock, Little Rock, AR
Harding University, Searcy, AR

DEGREES AWARDED:

Doctor of Philosophy, Earth Sciences, 2023, University of Oregon
Bachelor of Science, Earth Science, 2017, University of Arkansas at Little Rock
Bachelor of Science, Nursing, 2012, Harding University

AREAS OF SPECIAL INTEREST:

Vertebrate Paleontology

Marine Tetrapod Evolution

Conservation Ecology and Paleobiology

Diversity, Equity, Inclusion, and Justice in the Geosciences

PROFESSIONAL EXPERIENCE:

Community Engagement Consultant, Oregon Department of Geology and Mineral Industries, 2023

Instructor of Record for ERTH 103 Exploring Earth History, University of Oregon, Spring 2021, Spring 2022

Instructor of Record for 407/507 geoSTORIES (STOrytelling for Resilience and Inclusion in Earth Sciences) Seminar

Graduate Employee, University of Oregon, 2017-2023

Paleontology Camp Instructor, Sternberg Museum, 2018-2022

ICU Registered Nurse, St. Vincent Infirmary, Little Rock, AR 2013-2017

GRANTS, AWARDS, AND HONORS:

Women in STEM Conference Award, University of Oregon, 2022

Department of Earth Sciences Baldwin Scholarship, University of Oregon, 2020, 2021, 2022

Community for Minorities in STEM Conference Award, University of Oregon, 2022

Gary E. Smith Professional Development Scholarship, University of Oregon, 2022

Department of Earth Sciences Teaching Excellence Award, University of Oregon, 2018, 2021

Women in STEM Leadership Award, University of Oregon, 2021

General University Scholarship, University of Oregon, 2018, 2020, 2021

David S. Easley Memorial Fellowship, University of Oregon, 2020

Department of Earth Sciences Good Citizen Award, University of Oregon, 2020

Thomas Condon Outstanding Work in Paleontology, University of Oregon, 2018, 2019

Student Research Grant, Geological Society of America, 2018

L. Lynn Hamilton General Scholarship, University of Oregon, 2018

Science Literacy Program Fellowship, University of Oregon, 2018

Travel Scholarship, University of Oregon, 2017

Outstanding Senior Geology Student, University of Arkansas at Little Rock, 2017

Field Camp Scholarship, Central Arkansas Gem, Mineral and Geology Society, 2017

Honors Scholar, Harding University, 2008-2012

International Baccalaureate Diploma, Jefferson County International Baccalaureate School, 2008

PUBLICATIONS:

Tate-Jones, M.K., C.M. Peredo, C.D. Marshall, and S.S.B. Hopkins. 2020. The dawn of Desmatophocidae: a new species of basal desmatophocid seal (Mammalia, Carnivora) from the Miocene of Oregon, USA. *Journal of Vertebrate Paleontology* 40:1-4.

ACKNOWLEDGMENTS

I would like to offer my heartfelt gratitude to all those who have supported me through this journey. Just as no one hikes the Pacific Crest Trail or runs a decathlon without a dedicated support team, these six years of professional and personal growth would never have been possible without all of you.

To my family: Aunt Becky for showing me *The Land Before Time* and thus igniting my lifelong love of fossils; Aunt Patti for inspiring the first inklings of my geology obsession by bringing me the most fascinating tumbled rocks; my brother Carter for his company on my research trips and timely help wrangling my code and truly abominable spreadsheets; Dad for all the texts about ducks, pink cars, and bald eagles to keep me grounded; Mom for bringing me to see my first pinnipeds at the Birmingham Zoo, teaching me to always be curious about the world around me, and always reminding me that I can do hard things; my husband Jacob for the countless delicious meals, loads of laundry, encouraging pep talks, grocery runs, editing assistance, walks and hikes, cups of coffee, and unflagging belief in my ability to live out this dream, even and especially when I did not believe in myself; and of course my cats Shupa and Puddles, but Puddles especially for keeping me company through hundreds of hours of grading, coding, writing, and figure-making.

To my friends: Amber, Fletcher, David, and Craig, the tried-and-true Arkansas gang, for keeping the windows open to life outside academia; all of the members of Rehearsals for Life who have come and gone over the past six years and especially Abigail, Manas, Jaclyn, Rory, Kaushal, and Steve, for showing me the messy, imperfect beauty of working in community for a common goal; the Rainbow Connection team with

Oregon Country Fair for connecting me to the broader Oregon community and embracing me for exactly who I am; Stacie and Beckett for dispensing wisdom, books, hilarity, and absurdly delicious meals and cocktails; Ellen and Shawna for the reality TV breaks; Michelle for letting me bully her into going birding and truly unforgettable adventures in New Orleans and D.C.; Allison for ensuring I never forgot about the importance of fantasy fiction and Ted Lasso, even during the crunch times; Monse for keeping me connected to the arts and to uncontrollable belly laughs; and Rachel, my soul sister, for truly too many things to count but especially teaching me to cross country ski and mutually keeping each other afloat as we plummeted through the raging waters of everything from health problems to global pandemics.

To my colleagues in paleontology: the current and past students of the Oregon Vertebrate Paleontology Lab, including Holley, Leonard, Paul, Win, Dana, Helena, Amanda, Megan W, Megan P, Rachel, Sarah, Max, Jordan, Andy, Kai, Lyzzy, Deanna, Thomas, and Emma, for the laughs, ideas, discussions, encouragement, and gingerbread replicas of Jurassic Park; Elena for inviting me across the pond to experience vertebrate paleontology, European style, as well as the incredible sights (and tastes!) of Venice; the Sternberg Science Camps crew, especially Marjie, Amber, Maggie, and David, for keeping silliness and whimsy at the heart of the natural sciences; the other professional pinniped nerds for providing knowledge and insight along the way, including Bobby Boessenecker, Justin Keller, James Rule, Austin Hocking, and Carlos Peredo; and Lisa White for her unparalleled mentorship, perspective, and support in pursuing the next stages of my professional path.

To my undergraduate professors René Shroat-Lewis and Michael “Dr. D” DeAngelis not only for inspiring my bone-deep love of Earth science and geologic history but also for encouraging me to pursue my dream of earning a doctorate studying in this field. None of this would have happened without you.

Last but not least, to my committee: Steve Frost for helping me wrap my head around geometric morphometrics and taxonomic diversification, especially during preparation for my comprehensive exams; Valerie Sahakian for her mentorship with regards to my work in DEI spaces and editorial assistance for grant proposals; Sam Hopkins for introducing me to “Toby” (who would eventually become my first dissertation chapter) and expert perspective on phylogenetic comparative methods and evolutionary theory during my second chapter; and Edward Davis for his unwavering confidence in my abilities, guidance on ecological niche modeling, and mentoring on career pathways both inside and outside academia.

Dedicated to Jacob F. Jones, who has been the steadfast lift beneath my flippers for this entire journey.

TABLE OF CONTENTS

LIST OF FIGURES

LIST OF TABLES

Table Page

Chapter II

Chapter II

Chapter III

CHAPTER I

INTRODUCTION

From the study of seals—those queer amphibious animals living at the interface of land and sea—we gain new respect for the far-limit possibilities of mammalian adaptation.

– Victor Scheffer, from *Adaptations for a Marine Existence* (Riedman, 1990)

1 Background

For the past 25 million years, pinnipeds have served as critical components of global marine ecosystems (Bowen, 1997; Estes et al., 2013; Cammen et al., 2019). Modern pinnipeds include 18 species in the Phocidae (true or earless seals), 15 species in the Otariidae (fur seals and sea lions or eared seals), and a single extant species of Odobenidae: *Odobenus rosmarus*, the modern walrus (Berta et al., 2018). Additionally, the fossil record contains evidence of over 100 extinct pinniped species going back to the late Oligocene (Berta et al., 2018; Valenzuela-Toro and Pyenson, 2019). Although phocids arose in the North Atlantic before expanding into the Southern Hemisphere and eventually the North Pacific (Rule et al., 2020), stem pinnipeds and early otarioid pinnipeds (otariids, odobenids, and the extinct desmatophocids) largely diversified in the North Pacific and have a particularly rich fossil record from the west coast of the United States (Tonomori and Taru, 2022). Pinnipeds perform essential ecosystem services, from regulating lower trophic levels (Heithaus et al., 2008) and redistributing nutrients in the water column (Theobald et al., 2006; McCauley et al., 2015) to serving as a critical food source for other tertiary marine and terrestrial predators (Fay, 1982; Bowen, 1997; Hammerschlag et al.,

2006) and restructuring benthic communities through the bioturbation of seafloor sediment (Ray et al., 2006).

Today, however, pinnipeds are experiencing the same disproportionate impacts from anthropogenic environmental degradation as other large-bodied marine predators (Springer et al., 2003; Estes et al., 2011; McCauley et al., 2015). Two species, the Japanese sea lion (*Zalophus japonicus*) and the Caribbean monk seal (*Neomonachus tropicalis*) have already been hunted extinction, and the IUCN considers 30% of the remaining species to be threatened with extinction by the consequences of human activity, including, pollution, fishery collapses, warming oceans, and habitat disruption and destruction (Kovacs et al., 2012; IUCN, 2022). Addressing these urgent threats will require timely and fiscally efficient conservation policies based on scientific evidence. Studying the fossil record of modern lineages provides insight into the evolutionary roots of their ecological niches as well as their responses to past environmental perturbations, thus providing us insight into how they are likely to respond to current environmental change according to their respective ecologies (Jablonski and Sepkoski, 1996; Dietl and Flessa, 2011; Dietl et al., 2015). Compared to other marine mammals, the pinniped fossil record remains relatively understudied (Valenzuela-Toro and Pyenson, 2019), limiting our ability to develop the long-term perspective needed for effective and dynamic conservation efforts. In this dissertation, I aim to advance our understanding of pinniped evolutionary history by describing newly discovered desmatophocid pinniped *Eodesmus condoni* (Chapter II), reconstructing the locomotor evolution of the Otarioidea (Chapter III), and using the fossil record of modern walrus *O. rosmarus* to model its response to a rapidly warming Arctic (Chapter IV).

2 Chapter II

The extinct pinniped clade Desmatophocidae inhabited the North Pacific from the Aquitanian through the early Tortonian stages of the Miocene. The first large-bodied pinnipeds, the desmatophocids are primarily represented by around ten species of the geologically younger allodesmine desmatophocids (Boessenecker and Churchill, 2013; Tonomori et al., 2018). Conversely, only two species are known of the geologically older desmatophocid subclade, genus *Desmatophoca* or the desmatophocines (Condon, 1906; Barnes, 1987; Deméré and Berta, 2002). Both the desmatophocines and allodesmines are relatively derived compared to the morphology of stem pinnipeds like the so-called "enaliarctines," *Pinnarctidion*, and *Pteronarctos*. In this chapter, I describe a new fossil pinniped cranium from the Oregon coast and through morphological examination and phylogenetic analysis I identify it as the most basal desmatophocid species yet discovered, herein named *Eodesmus condoni*. *E. condoni* is the sixth pinniped species recovered from the Iron Mountain Bed (17.3–16.6 Ma) of the Astoria Formation, a remarkable taxonomic diversity that today is reached only in the highly productive waters of the polar regions (King, 1983). This diverse fauna lends support to the hypothesis that the elevated ocean productivity caused by the Mid-Miocene Climatic Optimum (18.0–16.5 Ma; Flower and Kennett, 1993; Böhme, 2003) supported the diversification of marine species (Lipps and Mitchell, 1976; Tsuchi, 1992; Pyenson et al., 2009).

3 Chapter III

While the publication of fossil otarioids like *E. condoni* is continuing to expand our understanding of their early diversity, we have yet to solve the mystery of their locomotor evolution. Significant evidence exists to support the plesiomorphy of hindlimb-dominated

swimming, with multiple recent studies identifying stem pinnipeds *Puijila darwini, Potamotherium valletoni*, and *Enaliarctos mealsi* as such (Bebej, 2009; Furbish, 2015; Paterson, 2017; Paterson et al., 2020). All modern phocids are highly adapted to hindlimb-propelled swimming, likely representing an extreme specialization on the ancestral condition (Hocking et al., 2021). Among otarioids, otariids rely on forelimb propulsion to swim while the walrus *O. rosmarus* uses a swimming somewhat intermediate to phocids and otariids, relying on forelimb propulsion at low speeds and hindlimb propulsion at higher speeds (Berta et al., 2018). This character distribution raises the question of whether the ancestor of the otarioids was forelimb-propelled with *O. rosmarus* representing a partial reversal to the ancestral condition, or was the otarioid progenitor hindlimb-propelled and otariids evolved forelimb propulsion separate from the minimal use of the forelimbs in *O. rosmarus*?

The fossil record represents an opportunity for investigating this conundrum. Indeed, recent analyses have resolved derived allodesmine desmatophocid *Allodesmus kernensis* as a forelimb-dominated swimmer (Bebej, 2009; Furbish, 2015). However, the linear morphometric analysis (Bebej, 2009) and ancestral trait reconstruction (Furbish, 2015) used in these and other similar studies rely on the availability of nearly complete specimens. While the Otarioidea are fairly well-represented in the fossil record in terms of number of specimens, most consist of isolated elements (Valenzuela-Toro and Pyenson, 2019), precluding the use of these previous methodologies. Therefore to investigate otarioid locomotor evolution, I used three-dimensional geometric morphometric methods to 1) quantify humerus morphology of forelimb- and hindlimb-propelled pinnipeds using a novel landmarking schema and Procrustes superimposition, 2) explore the variation of humerus morphology between locomotor categories via principal components analysis, 3) assess the utility of humerus morphology for diagnosing

swimming mode with flexible discriminant analysis, and finally 4) predict the swimming modes of fossil otarioids with the discriminant analysis. I found that the discriminant analysis correctly classified the modern taxa 90% of the time. Fossil classifications supported an ancestrally hindlimb-propelled state for Pinnipedia as well as for Otarioidea, with desmatophocid *Allodesmus kernensis*, odobenid *Pontolis barroni*, and the ancestor of modern Otariidae each separately acquiring forelimb propulsion, likely through the coopting of humeral structures that first evolved to facilitate the lunging terrestrial locomotion style used by modern otarioids.

4 Chapter IV

The range of environmental conditions within which a species can thrive forms another important dimension of ecology and is particularly relevant considering the rapidly accelerating environmental change mediated by human activity. Nowhere is this change more apparent than in the Arctic, which is warming two to four times as quickly as the rest of the planet (Yletyinen, 2019; Huntington et al., 2020; Turner et al., 2020; Jacobs et al., 2021; Rantanen et al., 2021). Consequently, sea ice is expected to disappear seasonally from the Arctic within the next two to three decades (Overland and Wang, 2013; Jahn et al., 2016; Notz and Stroeve, 2018; Diebold and Rudebusch, 2021). Multiple species of Arctic pinnipeds rely on ice for activities such as hauling out between feedings, pupping, maternal care, and mating (King, 1983), including the recent poster child of climate change, the walrus *Odobenus rosmarus*. However, the Pleistocene and Holocene fossil record for *O. rosmarus* includes specimens found far south of the southernmost extent of sea ice during even the coldest glacial periods. The paleodistribution of walruses suggests that despite the modern correlation between walrus range and sea ice, the full breadth of their ecological niche may include ice-free conditions.

To test this hypothesis, I first evaluated whether modern and fossil walrus ecospace occupation is significantly different using a permutational multivariate analysis of variance (PERMANOVA) and a principal components analysis (PCA). I then constructed two sets of ecological niche models (ENMs) from modern and fossil occurrences of *O. rosmarus*, respectively, using the maximum entropy algorithm, and projected these models to 2050 and 2100. The PERMANOVA supported a significant difference between the ecospace inhabited by modern and fossil walrus populations ($p = 0.0001$; $R^2 = 0.125$). Similarly, the PCA revealed that modern walrus populations indeed inhabit only a portion of their past ecospace, including the ice-free conditions likely to characterize the Arctic in the upcoming decades. The ENM projections also supported these findings. Furthermore, while the future projections derived from the modern ENM predict an 18% decrease in suitable walrus habitat by 2100, the fossil model projections predict no appreciable change in range over the next century. Although I consider an intermediate scenario more realistic than either endmember, our results nonetheless present encouraging evidence that with adequate conservation, walruses may adapt to the changing Arctic climate if other anthropogenic elements such as overfishing, oceanic pollution, and habitat disruption through shipping, drilling, and seafloor mining are mediated.

5 Co-authorships and Previous Publications

Chapter II is co-authored with C. M. Peredo, C. D. Marshall, and S. S. B. Hopkins and is published in the *Journal of Vertebrate Paleontology*. Chapter III is also co-authored with S. S. B. Hopkins and is in preparation for submission to the *Journal of Vertebrate Paleontology*. Chapter IV is co-authored with E. B. Davis and is in review with the journal *Frontiers of Biogeography*.

CHAPTER II

THE DAWN OF DESMATOPHOCIDAE: A NEW SPECIES OF BASAL DESMATOPHOCID SEAL (MAMMALIA, CARNIVORA) FROM THE MIOCENE OF OREGON, U.S.A.

From Tate-Jones, M. K., C. M. Peredo, C. D. Marshall, and S. S. B. Hopkins. 2020. The dawn of Desmatophocidae: a new species of basal desmatophocid seal (Mammalia, Carnivora) from the Miocene of Oregon, U.S.A. Journal of Vertebrate Paleontology. DOI: 10.1080/02724634.2020.1789867.

1 Introduction

The pinniped family Desmatophocidae originated in the early Miocene and dispersed throughout the North Pacific before their final extinction approximately 10 Ma (Barnes, 1987; Boessenecker and Churchill, 2018). Not only were Desmatophocidae the first large-bodied pinnipeds, but they also represent the only extinct family within crown Pinnipedia (Churchill et al., 2015; Berta et al., 2018). Desmatophocids were relatively diverse and, unlike their sister clade Phocidae (Dewaele et al., 2018), left behind a particularly rich fossil record of numerous well-preserved specimens, with a significant amount of articulated and cranial material. Two monophyletic subfamilies have been identified within Desmatophocidae: the Desmatophocinae and Allodesminae (Mitchell, 1966, 1968). Much attention has been given in particular to the geologically younger allodesmine pinnipeds, centering on debates regarding the number of species, how they relate to one another, and what led to their eventual extinction (Barnes, 1972;

Barnes and Hirota, 1994; Boessenecker and Churchill, 2018; Tonomori et al., 2018). Knowledge of desmatophocid diversity prior to the appearance of the allodesmines, however, has been limited to only the two species of desmatophocines, the type species *Desmatophoca oregonensis* and *Desmatophoca brachycephala* (Condon, 1906; Barnes, 1972; Deméré and Berta, 2002). The lack of knowledge of earlier, less derived desmatophocid species hinders our ability to confidently resolve the placement and structure of Desmatophocidae within the pinniped phylogeny.

This study sheds new light on family Desmatophocidae by describing a new genus and species of desmatophocid represented by a nearly complete cranium. Originating from the Lower Miocene Iron Mountain Bed of the Astoria Formation in Oregon, the specimen we describe here was collected nearly twenty years ago, erroneously identified as *Zalophus*, and stored without further examination until the present study. As noted by Valenzuela-Toro and Pyenson (2019), a considerable number of pinnipedimorph fossils remain unstudied or incorrectly catalogued in museum collections, some of which undoubtedly represent species that could illuminate previously uncertain regions of the pinniped tree. This study presents a morphological and cladistic analysis of just such a specimen.

Institutional Abbreviations—UOMNCH — University of Oregon Museum of Natural and Cultural History, Eugene, Oregon, U.S.A.; UO—University of Oregon, Eugene, Oregon, U.S.A.; USNM—United States National Museum of Natural History, Washington, D.C., U.S.A.

2 Material and Methods

2.1 Material Examined

For the purpose of this study, we examined *Allodesmus kernensis* (USNM 25227; Kellogg, 1922), *Desmatophoca brachycephala* (USNM 251201, cast of holotype LACM 120199; Barnes 1987), *Desmatophoca oregonensis* (UO MNCH F-735, holotype; USNM 335478; Condon, 1906; Deméré and Berta, 2002), *Enaliarctos barnesi* (USNM 314295; Berta, 1991), *Enaliarctos emlongi* (USNM 250345; Berta, 1991), *Enaliarctos mitchelli* (USNM 175637; Barnes, 1979), *Enaliarctos tedfordi* (USNM 206273; Berta, 1991), *Erignathus barbatus* (USNM 16116, 269126), *Imagotaria downsi* (USNM 335594; Mitchell, 1968), *Monachus monachus* (USNM 219059), *Pinnarctidion rayi* (USNM 250321, 314325; Berta, 1994), *Proneotherium repenningi* (USNM 335526, 215068, 205334; Kohno et al., 1994), *Pteronarctos goedertae* (USNM 250320, 335432; Barnes, 1989), *Zalophus californianus* (USNM 396062, 21735), and USNM 335445, an unpublished pinniped skull. USNM 335445 represents an undescribed desmatophocid-like pinniped from the Astoria Formation of Central Oregon. Preliminary work indicates that it may be sister to UOMNCH F-68583 (described herein) and we have included it in our phylogenetic analysis to determine its placement, a full description and analysis of USNM 335445 and its relationship to other pinnipeds is beyond the scope of this study and will be undertaken separately.

2.2 Anatomical Description

Anatomical terminology follows Deméré and Berta (2002) and Boessenecker and Churchill (2018) with ontogenetic stage assignment following Siversten (1954). The description addresses whichever side of the skull is more complete unless otherwise stated. Measurements were taken with Mitutoyo 500-171-30 Digimatic 150 mm digital calipers to the nearest tenth of a

millimeter. Angles were calculated using the angle tool in tpsDig2 2.31 (Rohlf, 2017). Photographs were taken with a Google Pixel 2.

2.3 Phylogenetic Methods

We added the new species to the 95-character, 24-taxon data matrix of Boessenecker and Churchill (2018) with the addition of three characters from the Tonomori et al. (2018) matrix. Our character list is provided in Appendix A. We also included the recently published *Allodesmus uraiporensis* (Tonomori et al., 2018) and the undescribed specimen USNM 335445. We could not include the enigmatic 'Desmatophocine B' (Barnes, 1972) because it lacks identified cranial material. *Allodesmus sadoensis* was also excluded from the analysis as we agree with the assessment of Tonomori et al. (2018), considering this taxon to be a junior synonym of *Allodesmus sinanoensis*. The character matrix was prepared in Mesquite 3.51 (Maddison and Maddison, 2018) and phylogenetic analysis was performed in TNT 1.5 (Goloboff and Catalano, 2016). We coded those characters with polymorphic states as ordered and the remainder as unordered. We conducted a new technology search using 10,000 replicates using sectorial and tree-fusing search options and an implied weight of K = 3. We assessed support for each node using a standard bootstrap analysis with 1,000 replicates.

3 Systematic Paleontology and Anatomical Description

3.1 Systematic Paleontology

MAMMALIA Linnaeus 1758

CARNIVORA Bowdich 1821

PINNIPEDIA Illiger 1881

DESMATOPHOCIDAE Hay 1930

3.1.1 Emended Diagnosis of Desmatophocidae—Pinnipedia differing from Phocidae, Odobenidae, and Otariidae, in possessing bulbous cheek teeth; a mortised, interlocking contact between the jugal and squamosal; a corner-like extension of the pterygoid process of the maxilla into a suborbital shelf; and a stylomastoid foramen distinct from the tympanohyal pit.

3.1.2 Type and Included Species of Desmatophocidae—*Eodesmus condoni* gen. et. sp. nov., *Desmatophoca oregonensis*, type species (Condon, 1906), *Desmatophoca brachycephala* (Barnes, 1987), *Atopotarus courseni* (Downs, 1956), *Allodesmus kernensis* (Kellogg, 1922), *Allodesmus naorai* (Kohno, 1996), *Allodesmus packardi* (Barnes, 1972), *Allodesmus sinanoensis* (Nagao, 1941), *Allodesmus demerei* (Boessenecker and Churchill, 2018), *Allodesmus uraiporensis* (Tonomori et al., 2018).

EODESMUS gen. nov.

3.1.3 Type and Only Included Species—*Eodesmus condoni* gen. et. sp. nov.

3.1.4 Diagnosis—as for type and only species.

3.1.5 Etymology—Greek *Eo-* meaning "dawn"; *-desmus* (Greek, masculine) from the naming conventions used for other taxa of Desmatophocidae and originating from the Greek "to bind."

EODESMUS CONDONI, sp. nov.

3.1.6 Holotype—UOMNCH F-68583, nearly complete cranium of a male individual lacking the incisive edge of the rostrum; both canines; the posterior edge of the left mastoid; right P1, P4, M1, and M2; and left P3, M1, and M2.

3.1.7 Etymology—In honor of Thomas Condon, who described the first desmatophocid (Condon, 1906).

3.1.8 Diagnosis—*Eodesmus condoni* can be diagnosed from other desmatophocids by wide anterior nares laterally bounded by the maxilla rather than premaxilla, the presence of a nasiolabialis fossa, a circular rather than dorsoventrally compressed foramen magnum, and posteroventrally protruding paraoccipital processes.

3.2 Geographical Location and Geology

3.2.1 Locality—The type specimen was found in float at UO Locality 4663 Moolack Beach (alternatively spelled as Moloch Beach in some publications, e.g., Deméré and Berta (2002) just south of Beverly Beach State Park, Lincoln County, Oregon (Fig. 1). This specimen was donated to the UOMNCH in December 2015 after collection by Andrew Berkholtz in the early 2000s. This locality is Paleobiology Database Locality Number 190995.

3.2.2 Horizon—The type specimen comes from the Iron Mountain Bed, a prominent horizon representing a near-shore facies in the Newport Embayment of the Astoria Formation (Armentrout, 1981). The Iron Mountain Bed consists of calcareously cemented, well-sorted volcaniclastic sandstone characterized by numerous concretions of varying sizes (Armentrout, 1981). The type specimen was preserved in a fine-grained, extremely hard concretionary boulder discovered in the boulder fields at Moolack Beach (spelled “Moloch” on the U.S. Geological Survey, Yaquina, Oregon, 15-minute topographic map, 1959 edition). Such concretions are characteristic of the Iron Mountain bed, which outcrops for 1.5 km at Moolack Beach (Munthe and Coombs, 1979; Armentrout, 1981; Barnes, 1990). Other higher and lower sections of the Astoria Formation, the singular Tertiary rock unit that outcrops at Moolack Beach (Barnes, 1990), largely consist of friable, poorly sorted sandy mudstones that differ significantly in lithology from the Iron Mountain bed (Colbath, 1985). The Iron Mountain bed has produced

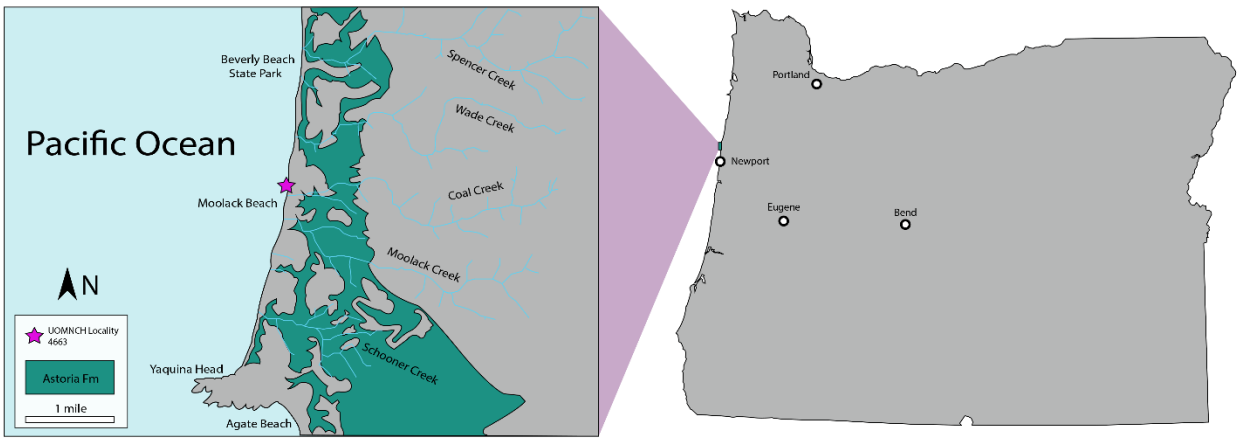

Figure 1. Map of central Oregon coastline with exposures of Astoria Formation with type locality for *Eodesmus condoni* gen. et. sp. nov. (UOMNCH F-68583) noted.

numerous vertebrate fossils preserved in similar concretions, including the type specimens for *Proneotherium repenningi*, *Pacifocotaria hadromma*, and *Desmatophoca oregonensis* (Condon, 1904; Barnes, 1992; Kohno et al., 1994; Deméré and Berta, 2002). *Enaliarctos* specimens have also been recovered from this horizon (Poust and Boessenecker, 2018). Notable non-pinnipedimorph taxa from this horizon include the baleen whale *Cophocetus oregonensis* (Packard and Kellogg, 1934) and the desmostylian *Desmostylus hesperus* (Domning, 2008), as well as terrestrial taxa such as the chalicothere *Tylocephalonyx* and the rhinoceros *Aphelops* (Coombs, 1979). Paleomagnetic data by Prothero et al. (2001) have dated the Iron Mountain Bed to 17.3–16.6 Ma, and these data along with the terrestrial fauna preserved here correlate this bed with the Hemingfordian.

3.3 Anatomical Description

Measurements taken from the skull are recorded in Table 1.

3.3.1 Ontogenetic Stage and Sex—The type specimen displays well-fused cranial sutures (suture age 35; Siversten, 1954). Its pronounced sagittal and lambdoidal crests indicate that the *Eodesmus condoni* holotype likely represents an adult male.

Table 1. Measurements (in millimetres) of cranial dimensions of *Eodesmus condoni* (gen. et. sp. nov.) (UOMNCH F-68583). Alveolar measurements are recorded from the right toothrow.

Total length, premaxilla to intercondylar notch	281.1
Facial length	171.6
Orbit length	62.1
Temporal fossa length	40.8
C^1-M^2 toothrow length	97.7
Braincase length	108.4
Braincase depth	72.7
Greatest transverse braincase width	103.6
Greatest width of anterior nares	43.3
Greatest length nasals	66.4
Greatest width nasals	30.7
Transverse width of rostrum at C^1	64.4
Narrowest width of rostrum	60.9
Transverse width of palate at M^2	74.3
Bizygomatic width	161.0
Transverse width at mastoid	163.0
Transverse width across tympanic bullae	103.0
Transverse width at paraoccipital process	122.7
Transverse width of condyles	68.4
Foramen magnum width	21.3
Foramen magnum depth	23.0
Anteroposterior length, mastoid and paraoccipital process	57.5
Width of internal choanae between pterygoid hamuli	23.2
Infraorbital foramen, depth/transverse width	9.3/12.7
Least interorbital width	39.1
Anteroposterior length of sagittal crest	124.8
Left P^1 crown height/anteroposterior length	9.0/9.1
Right P^2 crown height/anteroposterior length	12.4/11.2
Left P^2 crown height/anteroposterior length	11.4/10.4
Right P^3 crown height/anteroposterior length	11.5/11.3
Left P^4 crown height/anteroposterior length	9.2/11.4
C^1 alveolus anteroposterior length/transverse width	13.1/9.1
M^1 alveolus anteroposterior length/transverse width	8.0/5.2
M^2 alveolus anteroposterior length/transverse width	6.1/6.0

3.3.2 Rostrum—The rostrum is anteroposteriorly elongate (74.6 mm as measured from the anterior margin of the narial opening to the anterior extent of the orbit; 27% of condylobasal length; Figs. 2, 3). The premaxilla forms the anterior rostral margin and is slightly anteriorly expanded to form a small prenarial shelf. The rostral margin is smoothly rounded, lacking the

distinctive transverse expansion for accommodation of the canines seen in dorsal view of other desmatophocids. The premaxillary-maxillary suture is well-fused and extends from the anterolateral margin of the rostral border to the lateral portion of the floor of the external nares. Unlike in all other desmatophocids, the premaxilla does not contact the nasals laterally and does not contribute to the lateral walls of the external nares at all. Instead, it defines only the floor of the premaxilla, forming an anteroposteriorly elongate process on either side of the nares, extending posterolaterally from the rostral border into the nares. These processes bound a medial, posteriorly flaring fossa between them (Fig. 3). The anterior narial opening is wide compared to the rest of Desmatophocidae at 66% of the rostral width at the canine alveoli, compared to 38-45% for specimens of *Desmatophoca oregonensis* and less for other desmatophocids as published in Deméré and Berta (2002). This comparative width appears to derive from the lack of contribution of the premaxilla to the lateral borders of the external nares.

Directly anterior to the orbit, the maxilla preserves a shallow but distinct nasolabialis fossa, a plesiomorphic characteristic seen in stem pinnipeds and the fossil phocid *Devinophoca* but not in other desmatophocids. Just lateral to the nasolabialis fossa, the confluence of the maxillofrontal suture with the anterior rim of the orbit forms a poorly developed antorbital process, a characteristic trait of desmatophocids. Along the lateral border of the maxilla, a low ridge extends posteriorly from the anterior aspect of the canine alveolus to the anterior root of the zygomatic arch, forming a shallow fossa below it and above the toothrow. Just anterolateral to the anterior extent of the maxilla-nasal suture, the maxilla projects slightly over the external nares in a low, blunted, anteromedially directed process. Laterally, the maxilla is slightly flared at the level of the canines. Anteriorly, the nasals protrude over the nares in an M-shaped projection and extend posteriorly to form a narrow V-shaped suture with the frontal at approximately the

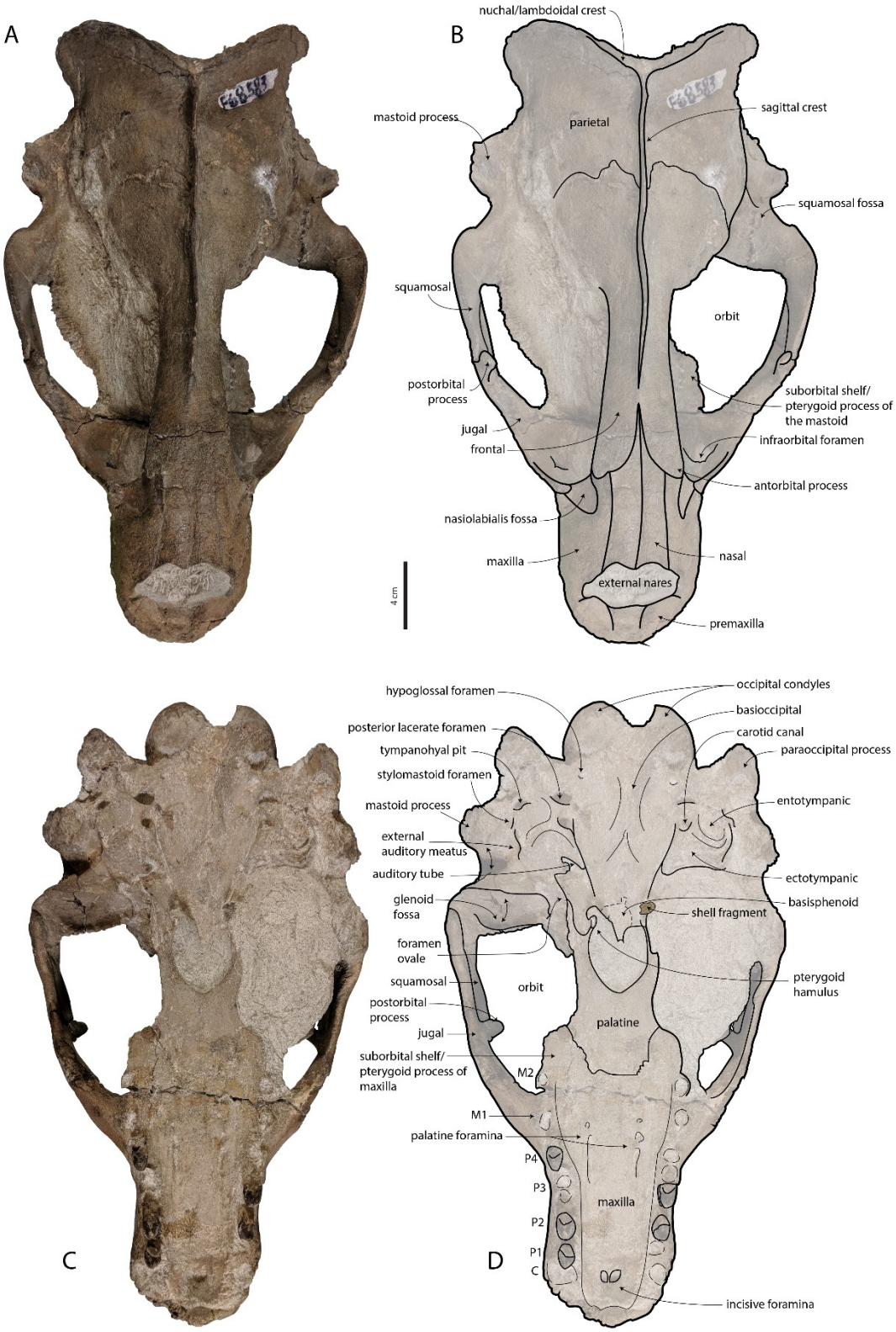

Figure 2. *Eodesmus condoni* gen. et. sp. nov. (UOMNCH F-68583). Holotype skull in dorsal (a, b) and ventral (c, d) views.

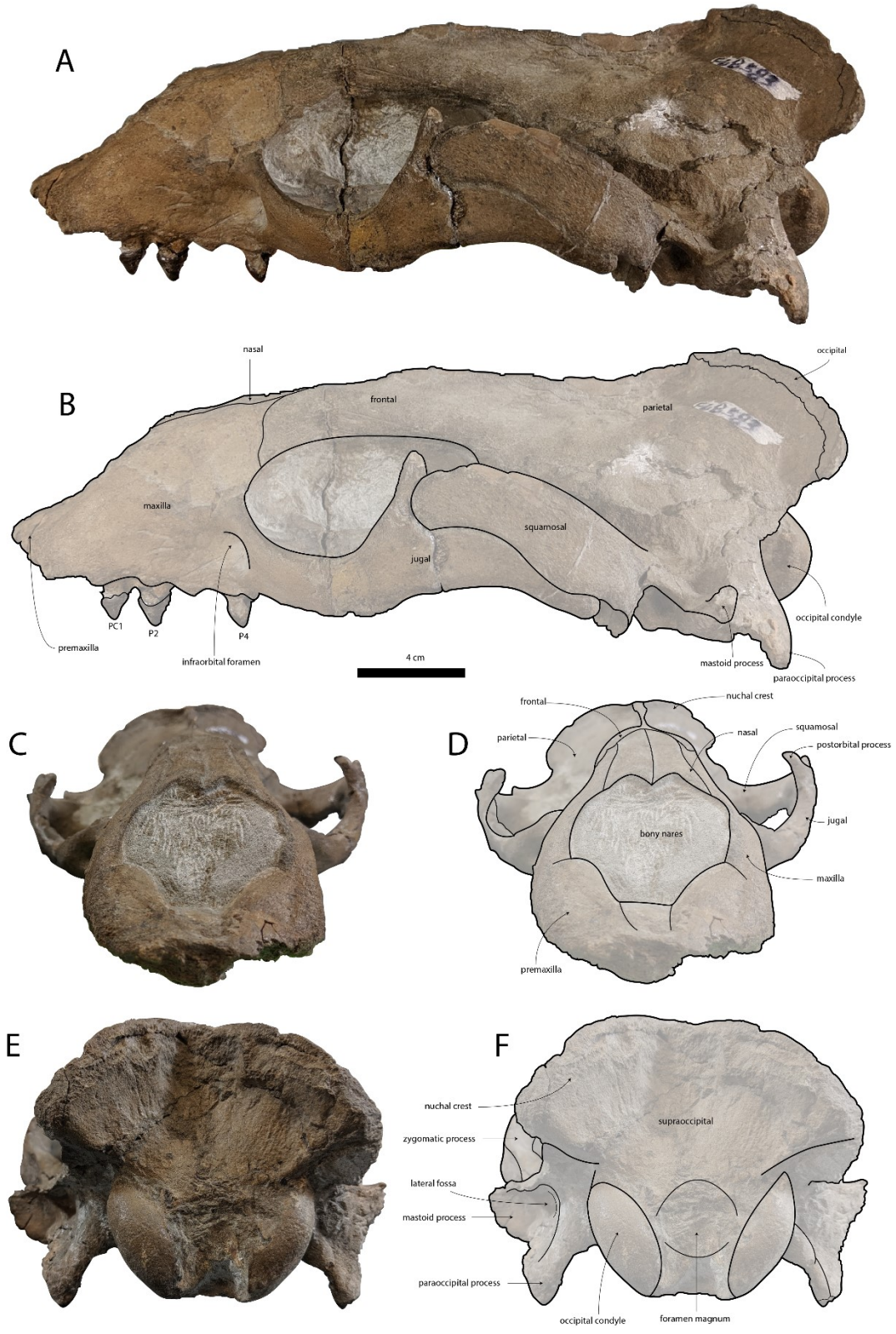

Figure 3. *Eodesmus condoni* gen. et. sp. nov. (UOMNCH F-68583). Holotype skull in lateral (a, b), rostral (c, d), and occipital (e, f) views.

level of the origination of the sagittal crest. The lateral edges of the nasals are approximately parallel to one another anterior before narrowing at the frontal-nasal-maxillary juncture, where they then converge into a narrow V-shaped nasal-frontal suture.

On the ventral aspect of the rostrum, the palate displays slight dorsal arching in the transverse plane and is widest at the level of M2. Two distinct, ovoid incisive foramina separated by a thin septum are preserved between the canine alveoli. At the level of P4, palatal foramina are also preserved. The anterior set are proceeded by shallow grooves and the second set are just posterior to the first. The toothrows are roughly parallel to one another up to the level of P4, where they flare slightly, extending onto the suborbital shelf formed by the palatine process of the maxilla. The lateral border of this shelf contacts the ventral root of the zygomatic process at a 45-degree angle just anterior to the M2 alveolus. The palatine-maxillary suture occurs at the level of the M2 alveolus and is medially transverse before abruptly flexing posterolaterally and extending to the posterior extent of the suborbital shelf. All other palatal sutures have been obliterated. From the lateral extent of the palatine-maxillary suture, the lateral borders of the palatine contract medially, forming the posterior corner of the suborbital shelf, before extending posteriorly to contact the pterygoid. The posterior border of the palatine is smooth and bluntly rounded, forming the anterior walls of the internal nares together with the pterygoids forming the posterior walls.

In lateral view, the pterygoid hamuli are triangular, gracile, laterally recurved, and laterally compressed. The pterygoid struts are widest at the level of the hamuli. They display a rugose texture and are characterized by two ridges extending posterolaterally from laterally adjacent to the hamuli and subsequently merging at the level of the common pit for the foramen

ovale and alisphenoid canal; the resultant singular ridge extends to the medial corner of the auditory bulla.

3.3.3 Orbital Region and Zygomatic Arch—In lateral aspect, the interorbital region is high and of approximately equal height with the braincase. The interorbital region as comprised by the frontals is relatively narrow. The sagittal crest initiates at approximately the level of the termination of the nasals. Along its length, the sagittal crest rises between 9.8 and 11.7 mm from the skull roof. The inner walls of the orbits are damaged, obscuring sutures, foramina, and the presence or absence of the orbital fissure. The lacrimal bone is not preserved.

Anteriorly, the jugal-maxillary suture is fully fused. Within the maxillary root of the zygomatic process, the infraorbital foramen is ovoid and exhibits slight anteroventral compression. Dorsally, its posterior outlet is visible within the orbit. The floor of the infraorbital foramen merges posteriorly with the suborbital shelf/pterygoid process of the maxilla. The zygomatic arch is laterally compressed and quite narrow from the dorsal perspective. In dorsal view, it extends laterally from the rostrum at the level of P3 at approximately 140° before abruptly recurving medially at the level of the glenoid fossa, where the zygoma is at its widest. At this juncture, it becomes dorsoventrally flattered. This flattened facet of the zygomatic root of the squamosal forms the squamosal fossa along with the dorsal aspect of the mastoid process. A slight ridge divides these two anterior and posterior portions of the squamosal fossa, which are approximately equal in size. This ridge overlies the external auditory meatus. The jugal-squamosal articulation is mortised and dorsoventrally expanded (Fig. 3). The posteroventral root of the jugal extends posteriorly to the level of the lateral extent of the glenoid fossa, forming a sigmoidal suture with the squamosal. The dorsal root of the jugal is triangular and forms the postorbital process; this process extends dorsally and interlocks posteriorly with the squamosal.

3.3.4 Braincase and Occiput—The braincase meets the interorbital region at an approximately right angle, forming a distinct corner. The braincase appears to have been dorsoventrally compressed post-burial, exhibiting fracturing along its lateral edges. These fractures obscure the region of the pseudosylvian sulcus. From its origin at the nasofrontal suture, the sagittal crest extends medially along the length of the frontals and parietals until merging with the lambdoidal (nuchal) crests. The lambdoidal crests diverge posterolaterally from the interparietal suture at 235° degrees to one another and posteriorly overhang the occipital shield. They then curve ventromedially before merging laterally with the mastoid process. The mastoid processes are large and dorsally triangular. The paraoccipital processes are not visible in dorsal view and are discussed below (see Basicranium). As a whole, the dorsal surface of the paraoccipital processes, the posterior surface of the mastoid processes, the posterolateral braincase, and the overhanging, anteriorly directed lambdoidal crests form deep lateral fossae on the braincase. The occipital shield exhibits some diagenetic fracturing but is otherwise relatively smooth. From its crest, the shield is slightly concave. From the lateral extent of the lambdoidal crests, the occipital shield narrows sharply before intersecting the dorsomedial surface of the occipital condyles. The occipital condyles are positioned unusually close to one another for a desmatophocid, bounding a small, rounded foramen magnum rather than the typical wide, dorsoventrally compressed morphology seen in the rest of Desmatophocidae (Fig. 3).

3.3.5 Basicranium—On the whole, the basicranium is broadly similar to that of desmatophocines. Anteriorly, the basisphenoid-basioccipital suture is visible but crushed, obscuring its exact morphology. Overall, the basioccipital is generally pentagonal. It is also characterized by the presence of a low, posteriorly narrow sagittal ridge that widens anteriorly before flattening at the level of the anterior extent of the auditory bullae. Anterior to this ridge,

the basioccipital is gently concave. Just anterior to the occipital condyles and on either side of this low ridge are the hypoglossal foramina, which are small and blind. The paraoccipital processes are large and triangular with excavated ventral surfaces. Unusually, they project from the posterior aspect of the basicranium at a sharp ventrolateral angle as opposed to the posteriorly directed paraoccipital processes of other desmatophocids. The mastoid processes project laterally and are approximately equal in size to the posteriorly located paraoccipital processes. Together, the anterior border of the mastoid process and the postglenoid process form an arched, bony roof that overhangs the anterolaterally directed external auditory meatus.

The auditory bullae are relatively flattened. Anteromedially, a small hooked projection extends medially over the common fossa for the auditory tube and median lacerate foramen. The ventral surfaces of the bullae are characterized by a recurved ridge originating at the posteromedial corner of the bulla before forking. One branch runs posterolaterally, just lateral to the carotid canal and posterior lacerate foramen to the anterolateral corner of the bulla. The other curves anterolaterally before flattening just medial to the external auditory meatus. The bullae protrude slightly posteroventrally, extending partially over the stylomastoid foramen and tympanohyal pit. The stylomastoid foramen and tympanohyal pit are small and of approximately equal size, obliquely ovoid, and directed dorsomedially into the bulla. Posteromedially to the bullae, the posterior lacerate foramina are large and elliptical with their main axes located transversely rather than anteroposteriorly as in *Desmatophoca oregonensis*.

3.3.6 Dentition—The preserved dentition and alveoli indicate an upper dental formula of I1-3, C1, P1-4, M1-2. Although the incisive border and incisor alveoli are not preserved, all pinnipeds except the most derived odobenids have three incisors and we have no reason to expect this species to differ (Drehmer et al., 2015; Winer et al., 2016). Preserved teeth include

the left P1, right and left P2, right P3, and left P4. Overall, the teeth are bulbous, peg-like, and homodont with vertically oriented roots. The left P1 is single-rooted and the alveolus of the right P1 both display single roots. P1 and the alveoli of M1 and M2 are single-rooted; P2-P4 are double-rooted. Each tooth features a single, bulbously triangular principal cusp. Buccally, the enamel is smooth and slightly more bulbous at the base. Lingually, a faintly crenulated cingulum is apparent on all of the teeth. Wear facets are present on the posteroventral surface of each of the teeth as well. The alveoli of M1 and M2 are distinctly smaller than those of the premolars.

3.3.7 Comparison to Other Pinnipedimorpha— *Eodesmus condoni* represents an important specimen for understanding the origination of Desmatophocidae as it possesses a unique combination of basal and derived traits. Unlike the basal pinnipedimorphs, *E. condoni* possesses characteristics of crown Pinnipedia such as homodont teeth, absence of the lacrimal bone and lacrimal foramen, and an expanded infraorbital foramen (Berta et al., 2018). However, it also possesses more basal traits such as the presence of a nasiolabialis fossa—a basal trait it shares with basal pinnipedimorphs and *Devinophoca*, the earliest fossil seal known from cranial material (Koretsky and Holec, 2002). Additionally, while the interorbital morphology is not preserved in *Eodesmus condoni*, the possible sister taxon of *E. condoni,* USNM 335445, lacks an orbital vacuity, as do the basal pinnipedimorphs and *Desmatophoca*.

Several characteristics preclude inclusion of *E. condoni* with any of the other three crown pinniped families. Presence of an M2, prenarial shelf, alisphenoid canal, pronounced paraoccipital processes, flattened tympanic bullae, and the shelf-like morphology of the pterygoid process of the maxilla exclude this specimen from Phocidae. *E. condoni* differs from Otarioidea (Otariidae + Odobenidae) in its V-shaped nasal-frontal suture, thin and laterally directed pterygoid strut, divided squamosal fossa, reduced M1 that is smaller than the premolars,

and its lack of antorbital and supraorbital processes. Additionally, its slightly divergent tooth rows, the smoothly convex anterolateral margin of the braincase, and the pentagonal shape of the basioccipital all rule out membership in Otariidae. Finally, it shares the diagnostic characters of its mortised jugal-squamosal articulation (Fig. 3) and the presence of a tympanohyal pit that is distinct from the stylomastoid foramen (Fig. 2) with the rest of Desmatophocidae.

4 Phylogenetic Results and Discussion

Our phylogenetic analysis with implied weighting recovered two most parsimonious trees with a best score of 32.661, consistency index = 0.443, and retention index = 0.683. We show the 50% consensus tree and report support values for this tree in Figure 4. As this paper focuses on desmatophocids, we limit our discussion of specific level relationships and synapomorphies to this clade. Overall, the relationships among major pinniped clades remain similar to the original results published with the Boessenecker and Churchill matrix (2018). *Enaliarctos*, *Pteronarctos*, and *Pinnarctidion* form a successive grade into crown Pinnipedia. Within Pinnipedia, our analysis resolved two lineages, Phocoidea (Desmatophocidae + Phocidae) and Otarioidea (Otariidae + Odobenidae). *Eodesmus condoni* sp. nov. and a yet undescribed specimen, USNM 335445, resolve as sister taxa in the most basal clade within Desmatophocidae. Together, these two specimens form a sister group to Desmatophocinae + Allodesminae in a poorly supported topology. This new taxon can be distinguished from the rest of Desmatophocidae by one ambiguous synapomorphy, the lack of contact between the premaxilla and the lateral border of the nasals (shared with *Odobenus*; character 1: state 2), and a symplesiomorphy, the presence of a nasiolabialis fossa (shared with basal pinnipedimorphs and *Devinophoca*; 11:0).

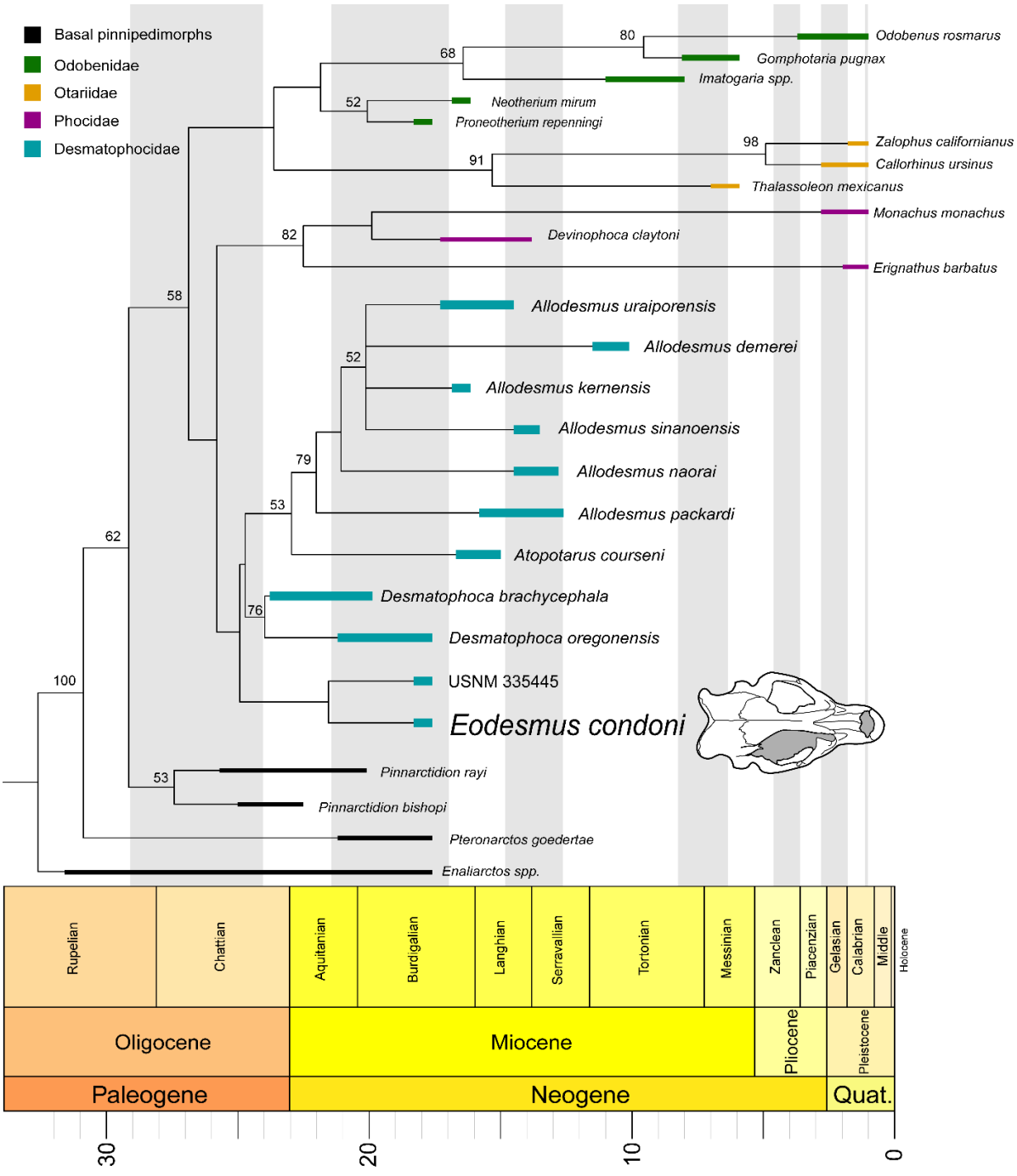

Figure 4. Phylogenetic tree showing position of *Eodesmus condoni* gen. et. sp. nov (UOMNCH F-68583). Time-calibrated most parsimonious tree from the analysis using implied weighting (K = 3). Terminal horizontal bars represent the age range of the taxa as determined by Boessnecker and Churchill (2018). We assigned the age range of *Eodesmus condoni* and USNM 335445 as 17.3–16.6 Ma because each of these specimens comes from the same horizon as *Proneotherium repenningi*, which was assigned to this time range by Boessenecker and Churchill (2018). Time-scaling was applied to the tree using the strap package (Bell and Lloyd, 2015) in R (R Core Team, 2019).

Additionally, inclusion of *Eodesmus condoni* gen. et sp. nov. provided better resolution to the topology of Desmatophocidae as a whole. Desmatophocidae is united by two unambiguous synapomorphies: the pterygoid process of the maxilla expanded laterally as into a corner-like suborbital shelf (8: 1) and a stylomastoid foramen distinct from the tympanohyal pit (33: 1). Desmatophocidae also possesses one ambiguous synapomorphy that it shares with *Imagotaria, Gomphotaria,* and *Odobenus*: round and bulbous (as opposed to transversely narrow) lower postcanines. Similarly, *Desmatophoca* is here recovered with moderate support (BS = 76) rather than poor (Boessenecker and Churchill, 2018). It is diagnosed by a single unambiguous synapomorphy: a mortised jugal-squamosal articulation without the dorsoventral expansion characteristic of other desmatophocids (22:1). *Desmatophoca* also shares an ambiguous synapomorphy with basal pinnipedimorphs, the lack of an orbital vacuity (17:0).

Allodesminae (*Atopotarus* + *Allodesmus*) is recovered with weak support (BS = 53) showing two unambiguous synapomorphies: divergent lower cheek tooth orientation (59:1) and the presence of a scapular undulation in place of the secondary spine on the scapulae (72:1). Ambiguous synapomorphies of allodesmines include an absent or indistinct genial tuberosity of the mandible (40:0; reversal to basal character trait; 40:0), the absence of a cingulum on the lower postcanines (61:2; shared with *Gomphotaria* and *Odobenus*; 61:2), and a large, dorsoventrally elliptical anterior narial opening with thick borders (shared with *Imagotaria, Gomphotaria* and *Odobenus*; 96:1). Within Allodesminae, *Atopotarus* resolves as the sister taxon to *Allodesmus*. The remaining allodesmine species are united with moderate support (BS=79). *Allodesmus packardi* and *Allodesmus naori* form a successively more derived grade leading to the final clade, a weakly supported polytomy (BS=52) containing *Allodesmus uraiporensis, Allodesmus kernensis, Allodesmus demerei,* and *Allodesmus sinanoensis*. Notably, we recovered

a very different placement for *Al. uraiporensis* and *Al. kernensis* than seen in the Tonomori et al. (2018) publication of this specimen. Tonomori et al. (2018) recovered *Al. uraiporensis* and *Al. kernensis* in a weakly supported (BS=53) clade intermediate between *Atopotarus* and the more derived allodesmines. However, as neither topology is well-supported, we do not consider this difference to be notable beyond the indication that the topology of Allodesminae is as yet unsettled.

One of the most notable features of this and similar phylogenetic analyses is the failure to conclusively resolve high level relationships within Pinnipedia. In our analysis, Pinnipedia itself is relatively poorly resolved (BS = 59), and both Phocoidea and Otarioidea are poorly supported. Even the monophyly of Odobenidae, one of the four traditionally recognized families within Pinnipedia, is poorly supported. These weaknesses parallel those of other recent phylogenetic analyses of pinnipeds (Deméré and Berta, 2002; Dewaele et al., 2017; Boessenecker and Churchill, 2018; Tonomori et al., 2018). Although most recent morphological phylogenetic analyses have recovered Phocidae as the immediate sister group to Desmatophocidae, this relationship has been poorly supported in each study. As noted by Boessenecker and Churchill, non-cladistic analyses have generally grouped Desmatophocidae with otariids and odobenids (Downs, 1956; Barnes, 1987, 1989; Barnes and Hirota, 1994). Though our results support the cladistically derived hypothesis, the poor support for both Phocoidea and Otarioidea in our analysis and those of others call for more extensive future investigation of these family level relationships with emphasis on the placement of Desmatophocidae. The lack of robust support for the placement of this extinct family demonstrates that the interfamilial relationships in crown Pinnipedia have yet to be fully settled.

5 Paleobiogeographic Context

Geospatially, *Eodesmus condoni* co-occurs with several basal pinnipedimorphs and early crown pinnipeds also found at the Iron Mountain bed. Basal taxa include *Enaliarctos sp*. (Poust and Boessenecker, 2018), *Pacificotaria hadromma* (Barnes, 1992), and *Pteronarctos goedertae* (Berta, 1994). Besides *E. condoni*, crown pinnipeds from this locality include the desmatophocid *Desmatophoca oregonensis* (Condon, 1906; Deméré and Berta, 2002) and the earliest known odobenid, the small-bodied walrus *Proneotherium repenningi* (Kohno et al., 1994). The presence of at least six pinnipedimorph species at a single locality represents a remarkable taxonomic diversity, particularly when compared to other similar localities from the early Miocene and late Oligocene, which typically only preserve one or two species of pinnipedimorph. Notably, this assemblage coincides with the Mid-Miocene Climatic Optimum (MMCO), a period of relative warming and subsequently increased ocean productivity from 18.0–16.5 Ma (Flower and Kennett, 1993; Bohme, 2003). Previous studies have indicated that this elevated productivity drove an increase in marine species richness (Lipps and Mitchell, 1976; Tsuchi, 1992; Pyenson et al., 2009). The diversity of the Iron Mountain bed represents an intriguing case study for further investigation of this hypothesized process. However, greater understanding of the genesis of the Iron Mountain bed with particular attention to the effects of time-averaging and other taphonomic biases is needed to satisfactorily investigate the relationship between pinnipedimorph diversity and the MMCO (Pyenson et al., 2009).

Although *Eodesmus condoni* represents the most basal desmatophocid yet described, the more derived *Desmatophoca brachycephala* precedes it chronologically. The holotype and single known specimen of *D. brachycephala* derives from the lower Astoria Formation and is dated to 23.0–20.4 Ma (Barnes, 1987). This occurrence of a more derived desmatophocid at least 3.1

million years before the appearance of *Eodesmus condoni* indicates the presence of a ghost lineage of eodesmine desmatophocids during the Aquitanian at the very least. Further fieldwork at older localities is needed to illuminate the history of this clade.

6 Conclusions

Here we describe a new genus and species of desmatophocid pinniped, *Eodesmus condoni* gen. et. sp. nov. from the Iron Mountain bed of the Astoria Formation of Oregon based on a nearly complete cranium. Our phylogenetic analysis resolves this new taxon as the most basal desmatophocid species identified to date. Our analyses also provide better resolution to the topology of the Desmatophocidae. *Eodesmus condoni* expands our knowledge of early pinnipedimorph diversity and further elucidates the relationships among fossil desmatophocids. However, our failure to recover strong support for high-level relationships among the major pinniped clades highlights the need for further phylogenetic work with an expanded subset of taxa and characters.

7 Bridge

As our understanding of the early diversity of otarioids expands with the description of new species like *E. condoni*, we gain new insight into when and how pinnipeds integrated into marine ecosystems. The way pinnipeds and other organisms interact with their respective ecosystems is largely a product of their locomotor mode. Whereas true seals and walruses produce thrust while swimming through lateral oscillation of their hindflippers, eared seals swim using forelimb propulsion in a stroke cycle sometimes known as “underwater flying.” How and why these idiosyncratic swimming modes arose remains an outstanding mystery in pinniped

paleoecology. In the next chapter, I turn my attention specifically to the evolution of otarioid locomotor modes to investigate the development of modern pinniped ecology.

CHAPTER III

FORELIMB-DOMINATED AQUATIC PROPULSION EVOLVED THREE TIMES IN OTARIOID PINNIPEDS AS REVEALED BY GEOMETRIC MORPHOMETRIC ANALYSES OF MODERN AND FOSSIL HUMERI

1 Introduction

The Pinnipedia (Illiger, 1811) are one of the most species-rich clades of secondarily aquatic vertebrates in the modern ocean. Second among marine tetrapods only to the cetaceans for number of species (Berta, 2020), modern pinnipeds include three major taxa: the Phocidae (Gray, 1821), also known as the true or earless seals (Fig. 1a); the Otariidae (Gray, 1825), the fur seals and sea lions (Fig. 1b); and the Odobenidae (Fig. 1c; Allen, 1880), sister taxon to the

FIGURE 1. The three modern subclades of Pinnipedia. **A**, Phocidae, or true seals, showing clockwise from top lefthand corner: *Mirounga leonina*, the southern elephant seal, in the Kerguelen Islands (photo by Antoine Lamielle); a juvenile *Pagophilus groenlandicus*, the harp seal, at False Cape Beach in Virginia, U.S.A. (photo by Albert Herring); and *Lobodon carcinophaga*, the crabeater seal, hauled out on the ice near Almirante Brown Station in Antarctica (photo by W. Bulach). **B**, Otariidae, or eared seals, showing from top to bottom: *Eumetopias jubatus*, the Steller sea lion, in a rookery in Alaska, U.S.A. (public domain photo by U.S. Fish and Wildlife Service); and *Zalophus californianus*, the California sea lion, resting near La Jolla, California, U.S.A. (photo by Mike's Birds). **C**, *Odobenus rosmarus*, the walrus and sole extant member of Odobenidae, on an ice floe in the Arctic (public domain photo by U.S. Fish and Wildlife Service). All photos are from Wikimedia Commons.

Otariidae and today represented by the singular extant walrus species *Odobenus rosmarus* (Linnaeus, 1758). Unlike other extant marine mammals like cetaceans and sirenians, pinnipeds have a uniquely amphibious lifestyle, relying on both the terrestrial and aquatic realms for survival (King, 1991; Berta et al., 2018). Furthermore, the swimming modes employed by pinnipeds differ significantly not only from those seen in other marine mammals but also between each of the three families. Phocids chiefly propel themselves via lateral oscillation of their hind flippers whereas otariids employ a bilateral stroke of the forelimbs for propulsion; *O. rosmarus* employs a type of combination swimming, sometimes using an otariid-like stroke cycle of the forelimbs at low speeds but relying on pelvic oscillation for high speed swimming (Howell, 1929; Backhouse, 1962; English, 1977; Gordon, 1981; Berta et al., 2018).

Such diversity of locomotor modalities is distinct from all other modern marine mammals which swim via dorsoventral undulation of either their tails, in the case of whales and sirenians, or their tails and hindlimbs, in the case of sea otters (Fish, 1996, 2016; Gingerich, 2003). Indeed, the disparity between pinniped swimming modes formed one of the primary arguments for pinniped diphyly, with otariids and odobenids hypothetically arising from one terrestrial ancestor and the phocids from another (Koretsky and Holec, 2002; Kuhn and Frey, 2012; Koretsky et al., 2016). However, molecular phylogenetic analyses have unequivocally supported a monophyletic Pinnipedia (Berta and Wyss, 1994; Arnason et al., 2006; Fulton et al., 2010; Nyakatura and Bininda-Emonds, 2012; Luan et al., 2013), raising the question of how these differing locomotor modes evolved from a single ancestral pinniped and what selective forces may have influenced the development of such different swimming modes.

Members of carnivoran clade Arctoidea, pinnipeds share a common ancestor with ursids (bears) and musteloids, which include the mustelids (weasels), procyonids (raccoons), mephitids

(skunks), and ailurids (red pandas) (Finarelli, 2008; Nyakatura and Bininda-Emonds, 2012; Luan et al., 2013). Both the ursids and musteloids also include secondarily aquatic species. Among the Ursidae, the polar bear *Ursus maritimus* is considered a marine mammal and although primarily adapted for ambulation on ice and land in terms of locomotor behavior, *U. maritimus* can swim long distances via alternating paddle-strokes of its forelimbs while dragging its hindlimbs (Fish, 1996; Lone et al., 2018). Several fossil and modern musteloids display varying degrees of aquaticism, from the semi-aquatic American mink *Neovison vison* and European river otter *Lutra lutra* to the fully aquatic sea otter *Enhydra lutris* (Mori et al., 2015), which is more behaviorally aquatic than any pinniped (Berta, 2020). Musteloids employ a range of swimming modes. Less aquatically specialized species swim using strategies from the quadrupedal paddling used by the mink *Mustela vison* to the somewhat unusual pectoral paddling observed in the domestic ferret *Mustela putorius furo* to the range of forelimb and/or hindlimb paddling and dorsoventrally undulatory swimming modes seen in American river otter *Lutra canadensis* (Fish, 1994). *E. lutris* uses its dorsoventrally flattened tail and flipper-like hindlimbs to provide thrust while swimming via dorsoventral undulation (Tarasoff et al., 2008), not altogether unlike the dorsoventral caudal undulation employed by whales and sirenians (Fish, 1996).

Perhaps surprisingly, the locomotor modes used by pinnipeds differ significantly from the swimming methods used by other arctoids, obscuring the trajectory by which the pinniped swimming modes may have arisen (Fish, 2016). When phocids or *O. rosmarus* are swimming rectilinearly, the animals propel themselves via alternating strokes of each hind flipper using lateral undulation of their hindlimbs, held with solar surfaces facing one another, via alternating adduction and abduction of the pes in the horizontal plane to produce thrust (Fish, 1996). They hold their forelimbs adducted at the side, pressed into bilaterally present axillary depressions in

the blubber of the torso to produce a hydrodynamic body shape for the reduction of drag (Backhouse, 1962; Fish, 1996). Although phocids and odobenids primarily rely on the hindlimbs for generating thrust while swimming, the forelimbs also play important roles in aquatic locomotion (Howell, 1929; Backhouse, 1962; Gordon, 1981, 1983). To execute turns, phocids and *O. rosmarus* will employ the forelimbs to produce lift by abducting the forelimb, extending the joints distal to the elbow, and maintaining the manus in a mid-prone-supine position so that the radius and radial digit form the leading edge of a hydroplane (Howell, 1929; Backhouse, 1962; Gordon, 1981). Occasionally, phocids will also use the foreflippers to paddle using alternating strokes when swimming slowly or will paddle on one side of the body to provide extra thrust for a tight turn. *O. rosmarus* uses this modality even more frequently than phocids, particularly while foraging along the seafloor (English, 1977; Gordon, 1981). Paddling is accomplished by first moving the forelimb into position via the recovery stroke, performed by extending the forearm and manus via elbow flexion, followed by the power stroke, in which the foreflipper is adducted, retracted, and pronated with the digits spread to provide maximal water resistance and therefore thrust (Backhouse, 1962). *O. rosmarus* also uses its forelimbs as stabilizers when it is feeding on the sea floor (Fay, 1982).

In contrast with both phocids and odobenids, otariids primarily employ pectoral oscillation of the forelimbs for thrust production with the hindlimbs passively trailed behind (English, 1977; Feldkamp, 1987a; Fish, 1996; Kuhn and Frey, 2012; Berta et al., 2018). At the beginning of the power stroke, the shoulder joint is in an extended position with the humerus in an abducted-protracted position, the elbow flexed, and the manus slightly extended (Howell, 1929; English, 1977). Subsequently, the shoulder joint undergoes flexion and the forelimb is simultaneously medially rotated, adducted, and retracted, with extension of the elbow joint and

flexion of the manus, so that at the end of the stroke the palmar surface of the flippers is appressed against the flank (Howell, 1929; English, 1977). To reposition the forelimb for the next power stroke via the recovery stroke, the foreflipper is then laterally rotated before the shoulder joint undergoes extension, protraction, and abduction, the elbow joint is flexed, and the manus is slightly extended (Howell, 1929; English, 1977). The hindlimbs are apparently less involved in otariid locomotion than the forelimbs are in that of phocids and odobenids, but they do function as rudders and occasionally brakes (English, 1977).

Given the disparity between pinniped swimming modes and those of their fissiped (terrestrial) arctoid relatives, understanding how and when these disparate swimming methods evolved requires investigation into the aquatic locomotion of fossil pinnipeds. The pinniped fossil record consists of over 100 extinct species (Valenzuela-Toro et al., 2018), including a number of stem "pinnipedimorphs" (herein referred to as stem pinnipeds), the enigmatic Desmatophocidae (Hay, 1930) which lived in the North Pacific from the mid-Arikareean to the early Hemphillian (Boessenecker and Churchill, 2018), and numerous extinct members of the three extant clades. Most previous studies have focused on reconstructing the locomotor modes of stem pinnipeds *Puijila darwini* (Paterson, 2017; Paterson et al., 2020) and *Enaliarctos mealsi* (Berta et al., 1989; Berta and Ray, 1990; Berta and Adam, 2001; Bebej, 2009; Furbish, 2015) and derived desmatophocid *Allodesmus kernensis* (synonymized with *Allodesmus kelloggi* by Deméré and Berta, 2002, and Boessenecker and Churchill, 2018; Berta and Adam, 2001; Bebej, 2009; Furbish, 2015), as they are each represented by nearly complete specimens. Notably, each of these three taxa display combinations of traits that, in modern species, are typically associated with either hindlimb- or forelimb-dominated propulsion, leading previous workers to infer that these species used a sort of combination-style swimming that involved both the forelimbs and

hindlimbs in propulsive strokes, not dissimilarly to *O. rosmarus* (Berta and Ray, 1990; Bebej, 2009; Furbish, 2015; Paterson, 2017). Nevertheless, each seems to show a greater morphological affinity for one style over the other. Basal taxa *P. darwini* and *E. mealsi* have generally been interpreted as combination swimmers with a preference for hindlimb propulsion (Bebej 2009, Paterson 2017). These results lend support to the hypothesis of an ancestral hindlimb-dominated swimmer, which Hocking et al. (2018) attribute to the need to liberate the forelimbs for prey manipulation while traveling in the aquatic environment. By this logic, the phocid swimming modality is a further specialization of the ancestral hindlimb-dominated swimming mode (Hocking et al., 2018, 2021).

Although significant evidence exists supporting the plesiomorphy of hindlimb propulsion in pinnipeds, the evolution of forelimb propulsion remains perplexing. *A. kernensis*, the only otarioid fossil known from a generally complex skeleton, has typically been resolved as a forelimb-dominated combination swimmer (Bebej, 2009; Furbish, 2015). The phylogenetic placement of the desmatophocids is controversial (Dewaele et al., 2017b; Boessenecker and Churchill, 2018; Paterson et al., 2020; Tate-Jones et al., 2020), but if Desmatophocidae is an otarioid as the most recent total evidence phylogenies indicate (Paterson et al., 2020; Rule et al., 2020), a forelimb-propelled *A. kernensis* in conjunction with the forelimb propulsion seen in modern otariids suggests that pectoral oscillation may indeed be ancestral to the Otarioidea, with reversal to the plesiomorphic condition at some point in the odobenid lineage (Gordon, 1979; Bebej, 2009). Such a scenario is supported by the reconstruction of partially known odobenid *Dusignathus seftoni* as a forelimb-dominated swimmer (Furbish, 2015) and morphological evidence that the highly derived Pleistocene odobenid *Valenictus chulavistensis* relied predominantly on forelimb propulsion (Deméré, 1994). However, these characterizations of *D.*

seftoni and *V. chulavistensis* are far from certain; Furbish (2015) notes that many of the characters used for trait reconstruction were absent for *D. seftoni*, decreasing the certainty of this classification, and Giffin (1992) interpreted the swimming of *V. chulavistensis* as comparable to that of *O. rosmarus* through examination of neural canal anatomy. So while the locomotor evolution of otarioid pinnipeds remains unresolved, this previous work provides a testable hypothesis: forelimb propulsion arose once at the base of Otarioidea with a partial reversal to the ancestral condition of hindlimb-dominated combination swimming at some point in the odobenid lineage.

As discussed, most previous locomotor studies examine species that are represented by nearly complete skeletons or which, in the case of *D. seftoni*, at least have multiple limb elements available, severely limiting exploration of locomotor modes in basal members of the otarioid families, none of which are represented by complete specimens and very few of which are represented by elements other than crania and humeri (Valenzuela-Toro et al., 2018). However, this latter bone offers a largely untapped resource for exploring the evolution of otarioid locomotion. The mammalian humerus displays a remarkable range of morphological diversity that has been shown to strongly correlate with function (Andersson, 2004; Fabre et al., 2014; MacLaren and Nauwelaerts, 2016; Jones et al., 2022), including locomotion. Furthermore, Muñoz (2021) found that the morphology of the carnivoran humerus is not only strongly correlated with locomotor mode but is also more influenced by locomotion than that of the femur, which tends to be more conserved.

Well over a century of work focusing specifically on the functional morphology of pinniped humeri provides a foundation for predicting how humeral shape may vary with specific aquatic locomotor functions, particularly with regards to phocids and otariids. With their reliance

on forelimb propulsion, the morphology of the otariid humerus (Fig. 2a) has been considered especially associated with swimming modality. Otariid humeri display an elongated deltoid crest and high greater tubercle which provides a long moment arm for forelimb adduction during thrust production via the pectoralis muscle, increasing the efficiency of the power stroke (Howell 1929). The same condition allows for an extended attachment of the deltoid muscle, which is responsible for generating the majority of the force of the recovery stroke (Howell, 1929; English, 1977), and a similarly extended attachment of the humerotrapezius muscle, allowing for strong, rapid extension of the humerus during this recovery stroke. Howell (1929) attributes the elevation of the greater tubercle above the level of the humeral head and the lesser tubercle in the California sea lion *Zalophus californianus* to the provision of increased leverage for the extension of the humerus via the supraspinatus muscle during the recovery stroke. Otariids also possess enlarged medial epicondyles compared to phocids, ostensibly for providing an anchor for the powerfully developed digital flexors as needed for the power stroke (Howell, 1929).

As previously discussed, although the phocid foreflipper is not generally used for primary thrust production, it nonetheless serves numerous important locomotor functions and thus phocid humeral morphology (Fig. 2b) has also been interpreted in relation to aquatic locomotion (Howell, 1929; Backhouse, 1962). Similar to otariids, the deltoid crest in phocids is significantly developed relative to the usual condition in fissiped carnivorans, but the phocid deltoid crest is generally proximodistally shorter and lateromedially wider than that of otariids. Howell (1929)

FIGURE 2 (next page). Dorsal, medial, ventral, and lateral views of the right humerus of the three modern pinniped clades: **A**, Otariidae, represented by the New Zealand fur seal *Arctocephalus forsteri*; **B**, Phocidae, represented by the harp seal *Pagophilus groenlandicus*; and **C**, Odobenidae, represented by the walrus *Odobenus rosmarus*. Each scale bar represents 5 cm.


A
B
C

hypothesized that the elevation of the crest in phocids resulted from the effort of the humerotrapezius and atlantoscapularis, each of which have broader if shorter attachment sites in phocids than otariids, to limit forelimb range of motion and to immobilize the forelimb against the body during sustained periods of swimming. Another major distinction between phocid and otariid humeri is the lesser tubercle (Berta et al., 2018). Although enlarged in all pinnipeds relative to other carnivorans (Wyss, 1988), this condition is even more pronounced in phocids, which possess massively developed lesser tubercles that extend further proximally than the greater tubercle or the humeral head. Howell (1929) attributes this condition partially to the greater development of the subscapularis in phocids, which holds the humerus in a more abducted resting position relative to otariids, although he considers this to be insufficient explanation for the enormity of the lesser tubercle. Laakkonen and Nihtilä (2021) accredit the elevation of the lesser tubercle above the humeral head to the provision of a long moment arm for the protraction and rotation of the humerus. These movements are of particular importance for braking, turning, and use of the forelimb as a hydroplane, considered to be the primary uses of the forelimb in phocids (Backhouse, 1962). While the phocid medial epicondyle is notably less developed than the otariid condition, the phocid lateral epicondyle is laterally protuberant with a medially convex edge compared to the comparatively faint otariid state (Berta et al., 2018), assumedly to anchor the respectively larger forearm extensors which allow for dorsal thrusts of the manus for initiating dives or ventral bending of the anterior portion of the body (Howell, 1929).

The humerus of *O. rosmarus* largely resembles the otariid condition (Murie, 1870; Howell, 1929) with several notable differences (Fig. 2c). Like otariids, it also possesses an elongated deltoid crest with an elevated greater tubercle, a large lesser tubercle whose proximal

extent does not quite extend to the level of the humeral head or the greater tubercle, and a medially protuberant medial epicondyle. Although this condition is similar to that which allows for forelimb-dominated swimming in otariids, Gordon (1983) attributes the elongation of the deltoid crest in *O. rosmarus* to the provision of a long moment arm for the forelimb adduction needed "push-up" phase of the forward lunge performed during terrestrial locomotion, raising the question of whether a proximodistally long deltoid crest first arose to assist with efficient terrestrial locomotion or, if otarioids are ancestrally forelimb-propelled, it evolved for forelimb-dominated aquatic locomotion, and was subsequently exapted for the terrestrial gait of *O. rosmarus*. Unlike otariid humeri, however, the proximal ventrolateral surface of the deltoid crest of *O. rosmarus* is wide like the condition seen in many phocids. Additionally, the lateral epicondyle protrudes in a laterally convex curve from the condyle before sloping back towards the axis of the shaft at its proximal aspect in a condition that differs from either otariids or phocids (Murie, 1870). However, phocid lateral epicondyles do display a greater degree of lateral protrusion than those of otariids (although the muscle attachment for the forearm extensors rises further proximally than in *O. rosmarus*), so the possibility remains that these conditions are functionally linked with hindlimb-dominated propulsion. This work on the functional morphology of pinniped humeri provides a foundation for exploring the relationship between swimming mode and humeral shape and thus for predicting the locomotor affinities of fossil otarioids.

To quantitatively analyze humeral morphology and its functional implications, I used three-dimensional geometric morphometrics (GMM) methods to first investigate the relationship between humeral morphology and swimming mode in modern pinnipeds and then to predict the locomotor affinities of fossil otarioids (Zelditch et al., 2004; Marramà and Kriwet, 2017).

Through these analyses, I can test the formerly stated hypothesis that forelimb propulsion is the plesiomorphic state for Otarioidea with a reversal to hindlimb-dominated combination swimming in the odobenid lineage.

2 Materials and Methods

2.1 Material Examined

We examined, photographed, and landmarked the humeri of 23 extant pinniped species represented by 41 individual adult specimens and 17 species of fossil pinniped. A list of all taxa and specimens included in this study is available in Table 1. This sample includes the smallest and second largest species of phocids (*Pusa sibirica* and *Mirounga angustirostris*, respectively) and the smallest and second largest species of otariids (*Arctocephalus galapagoensis* and *Z. californianus*, respectively). When possible, I landmarked right humeri; the landmarks of left humeri were reflected during the Procrustes analysis. When available, I landmarked a male and female humerus to include the widest range of intraspecific morphological variation and because the fossil record likely consists of both male and female specimens. All modern specimens are housed in the Smithsonian National Museum of Natural History (USNM) and fossil specimens are housed at both the USNM and the Natural History Museum of Los Angeles County (LACM).

2.2 Phylogenetic Information

Using all the taxa included in this study, I constructed a phylogeny in Mesquite using previously published trees as I subsequently explain (Fig. 3). Because I landmarked at least two specimens for most species, I included multiple representatives of a single species in our tree as a polytomy. For the placement of stem pinnipeds *Potamotherium valletoni* and *Pinnarctidion rayi*, I used the topology of Paterson et al. (2020). Family-level topology derives

Table 1. List of landmarked specimens representing fossil and extant taxa. USNM = Smithsonian National Museum of Natural History; LACM = Natural History Museum of Los Angeles County.

	Taxon	Specimen(s)		Taxon	Specimen(s)
	Fossil Taxa			**Extant Phocids**	
1.	*Potamotherium valletoni*	USNM 214984	28.	*Cystophora cristata*	USNM 188962
2.	*Pinnarctidion rayi*	USNM 250321	29.		USNM 593970
3.	*Desmatophoca oregonensis*	USNM 33524	30.	*Erignathus barbatus*	USNM 16116
4.	*Allodesmus kernensis*	LACM 4320	31.		USNM 269126
5.	*Pithanotaria starri*	LACM 52773	32.	*Halichoerus grypus*	USNM 446405
6.	*Thalassoleon mexicanus*	LACM 128005	33.		USNM 446406
7.	*Neotherium mirum*	LACM 4319	34.	*Histriophoca fasciata*	USNM 504959
8.	*Imagotaria downsi*	USNM 23865	35.		USNM 504960
9.	*Pontolis barroni*	LACM 214848	36.	*Hydrurga leptonyx*	USNM 396931
10.	*Dusignathus seftoni*	USNM 314263	37.	*Leptonychotes weddellii*	USNM 504871
11.	*Pliopedia pacifica*	USNM 187328	38.		USNM 550118
12.	*Valenictus imperialensis*	LACM 3926	39.	*Mirounga angustirostris*	USNM 12441
			40.	*Monachus monachus*	USNM 219059
	Extant Otarioids				
13.	*Odobenus rosmarus*	USNM 21331	41.	*Neomonachus schauinslandi*	USNM 334577
14.		USNM 500252	42.		USNM 395997
15.		USNM 550040	43.		USNM 395999
16.	*Arctocephalus australis*	USNM 23331	44.	*Ommatophoca rossii*	USNM 275206
17.		USNM 501120	45.		USNM 302975
18.	*Arctocephalus forsteri*	USNM 396921	46.	*Pagophilus groenlandicus*	USNM 593976
19.		USNM 504891	47.		USNM 594013
20.	*Arctocephalus galapagoensis*	USNM 392266	48.	*Phoca vitulina*	USNM 594207
21.	*Callorhinus ursinus*	USNM 219847	49.	*Pusa capsica*	USNM 175689
22.		USNM 219848	50.	*Pusa hispida*	USNM 16106
23.	*Neophoca cinerea*	USNM 484382	51.		USNM 7102
24.	*Otaria flavescens*	USNM 484912	52.	*Pusa sibirica*	550038
25.		USNM 95063			
26.	*Zalophus californianus*	USNM 14410			
27.		USNM 504991			

from the phylogenies of Furbish (2015) and Paterson et al. (2020): phocids are the outgroup to the Otarioidea with Desmatophocidae as the earliest diverging member of the otarioids, with placement of the desmatophocids resolved with moderate support (0.72 and 0.75, respectively). I acknowledge that significant debate exists regarding the placement of the extinct pinniped family Desmatophocidae. Initially, Kellogg (1922) classified desmatophocids as basal otariids, a

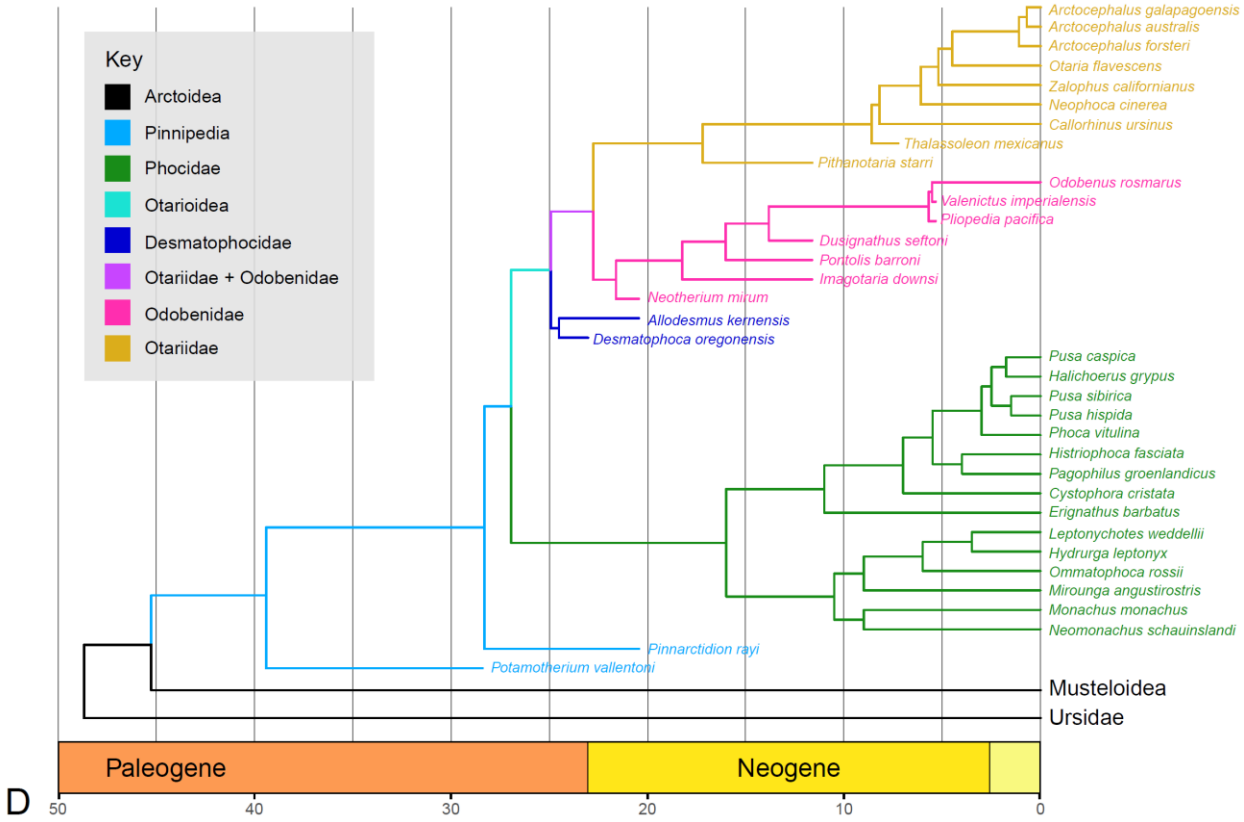

FIGURE 3. Phylogenetic topology used for this study. Relationships between arctoid subclades, stem pinnipeds, and the crown pinniped subclades Phocidae, Desmatophocidae, Otariidae, and Odobenidae after Paterson et al. (2020). Interclade relationships of Phocidae, Desmatophocidae, Odobenidae, and Otariidae after Rule et al. (2020), Tate-Jones et al. (2020), Magallanes et al. (2018), and Boessenecker and Churchill (2014), respectively. Time-scaling applied to tree using the strap package (Bell and Lloyd, 2015) in R (R Core Team 2021).

placement supported by later workers as well (Simpson, 1945; Mitchell, 1966, 1968; Barnes, 1989; Barnes and Hirota, 1994). Others also allied Desmatophocidae with Otarioidea but as the sister taxon to Odobenidae (Berta et al., 1989; Rule et al., 2020). A number of relatively recent phylogenetic analyses have alternately resolved desmatophocids as sister taxon to Phocidae (Berta and Wyss, 1994; Boessenecker and Churchill, 2015, 2018; Tanaka and Kohno, 2015; Dewaele et al., 2017a; Tonomori et al., 2018; Velez-Juarbe, 2018; Tate-Jones et al., 2020). First, Furbish (2015) is the only phylogeny that specifically examines the placement of

desmatophocids. Secondly, only Furbish (2015), Paterson et al. (2020), and Rule et al. (2020) use both molecular and morphological data for the phylogenetic reconstruction of family-level relationships in Pinnipedia and support for the Rule et al. 2020 resolution was lower (0.59) than that of the other two studies. Thirdly, all currently known desmatophocids hail from the North Pacific, which is also the region where odobenids and otariids first diversified, whereas all early-diverging phocids have been found in the North Atlantic and Tethys basins (Berta et al., 2018). Finally, current literature strongly supports the use of probabilistic phylogenetic reconstruction methods and total evidence datasets with both molecular and morphological data for the most accurate topological resolution and highest nodal support (O'Reilly et al., 2018; Puttick et al., 2019; Smith, 2019; Mongiardino Koch et al., 2021). For the topology for intrafamilial relationships, I also relied on total evidence phylogenies where available, referring to Boessenecker and Churchill et al. (2014) for Otariidae, to Rule et al. (2020) for Phocidae, and to Boessenecker and Churchill (2018), Tonomori et al. (2018), and Tate-Jones et al. (2020) for Desmatophocidae. As *O. rosmarus* is the only modern species of Odobenidae, total evidence phylogenies are not available, so I used the morphological phylogenies from Magallanes et al. (2018) and Biewer et al. (2020) for the odobenid topology.

To timescale the phylogeny, I followed the protocol of (Morales-García et al., 2021) using the "equal" method (Brusatte et al., 2008) in package 'paleotree' (Bapst, 2012). I retrieved first and last appearance data for fossil taxa from the Paleobiology Database (pbdb.org) and divergence dates for nodal constraint from the literature (Higdon et al., 2007; Velez-Juarbe, 2017; Magallanes et al., 2018; Biewer et al., 2020; Paterson et al., 2020; Rule et al., 2020; Tate-Jones et al., 2020). The time-scaled phylogeny is available in Appendix D.

2.3 Geometric Morphometrics

Geometric morphometric methods (GMM) are a set of statistical tools used to analyze the morphological variation of biological structures and can be used to infer functional adaptations including locomotor modes (Zelditch et al., 2012). To quantify the morphology of pinniped humeri, I developed a landmarking schema consisting of 26 fixed landmarks including a combination of Type I (homologous) and Type II (based on maxima and minima) landmarks (Fig. 4; Table 2). This schema derives from both our own observations and previous studies examining humeral morphology (Milne et al., 2009; Richards et al., 2022). I landmarked all

Table 2. Landmarks used to quantify the three-dimensional morphology of pinniped humeri.

1.	Proximal apex of the lesser tubercle
2.	Distal extent of the lesser tubercle
3.	Lateral extent of the lesser tubercle
4.	Medial extent of the lesser tubercle
5.	Proximal apex of the greater tubercle
6.	Medial extent of head at confluence with the lesser tubercle
7.	Head at distodorsal edge
8.	Lateral extent of head at confluence with greater tubercle/deltoid crest
9.	Proximoventral extent of head at top of bicipital groove
10.	Head at center of free surface
11.	Bicipital groove
12.	Laterodistal extent of deltoid crest
13.	Distal extent of deltoid crest
14.	Proximolateral extent of ventral surface of humeral condyle
15.	Distolateral extent of humeral condyle
16.	Proximolateral extent of dorsal surface of humeral condyle
17.	Proximal extent of dorsal surface of humeral condyle
18.	Point of maximal depth of olecranon fossa
19.	Proximomedial extent of dorsal surface of humeral condyle
20.	Distomedial extent of humeral condyle
21.	Proximomedial extent of ventral surface of humeral condyle
22.	Inflection point of proximal edge of ventral surface of humeral condyle
23.	Inflection point of distal extent of humeral condyle
24.	Distomedial extent of medial epicondyle
25.	Proximomedial extent of medial epicondyle
26.	Proximal extent of lateral epicondyle

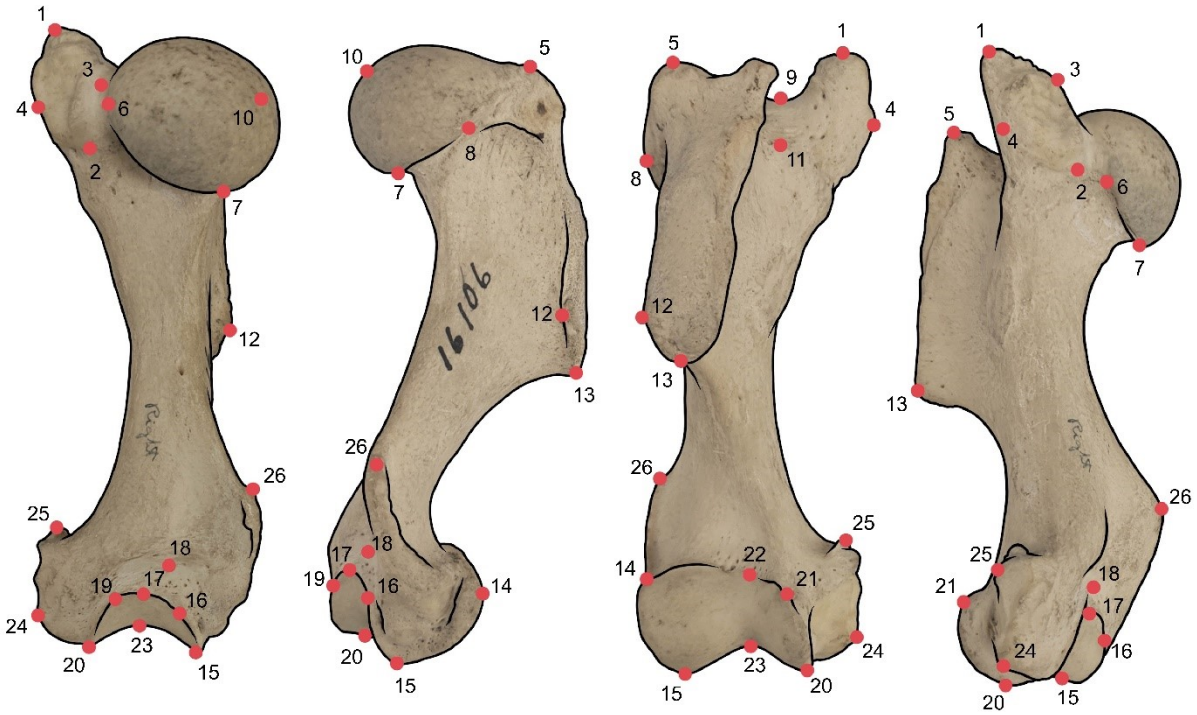

FIGURE 4. In order of right to left, dorsal, lateral, ventral, and medial views of the landmarks used in this study as shown on the left humerus of the spotted seal *Phoca hispida*. Numbers correspond to the landmarks listed in Table 2.

humeri using a Revware Microscribe G2LX with a reported position accuracy of 0.30 mm; the 3D coordinates (x, y, z) were imported into Excel using the Revware MicroScribe Utility Software package.

To analyze shape variation between humeri associated with specific swimming modalities, I designated otariids as forelimb-propelled swimmers and phocids and odobenids as hindlimb-propelled swimmers. I acknowledge that these designations collapse the true diversity of pinniped locomotor modes into an artificial binary but chose this framework for the sake of analytical simplicity. I then ingested the landmark data into R (R Core Team, 2021) and used the 'gpagen' function in R package geomorph version 4.0.4 (Baken et al., 2021; Adams et al., 2022) to perform a generalized Procrustes analysis (GPA) on the landmark data to remove non-shape variation from between the specimens, such as size, orientation, and positioning (Rohlf and

Slice, 1990). I then performed a principal components analysis (PCA) to reduce the dimensionality of the dataset and to visualize its variation with R package ggplot2 (Wickham, 2016; Marramà and Kriwet, 2017).

2.4 Flexible Discriminant Analyses

To test the hypothesis that the three dimensional morphology of pinniped humeri distinguishes between hindlimb- and forelimb-propelled swimmers, I used flexible discriminant analyses (FDA). Similar to linear discriminant analysis, FDA finds a combination of predictors that maximize the separation between groups, but FDA allows for non-linear decision boundaries by fitting flexible functions to the data rather than being limited to a line (Hastie et al., 1994). I performed two flexible discriminant analyses (FDAs), one without phylogenetic correction (npFDA) and one with (pFDA), so that I could assess the degree of impact phylogeny had on shape variation and classification rates. I conducted the npFDA using the 'fda' function in R package mda version 0.5.3 (2022) and the pFDA following the protocol of Morales-García et al. (2021) which uses source code 'phylo.fda.v0.2.R' (Motani and Schmitz 2011). I trained the FDAs on extant taxa with known locomotor modes with the principal components (PCs) that accounted for up to 90% of the variation in the dataset. As part of the pFDA, I also calculated the optimal lambda, a parameter that quantifies the degree to which the trait data of a group of species are influenced by their shared evolutionary history (Pagel, 1999; Motani and Schmitz, 2011). I calculated confusion matrices for the FDAs, the posterior classification rates for the training (modern) dataset, and the relative contribution of each PC to the discriminant function. Finally, I used the FDAs to classify the fossil taxa and calculated posterior probabilities and discriminant scores for each. I then plotted the mean discriminant score for each species on a

phylogeny using the R package phytools (Revell, 2012). The coefficients of the FDAs, by which each PC is multiplied to form the discriminant decision rule, are also calculated.

3 Results

3.1 Humeral Morphology and Aquatic Locomotion

Using 3D GMM, I found that humeral morphology correlates with pinniped swimming mode. In Fig. 5, I show a visualization of PC1 and PC3, as these were the two PCs that contributed the most to the FDAs (see following section). PC1 accounts for 32.7% of the variation and PC3 for 10.4% of the variation. PC1 largely discriminates between otarioids on the negative end of the axis and phocids on the positive end of the axis. Taxa with negative PC1 scores have a relatively long deltoid crest that runs parallel to the shaft and extends into an exaggerated greater tubercle that reaches further proximally than either the humeral head or the lesser tubercle, which is located just ventrally to the comparatively slightly more proximally elevated head. The two tubercles are separated by a narrow intertubercular fossa. The medial epicondyle is proximodistally short and its distal extent arises from the shaft slightly proximally to the medial keel of the condyle and its proximal extent merges again with the shaft at approximately the same level as does the lateral epicondyle. The olecranon fossa is small and limited to a shallow indentation just proximal to the ventroproximal edge of the condyle. Comparatively, taxa with positive PC1 values have a shorter deltoid crest that tilts away from the shaft in the ventrodistal direction. The lesser tubercle is bulbous, medially offset from the humeral head, and extends further proximally than the humeral head or the comparatively reduced greater tubercle. A wide intertubercular fossa separates the two tubercles. The medial

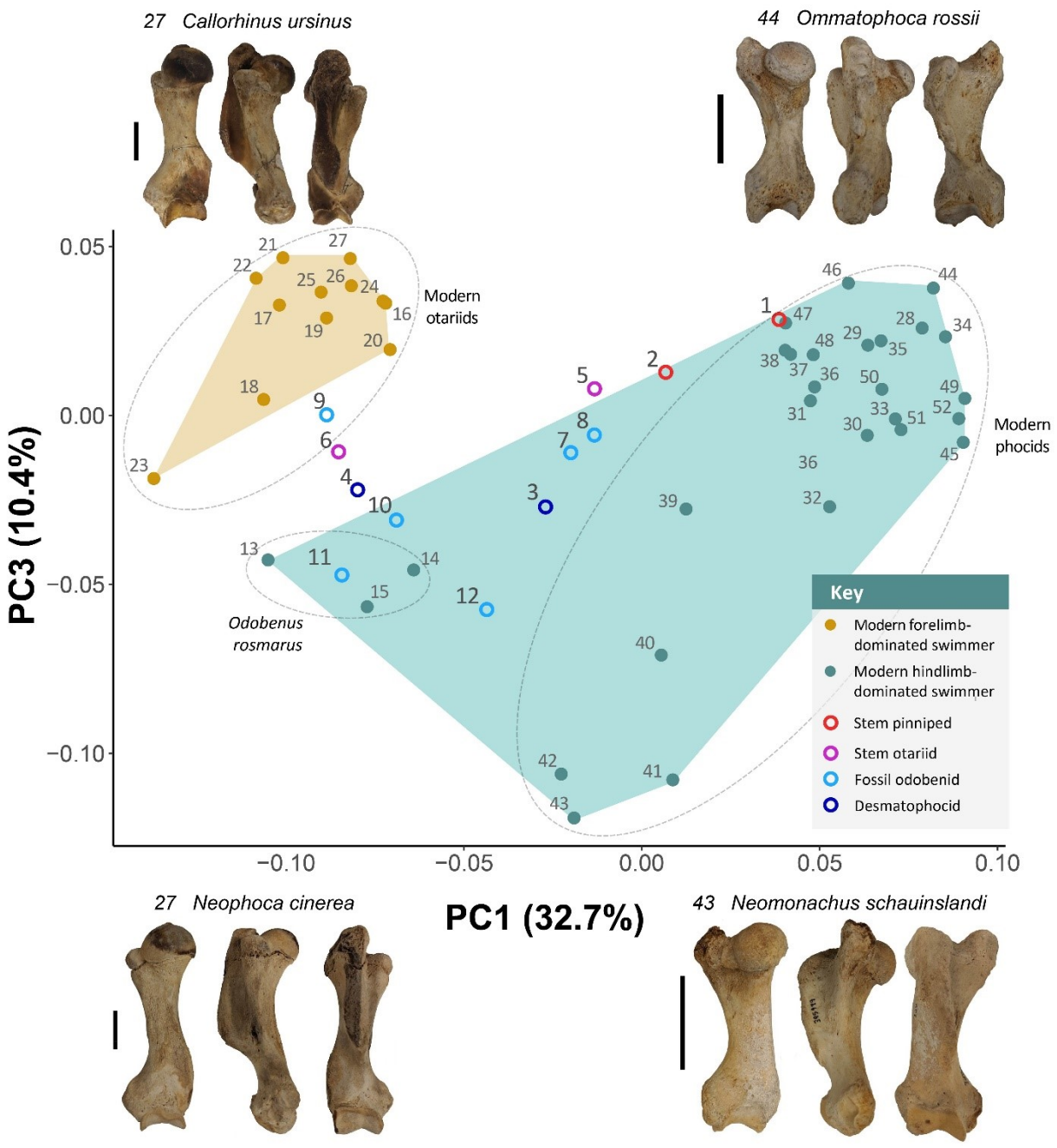

FIGURE 5. Scatter plot of the results of the principal components analysis showing principal components (PCs) 1 and 3, the two main contributors to the flexible discriminant analyses. Extant taxa are indicated by solid points and extinct taxa by unfilled points. Convex hulls are shown for extant hindlimb-dominated swimmers (teal) and forelimb-dominated swimmers (gold). The humeri of selected taxa are shown to demonstrate the range of morphologies associated with the maxima and minima of the PCs. See Table 1 for taxon names.

and lateral epicondyles are proximodistally longer than the condition seen in taxa with negative PC1 values, with the lateral epicondyle extending further proximally than the medial epicondyle. The olecranon fossa is broad and shallowly concave.

The PC3 axis forms a continuum between two distinct morphologies that are less taxonomically discriminatory than PC1, although the otariids do fall exclusively towards the positive end of the spectrum. The minimum for PC3 represents humeri with a broad deltoid crest that extends proximally past the humeral head to approximately the same level as the robust, medially protuberant lesser tubercle. The tubercles are separated by a deep, wide intertubercular fossa. The medial and lateral epicondyles are each fairly symmetrical around the humeral condyle and are approximately equal in proximodistal length to one another. The olecranon fossa is extremely shallow. The positive end of the PC3 axis represents humeri with a narrow deltoid crest that extends proximally into a greater tubercle that rises past the humeral head and the comparatively smaller lesser tubercle. The medial epicondyle is proximodistally shorter than that structure in specimens represented by negative PC3 values but is also bulbously protuberant rather than flat. The lateral epicondyle extends further proximally than the medial epicondyle to the approximate halfway between the distal extent of the humerus and the distal extent of humeral head. The olecranon fossa is slightly deeper and wider than the condition at the PC3 minimum. Monk seals cluster towards the minimum of PC3. *O. rosmarus*, a male *Mirounga angustirostris* (the northern elephant seal), a male *Halichoerus grypus* (the grey seal), and a female *Neophoca cinerea* (the Australian sea lion) cluster around the median. The remaining taxa cluster towards the PC3 maximum.

We also projected the humeral shape of fossil taxa into the morphospace of extant taxa. Stem pinnipeds *P. valletoni* and *P. rayi* fall near the upper limit of the hindlimb morphospace, in

line with previous predictions that hindlimb-dominated swimming is the ancestral state in pinnipeds (Furbish, 2015; Paterson et al., 2020; Hocking et al., 2021). Early diverging desmatophocid *Desmatophoca oregonensis* falls within the hindlimb-dominated morphospace intermediate to phocids and odobenids, but derived desmatophocid *A. kernensis* falls outside of modern morphospace. The two fossil otariids, the basal *Pithanotaria starri* and later branching *Thalassoleon mexicanus*, similarly fall in the space intermediate to the modern hindlimb and forelimb morphospaces, but *P. starri* has a higher PC1 value than any of the modern otariids and falls very close to the two stem pinnipeds. Except for *Pontolis barroni*, all of the fossil walruses fall within the hindlimb-dominated morphospace. The early walruses *Neotherium mirum* and *Imagotaria downsi* cluster relatively close to early otariid *P. starri* and stem pinniped *P. rayi*, while *P. barroni* falls just outside the modern otariid morphospace. The neodobenids *D. seftoni*, *Pliopedia pacifica*, and *Valenictus imperialiensis* all cluster near modern *O. rosmarus*. Notably, most of the fossil species fall outside regions occupied by modern pinnipeds.

3.2 Inferring Locomotor Mode from Pinniped Humeral Morphology

To train the FDAs, I used the first 13 PCs (Appendix E), which accounted for 88.8% of the total variation in the dataset. The posterior classification rates and discriminant scores for each species are recorded in Table 3 and probability density functions displaying the distribution of discriminant scores for each FDA are shown in Figure 6. The coefficients of the FDAs, which quantify the degree to which each PC contributes to the discriminant function, are recorded in Table 4. Both FDAs performed remarkably well: the npFDA correctly classified both hindlimb- and forelimb-dominated swimmers 100% of the time and the pFDA had an overall correct classification rate of 90% with correct identification of all of the hindlimb swimmers and four out of 12 forelimb swimmers incorrectly classified as hindlimb swimmers (Table 3). The

Table 3. Results of phylogenetically uncorrected and corrected flexible discriminant analyses (FDAs). Numbers correlate with specimens listed in Table 1; DS = discriminant score. Continued onto the subsequent page.

		Uncorrected FDA Results				Phylogenetically Corrected FDA Results			
	Taxon Name	**Predicted Class**	**Forelimb Probability**	**Hindlimb Probability**	**DS**	**Predicted Class**	**Forelimb Probability**	**Hindlimb Probability**	**DS**
	Fossil Taxa								
1.	*Potamotherium vallentoni*	Hindlimb	0.000	1.000	0.06	Hindlimb	0.324	0.676	-0.30
2.	*Pinnarctidion rayi*	Hindlimb	0.000	1.000	0.60	Hindlimb	0.231	0.769	0.30
3.	*Desmatophoca oregonensis*	Hindlimb	0.000	1.000	0.84	Hindlimb	0.131	0.869	1.17
4.	*Allodesmus kernensis*	Forelimb	0.972	0.028	-1.99	Forelimb	0.651	0.349	-2.03
5.	*Pithanotaria starri*	Hindlimb	0.000	1.000	-0.28	Hindlimb	0.158	0.842	0.89
6.	*Thalassoleon mexicanus*	Forelimb	1.000	0.000	-2.98	Hindlimb	0.340	0.660	-0.39
7.	*Neotherium mirum*	Hindlimb	0.327	0.673	-1.36	Hindlimb	0.436	0.564	-0.91
8.	*Imagotaria downsi*	Hindlimb	0.001	0.999	-0.46	Hindlimb	0.261	0.739	0.09
9.	*Pontolis barroni*	Forelimb	1.000	0.000	-3.45	Forelimb	0.724	0.276	-2.46
10.	*Dusignathus seftoni*	Hindlimb	0.123	0.877	-1.17	Hindlimb	0.340	0.660	-0.39
11.	*Pliopedia pacifica*	Hindlimb	0.032	0.968	-0.96	Hindlimb	0.426	0.574	-0.85
12.	*Valenictus imperialensis*	Hindlimb	0.000	1.000	-0.10	Hindlimb	0.220	0.780	0.37
	Extant Otarioids								
13.	*Odobenus rosmarus*	Hindlimb	0.000	1.000	0.16	Hindlimb	0.294	0.706	-0.12
14.		Hindlimb	0.000	1.000	1.51	Hindlimb	0.176	0.824	0.73
15.		Hindlimb	0.000	1.000	0.29	Hindlimb	0.231	0.769	0.29
16.	*Arctocephalus australis*	Forelimb	1.000	0.000	-3.26	Hindlimb	0.321	0.679	-0.28
17.		Forelimb	1.000	0.000	-5.33	Forelimb	0.591	0.409	-1.70
18.	*Arctocephalus forsteri*	Forelimb	1.000	0.000	-5.89	Forelimb	0.651	0.349	-2.03
19.		Forelimb	1.000	0.000	-5.50	Forelimb	0.627	0.373	-1.90
20.	*Arctocephalus galapagoensis*	Forelimb	0.999	0.001	-2.60	Hindlimb	0.254	0.746	0.13
21.	*Callorhinus ursinus*	Forelimb	1.000	0.000	-5.27	Forelimb	0.605	0.395	-1.78
22.		Forelimb	1.000	0.000	-4.60	Forelimb	0.571	0.429	-1.60
23.	*Neophoca cinerea*	Forelimb	1.000	0.000	-5.58	Forelimb	0.706	0.294	-2.35
24.	*Otaria flavescens*	Forelimb	1.000	0.000	-4.13	Hindlimb	0.442	0.558	-0.94
25.		Forelimb	1.000	0.000	-4.86	Forelimb	0.553	0.447	-1.51

Table 3. Continued from previous page.

		Uncorrected FDA Results				Phylogenetically Corrected FDA Results			
	Taxon Name	**Predicted Class**	**Forelimb Probability**	**Hindlimb Probability**	**DS**	**Predicted Class**	**Forelimb Probability**	**Hindlimb Probability**	**DS**
26.	*Zalophus californianus*	Forelimb	1.000	0.000	-4.04	Hindlimb	0.432	0.568	-0.89
27.		Forelimb	1.000	0.000	-5.22	Forelimb	0.604	0.396	-1.77
	Extant Phocids								
28.	*Cystophora cristata*	Hindlimb	0.000	1.000	1.30	Hindlimb	0.280	0.720	-0.03
29.		Hindlimb	0.000	1.000	2.21	Hindlimb	0.212	0.788	0.44
30.	*Erignathus barbatus*	Hindlimb	0.000	1.000	3.07	Hindlimb	0.138	0.862	1.10
31.		Hindlimb	0.000	1.000	1.67	Hindlimb	0.254	0.746	0.14
32.	*Halichoerus grypus*	Hindlimb	0.000	1.000	3.83	Hindlimb	0.111	0.889	1.41
33.		Hindlimb	0.000	1.000	1.85	Hindlimb	0.259	0.741	0.10
34.	*Histriophoca fasciata*	Hindlimb	0.000	1.000	2.21	Hindlimb	0.198	0.802	0.55
35.		Hindlimb	0.000	1.000	1.93	Hindlimb	0.242	0.758	0.22
36.	*Hydrurga leptonyx*	Hindlimb	0.000	1.000	2.08	Hindlimb	0.222	0.778	0.36
37.	*Leptonychotes weddellii*	Hindlimb	0.000	1.000	1.35	Hindlimb	0.287	0.713	-0.08
38.		Hindlimb	0.000	1.000	1.88	Hindlimb	0.237	0.763	0.25
39.	*Mirounga angustirostris*	Hindlimb	0.000	1.000	2.54	Hindlimb	0.180	0.820	0.69
40.	*Monachus monachus*	Hindlimb	0.000	1.000	2.91	Hindlimb	0.139	0.861	1.09
41.	*Neomonachus schauinslandi*	Hindlimb	0.000	1.000	3.05	Hindlimb	0.112	0.888	1.40
42.		Hindlimb	0.000	1.000	1.79	Hindlimb	0.237	0.763	0.25
43.		Hindlimb	0.000	1.000	2.69	Hindlimb	0.149	0.851	0.98
44.	*Ommatophoca rossii*	Hindlimb	0.000	1.000	1.23	Hindlimb	0.250	0.750	0.16
45.		Hindlimb	0.000	1.000	4.27	Hindlimb	0.080	0.920	1.87
46.	*Pagophilus groenlandicus*	Hindlimb	0.000	1.000	0.67	Hindlimb	0.350	0.650	-0.45
47.		Hindlimb	0.000	1.000	0.49	Hindlimb	0.422	0.578	-0.83
48.	*Phoca vitulina*	Hindlimb	0.000	1.000	1.58	Hindlimb	0.285	0.715	-0.06
49.	*Pusa caspica*	Hindlimb	0.000	1.000	2.79	Hindlimb	0.157	0.843	0.90
50.	*Pusa hispida*	Hindlimb	0.000	1.000	1.64	Hindlimb	0.230	0.770	0.30
51.		Hindlimb	0.000	1.000	2.18	Hindlimb	0.199	0.801	0.54
52.	*Pusa sibirica*	Hindlimb	0.000	1.000	3.07	Hindlimb	0.132	0.868	1.16

Table 4. The contribution of each of the first 13 principal components (PCs) to the phylogenetically uncorrected FDA (npFDA) and phylogenetically corrected FDA (pFDA), which quantify the contribution of each principal component (PC) to the discriminant function.

PC	npFDA Coefficient	pFDA Coefficient
1	36.35	8.73
2	-1.62	-0.87
3	-35.33	-8.22
4	-4.40	-1.14
5	-20.46	-2.79
6	-16.04	-2.76
7	3.31	0.96
8	8.36	2.38
9	12.23	2.18
10	-4.37	-1.33
11	7.15	2.14
12	-1.95	-0.24
13	-13.87	-2.88

incorrectly classified specimens from the pFDA include a male *Z. californianus* with a phylogenetically corrected discriminant score (pDS) of -0.89 and uncorrected discriminant score (npDS) of -1.20, a male *Otaria flavescens* (pDS = -0.94, npDS = -1.22), a male *Arctocephalus australis* (pDS = -0.28, npDS = -0.96), and an *Arctocephalus galapagoensis* of unknown sex (pDS = 0.13, npDS = -0.77). The locomotor groups are well-separated in both FDAs with some overlap between the groups in the pFDA (Fig. 6).

The swimming mode predictions for fossil taxa are recorded in Table 3 along with the posterior classification rates and discriminant scores. Predictions were consistent between the npFDA and the pFDA with the exception of otariid *T. mexicanus*. Both stem pinnipeds were classified as hindlimb-dominated swimmers (*P. valletoni*: pDS = -0.30, npDS = 0.06; *P. rayi*: pDS = 0.30, npFD = 0.60). This finding is consistent with the morphospace occupied by these species in the PCA and with previous predictions that hindlimb-dominated swimming is

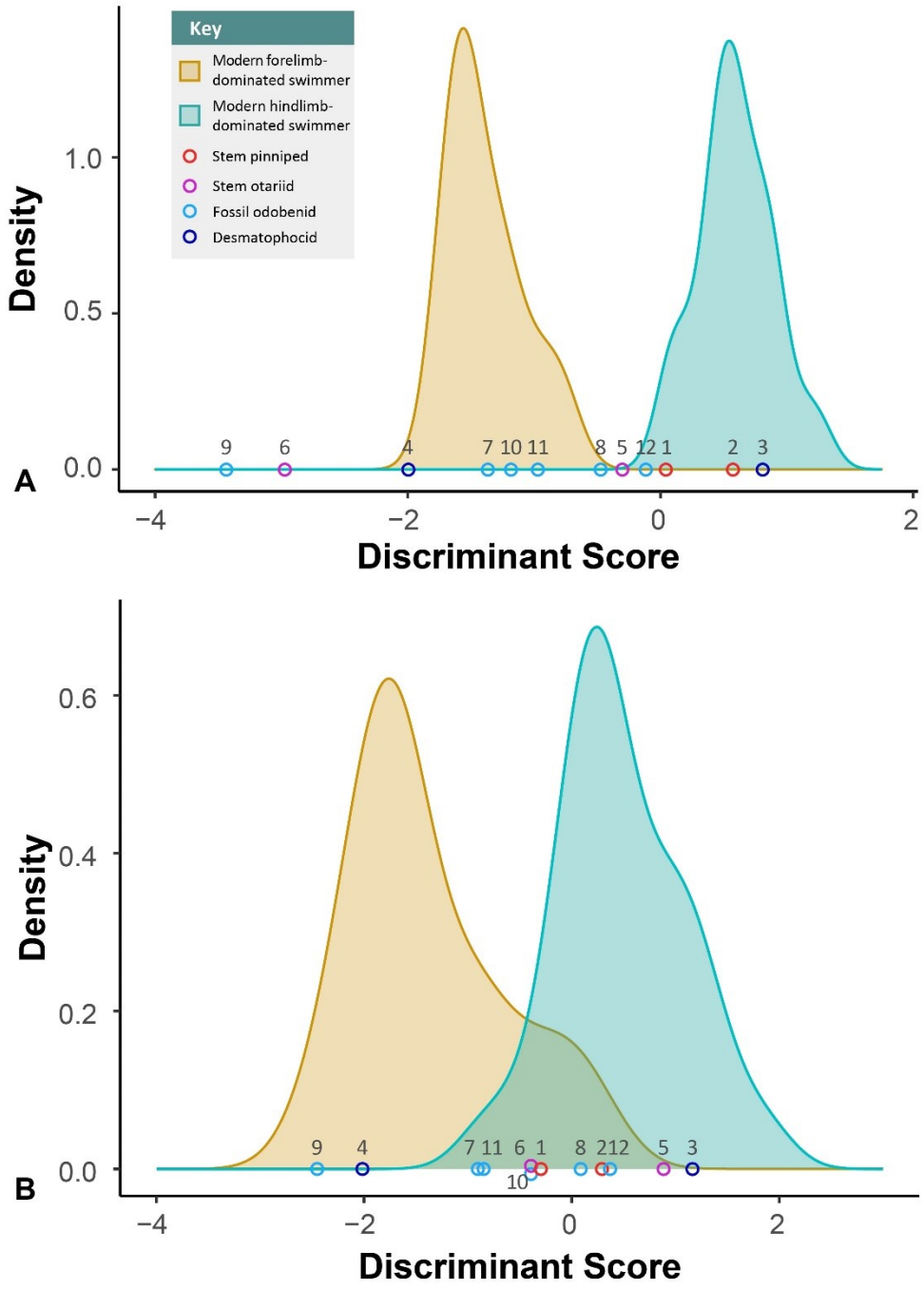

FIGURE 6. Probability density functions for the uncorrected flexible discriminant analysis (FDA, **A**) and the phylogenetically corrected FDA (**B**). Unfilled points show the discriminant scores for each of the fossil taxa. See Table 1 for taxon names.

ancestral for pinnipeds (Bebej, 2009; Paterson, 2017; Hocking et al., 2018). Similarly, the most basal members of the otarioid clades were classified as hindlimb-dominated swimmers: otariid *P. starri* (pDS = 0.89, npDS = -0.28), desmatophocid *D. oregonensis* (pFDA pDS = 1.17, npDS = 0.84), and odobenids *N. mirum* (pDS = -0.91, npDS = -1.36) and *I. downsi* (pDS = 0.09, npDS = -0.46). Later-diverging odobenids *D. seftoni* (pDS = -0.39, npDS = -1.17), *P. pacifica* (pDS = -0.85, npDS = -0.96), and *V. imperialensis* (pDS = 0.37, npDS = -0.96) were all resolved as hindlimb-dominated swimmers. The only difference in predicted swimming modes for fossil taxa between the two FDAs was the classification of the otariid *Thalassoleon mexicanus*, which diverged after *P. starri* but before crown Otariidae, as a forelimb-dominated swimmer in the npFDA (npDS = -2.98) and as hindlimb-dominated swimmer in the pFDA (pDS = -0.39).

4 Discussion

4.1 Implications of Pinniped Humerus Morphology for Locomotor Function

Overall, I found that humeral shape is significantly influenced not only by phylogeny (optimal lambda = 0.52) but also by aquatic locomotor mode. The results of our PCA indicate that the humeral morphospace occupied by forelimb-dominated swimmers is limited towards the negative end of PC1 and the positive end of PC2 and is characterized by a long, narrow deltoid crest that extends into a tall greater tubercle that reaches proximally past the humeral head and the lesser tubercle; a shallow, narrow intertubercular fossa; a proximodistally short but medially bulbous medial epicondyle; a broad, shallowly concave olecranon fossa; and a proximodistally long lateral epicondyle. The humeri of hindlimb-dominated swimmers, alternately, occupy a wider morphospace than the forelimb-dominated swimmers, with representatives from both

extremes of PC3 and occupying nearly the entire range of PC1 as well, although phocids are largely limited to the positive end of the PC1 axis. Both the markedly smaller morphospace for forelimb-dominated swimmers compared to hindlimb-dominated swimmers and the positioning of *A. kernensis*, *T. mexicanus*, and *P. barroni* close to the convex hull surrounding the modern forelimb swimmers indicates that forelimb propulsion constrains the overall morphology of the humerus. Alternately, the greater area of the morphospace occupied by hindlimb-dominated swimmers likely reflects both the wider phylogenetic and ecological diversity of this group. It also raises the possibility that primary dependence on the hindlimbs for aquatic locomotion releases the forelimbs from locomotor constraint, allowing for a wider range of forelimb morphologies as well as functions. Indeed, hindlimb-dominated swimmers utilize their forelimbs for a wide range of activities other than aquatic locomotion, including prey manipulation (Backhouse, 1962; Hocking et al., 2017, 2018), underwater "clapping" against the torso by grey seals (*H. grypus*) (Hocking et al., 2020), extensive scratching (Backhouse, 1962), digging through ice to create breathing holes (Stirling, 1977; Laakkonen and Nihtilä, 2021), and hollowing out snowbanks into lairs for hauling out, birthing, and protecting young (Helle et al., 1984; Lydersen and Gjertz, 1986). Grey seals (*H. grypus*) even use their forelimbs during terrestrial locomotion to propel the body forwards while the pelvis is still lifted from the ground, primarily through hyperextension and flexion of the phalanges and metacarpals (Backhouse 1962).

As expected, the specific morphology of the major structures of the humerus correlates with swimming modes in generally predictable ways. Here I discuss the implications of the particular morphology of each of the major structures for aquatic locomotion as identified by our analyses.

4.1.1 Deltoid Crest and Greater Tubercle—At the PC1 minimum, the deltoid crest is proximodistally long, extending proximally past both the humeral head and the lesser tubercle, with a ventral edge that is relatively narrow and runs approximately parallel to the shaft. The positive end of PC1 represents a proximodistally shorter crest that rises proximally to a level intermediate between the proximal extent of the lesser tubercle and the lower humeral head; the ventral surface of the deltoid crest is wider than the condition at the opposite end of PC1 and it also tilts away from the shaft towards is distal extent. Along PC3, the minimum is represented by a proximodistally long deltoid crest that runs parallel to the shaft with its lateral-most extent located just proximal to halfway along its length, with a greater tubercle than extends proximally past the head to approximately the same level as the lesser tubercle. At the PC3 maximum, the deltoid crest is slightly shorter than the condition seen at the minimum and tilts distally away from the shaft with its lateral-most extent located just proximolaterally to its furthest distal extent; the greater tubercle extends proximally to both the humeral head and the lesser tubercle.

With at least ten different muscles attaching to the deltoid crest and greater tubercle, these structures have significant relevance to pinniped forelimb movements. The two largest muscles attaching to the deltoid crest are the deltoid muscle, inserting to the lateral aspect of the deltoid crest, and the pectoralis muscles, inserting to the medial aspect of the deltoid crest, which have opposing functions. The deltoid muscle works with other muscles that attach to the deltoid, including the humerotrapezius, atlantoscapularis, supraspinatus, brachioradialis, cephalohumeralis, and infraspinatus, to accomplish both the recovery stroke and the abduction-protraction needed to execute braking or turning. The pectoralis works with the latissimus dorsi, which attaches to the insertional edge of the pectoralis, to produce the power stroke in *Z. californianus* (Howell 1929); in *Phoca vitulina*, the pectoralis and latissimus dorsi, each of

which insert to the medial lip of the deltoid crest, produce the rhythmic lateral undulations of the caudal portion of the body used during hindlimb propulsion (Howell 1929). In phocids, the atlantoscapularis and humerotrapezius also work to hold the forelimb against the body to maintain a hydrodynamic shape during hindlimb propulsion. Howell (1929) attributes the shortness of the greater tubercle in *P. vitulina* and other phocids to a comparatively underdeveloped supraspinatus, responsible for humeral extension and therefore less important to phocids than otariids. Notably, although the deltoid crest in *P. valletoni* is relatively short, similar to the phocid condition, its greater tubercle extends proximally past the height of the head and lesser tubercle. This trait could indicate that *P. valletoni* relied more on forelimb propulsion, perhaps via paddling as seen in semi-aquatic musteloids (Samuels et al., 2013; Fabre et al., 2015), than later stem pinnipeds like *P. rayi* and *E. mealsi*, each of which have greater tubercles that do not reach the level of the head or lesser tubercle. Furthermore, unlike other otarioids, early otariid *P. starri* has a relatively short deltoid crest that, other than extending past the level of the humeral head and lesser tubercle in a tall greater tubercle, is more similar to the condition seen in phocids and stem pinnipeds than other otarioids. This condition is also seen in early desmatophocid otarioid *D. oregonensis*. This lends further support to their classification as hindlimb-dominated swimmers.

Our findings that a proximodistally long deltoid crest and tall, proximally extended greater tubercle are associated with a forelimb-dominated swimming style are expected as this condition provides a long moment arm for the adduction, abduction, and rotation of the forelimb needed for the stroke cycle (Howell, 1929; Gordon, 1983). However, as previously stated, this condition is not solely indicative of forelimb propulsion as the elongated deltoid crest also allows for the forelimb adduction needed during the forward lunge phase of terrestrial locomotion in *O.*

rosmarus (English, 1977; Gordon, 1981). Furthermore, this condition also characterizes all the fossil otarioids in our analysis with the exception of *P. starri* and *D. oregonensis*, regardless of whether the FDAs classified them as hindlimb- or forelimb-dominated swimmers. Although previous workers have discussed an apparent tradeoff between the functional constraints of aquatic versus terrestrial locomotion (Gingerich, 2003; Botton-Divet et al., 2016; Berta et al., 2018; Hocking et al., 2021), our findings raise the possibility that this condition originally evolved not for aquatic forelimb propulsion but rather to allow for efficient terrestrial locomotion with an aquatically adapted bauplan. This condition was then exapted for forelimb propulsion in otariids, *A. kernensis*, and *P. barroni*. Whereas the majority of locomotor propulsion in fissiped carnivorans originates in the hindlimbs, otariids generate the majority of the force for terrestrial locomotion with their forelimbs (English, 1976, 1977; Beentjes, 1990). Further investigation of functional morphology of the forelimb with regards to terrestrial locomotion in otarioids is needed.

In opposition to the proximodistally long deltoid crest seen in otarioids, most phocids possess a deltoid crest that is lateromedially wider than the condition in most otariids, seen in the PCA at the maximum of PC1 and at the minimum of PC3. *O. rosmarus* also possesses a laterally expanded deltoid crest. This trait appears to accommodate a lateral placement of the humerotrapezius in phocids compared to its attachment in *Z. californianus* along the ventral edge of the deltoid crest. Although the longer attachment of the humerotrapezius in *Z. californianus* allows for stronger, faster extension of the humerus during the recovery stroke needed for rapid forelimb propulsion (English, 1977), its shorter, more laterally placed attachment in phocids seems to represent an adaptation for immobilizing the forelimb against the body during sustained periods of rectilinear swimming (Howell, 1929). The broader attachment for the humerotrapezius

both limits the range of motion and allows for more energy efficient muscle contraction while the forelimbs are being held against the body. Notably, this lateromedially wide surface of the deltoid crest does not appear in any of the fossil stem pinnipeds or otarioids, indicating a strong phylogenetic component to this condition.

The phocid deltoid crest also forms an acute angle to the humeral shaft from its vertex at the greater tubercle as opposed to running parallel to the shaft as seen in most otarioids. The phocid condition also appears in stem pinnipeds *P. valletoni*, *P. rayi*, and *D. oregonensis*. This condition potentially results from a broader attachment site for the brachialis muscle, which attaches to the shaft just dorsal to the lateral edge of the deltoid crest and assists with flexion of the elbow joint, a critical movement in braking and turning. Although previous workers have considered biceps muscle to be the primary actor in elbow flexion/braking (Howell, 1929; English, 1977), the large insertion of the brachialis in phocids indicates that it may also be significantly involved. The presence of this condition in the stem pinnipeds as well as *D. oregonensis* suggests that it is the plesiomorphic condition for pinnipeds.

4.1.2 Lesser Tubercle— Another point of differentiation between the humeral morphology associated with each swimming mode is the lesser tubercle. At the negative end of the PC 1 axis, where the otariids and *O. rosmarus* fall, the lesser tubercle is located just mediodorsally to the head, is relatively appressed to the medial edge of the head and extends proximally neither as far as the top of the head nor the top of the greater tubercle. At the positive end of PC1, where the phocids fall, the lesser tubercle is broader than the condition at the negative end, strongly medially offset from the head, and extends proximally past the top of the head and the greater tubercle. The negative end of PC3, where the monk seals fall, is characterized by a wide, medially offset lesser tubercle that is approximately equal in height to

the greater tubercle; at the positive end of PC3, where the otariids and phocine seals fall, the lesser tubercle is still relatively wide but is slightly less offset from the humeral head and does not extend as far proximally as either the head or the greater tubercle.

Compared to fissiped carnivorans, the lesser tubercle is highly developed in all pinnipeds (Wyss, 1988; Berta et al., 2018), even in basal taxa *P. valletoni* (Savage, 1957), *E. mealsi* (Berta and Ray, 1990), and *P. rayi* (Berta, 1994), allowing for a broad attachment site of the subscapularis muscle, which is responsible for medial rotation and adduction of the humerus. However, the lesser tubercle is particularly enormous in phocids, extending further proximally than the head or the greater tubercle. In otarioids, while the lesser tubercle is still substantial, it is less prominent than in phocids and does not extend as far proximally as the greater tubercle or the top of the humerus head. As previously discussed, the phocid condition likely results both from the more abducted resting position of the humerus in phocids relative to otarioids (Howell, 1929) and the provision of a longer moment arm for protraction and rotation of the humerus for braking, turning, and use of the forelimb as a hydroplane (Backhouse, 1962; Laakkonen and Nihtilä, 2021). Dewaele et al. (2017) further discuss this condition and posit that the large lesser tubercle allows for energy efficiency in maintaining the medial rotation of the humerus while the forelimb is held against the torso during hindlimb-propelled rectilinear swimming.

In stem pinnipeds *P. valletoni* and *P. rayi*, the proximal extent of the lesser tuberosity is already inflated compared to the fissiped condition but its proximal extent stops well short of the level reached by the proximal extent of the humeral head or greater tubercle (Savage, 1957; Berta and Ray, 1990; Berta, 1994). I also observed this condition in otariid *T. mexicanus* and odobenids *N. mirum*, *I. downsi*, and *P. barroni*. In stem otariid *P. starri*, the height of the lesser tubercle is intermediate between the tall greater tubercle and the humeral head. Each of these

similar conditions implies a less developed subscapularis in these taxa than seen in modern phocids, possibly because they utilized their forelimbs more regularly when swimming than phocids. In derived odobenids *P. pacifica* and especially *V. imperialensis*, the lesser tubercle is rather enormous despite its proximal extent falling short of the humeral head and greater tubercle; it bows distomedially outwards from the shaft of the humerus and its proximal confluence with the humeral head. This latter condition likely also contributes to efficient medial rotation and adduction of the humerus during hindlimb-propelled swimming, indicating that *P. pacifica* and *V. imperialensis* might have relied more heavily on hindlimb propulsion than their earlier relatives.

4.1.3 Medial Epicondyle—On PC1, negative values represent a medial epicondyle that is medially inflated with a base that is proximomedially offset from landmark 20 (the mediodistal extent of the humeral condyle) and reaches proximally just short of the proximal extent of the lateral epicondyle. Positive PC1 values are associated with a medial epicondyle with a base that is just mediodorsal to landmark 20 and is proximodistally shorter than the lateral epicondyle. At the PC3 minimum, the distal base of the medial epicondyle is closely associated with landmark 20 and it is approximately equal in proximodistal length to the lateral epicondyle. At the PC3 maximum, the medial epicondyle is proximomedially offset from the condyle and proximodistally shorter than the lateral epicondyle.

The medially expanded medial epicondyle associated with the forelimb-dominated morphospace provides a more secure elbow joint by providing an anchor for the enlarged medial collateral ligament (English 1977) and allows for the attachment of well-developed forearm and hand flexors (Milne et al., 2009), increasing the efficiency of the power stroke in modern otariids (Howell, 1929; English, 1976). The plesiomorphic condition for this trait appears to be a medial

epicondyle that forms a large, broad flank at approximately the same level as the base of the trochlea, as observed in *P. darwini* (Paterson, 2017), *P. valletoni* (Savage, 1957), and *P. rayi* (Berta, 1994). This is similar to the condition in mustelids (Schutz and Guralnick, 2007). This condition is also retained in *D. oregonensis* (Deméré and Berta, 2002) and *A. kernensis*. Stem otariid *P. starri* possesses a somewhat poorly developed medial epicondyle compared to living otariids; while the medial epicondyle of *T. mexicanus* is more prominent than that of *P. starri*, it is also less medially protuberant than that of living otariids. The medial epicondyle of the fossil odobenids is somewhat varied in morphology, from the comparatively weakly developed epicondyle in *N. mirum* and *I. downsi* to the subtriangular, intermediately protuberant condition seen in *P. pacifica* to the massively medially enlarged epicondyle seen in *D. seftoni* and particularly *V. imperialiensis* where the medial epicondyle nearly doubles the width of the distal end of the humerus.

Although Howell (1929) attributed the greatly developed medial epicondyle seen in *Z. californianus* to the flexors of the lower arm as needed for a more efficient power stroke, the presence of this condition in hindlimb-dominated modern *O. rosmarus* as well as *D. seftoni* and *V. imperialiensis*, both categorized by our analysis as hindlimb-dominated, calls this assumption into question. Gordon (1981) reports that during the forward lunge phase of the terrestrial gait of *O. rosmarus*, the manus remains flexed as the forelimb is retracted, but it seems unlikely that such a behavior would account for the enormous development of the medial epicondyle seen in derived odobenids. The functional role of the morphology of this structure in walruses as well as how and if it relates to aquatic locomotion remains an open question.

4.1.4 Lateral Epicondyle—In our PCA, the negative end of both PC1 and PC3 represents a lateral epicondyle that extends approximately as far proximally as the medial

epicondyle and flares proximolaterally from its base. At the positive end of both PC1 and PC3, the lateral epicondyle extends further proximally than the medial epicondyle to slightly less than halfway up the length of the shaft; it also flares at a slight angle proximally from its base. This landmark configuration limits the utility of understanding the functionality of these character states as it does not fully capture the variation in this structure because the only landmark describing the lateral epicondyle is landmark 26 (apex of the lateral epicondyle). This landmark largely shows only the relative height of this structure along the bone and not its differentiation from the shaft. Further investigation into the variation in this structure is therefore needed.

From qualitative observations, I noted that the apex of the lateral epicondyle in otariids was higher than the condition in phocids, but the condyle itself was largely confluent with the humeral shaft, whereas the lateral epicondyle formed a structure distinct from the humeral shaft in phocids and, notably, *O. rosmarus*. In the latter, the lateral epicondyle is proximodistally shorter than the medial epicondyle and bows laterally out from its confluence with the lateral base of the condyle in a convex curve that is even more laterally protuberant than the condition of many phocid species. I also noted that the relative height of the lateral epicondyle varied significantly between species within the Phocidae. I consider it likely that this condition varies according to influences other than locomotion, but it remains unclear whether this results from other ecological adaptations or random phylogenetic variation. As the lateral epicondyle primarily serves as the attachment site for forearm extensors (Howell, 1929), this could be a point of variation related to the various uses of the forelimb and manus available to hindlimb-dominated swimmers.

In the fossil taxa, stem pinnipeds *P. valletoni* and *P. rayi* possess a tall, flank-like lateral epicondyle that rises proximally to approximately halfway along the shaft. *D. oregonensis* has a

low lateral epicondyle that consists only of a slight crook in the lateral edge of the shaft just proximal to the proximodorsal edge of the condyle; it is approximately equal in proximodistal height to the medial epicondyle. Interestingly, *A. kernensis*, which was categorized as a forelimb-dominated swimmer by our analysis as well as other studies (Bebej, 2009; Furbish, 2015), possesses a lateral epicondyle that more resembles the condition in phocids as opposed to modern otariids. Its lateral edge forms a convex curve from the laterodistal edge of the condyle before an inflection point at which it sharply curves back towards the shaft, forming a distinctive structure from the main shaft. The lateral epicondyle of early otariid *P. starri* is relatively similar to the tall, flank-like condition seen in the stem pinnipeds, although it does not extend as far proximally as the stem species. *T. mexicanus* has a lateral epicondyle that forms a broad lateral convex bend in the lateral edge of the distal shaft. Although the *O. rosmarus* condition is approached in *Valenictus*, in the other odobenids, the lateral epicondyle approximates the morphology of *D. oregonensis*. The reason for the greater development of the lateral epicondyle in *Odobenus* and *Valenictus* compared to early odobenids is unclear, although it is possibly a product of allometry. Extension of the manus seems unimportant in the terrestrial locomotion of modern walruses (Gordon 1981), and it is not readily apparent how and if the greater development of the lateral epicondyle in these two derived odobenids would impact aquatic locomotion.

4.2 The Evolution of Swimming Modalities in Otarioid Pinnipeds

In Figure 7, I show the average discriminant scores associated with each taxon plotted across the pinniped phylogeny. According to the results of our FDAs, both the stem pinnipeds and the earliest diverging members of otarioid clades Desmatophocidae, Otariidae, and Odobenidae were likely all hindlimb-propelled swimmers. The classification of *P. valletoni* and

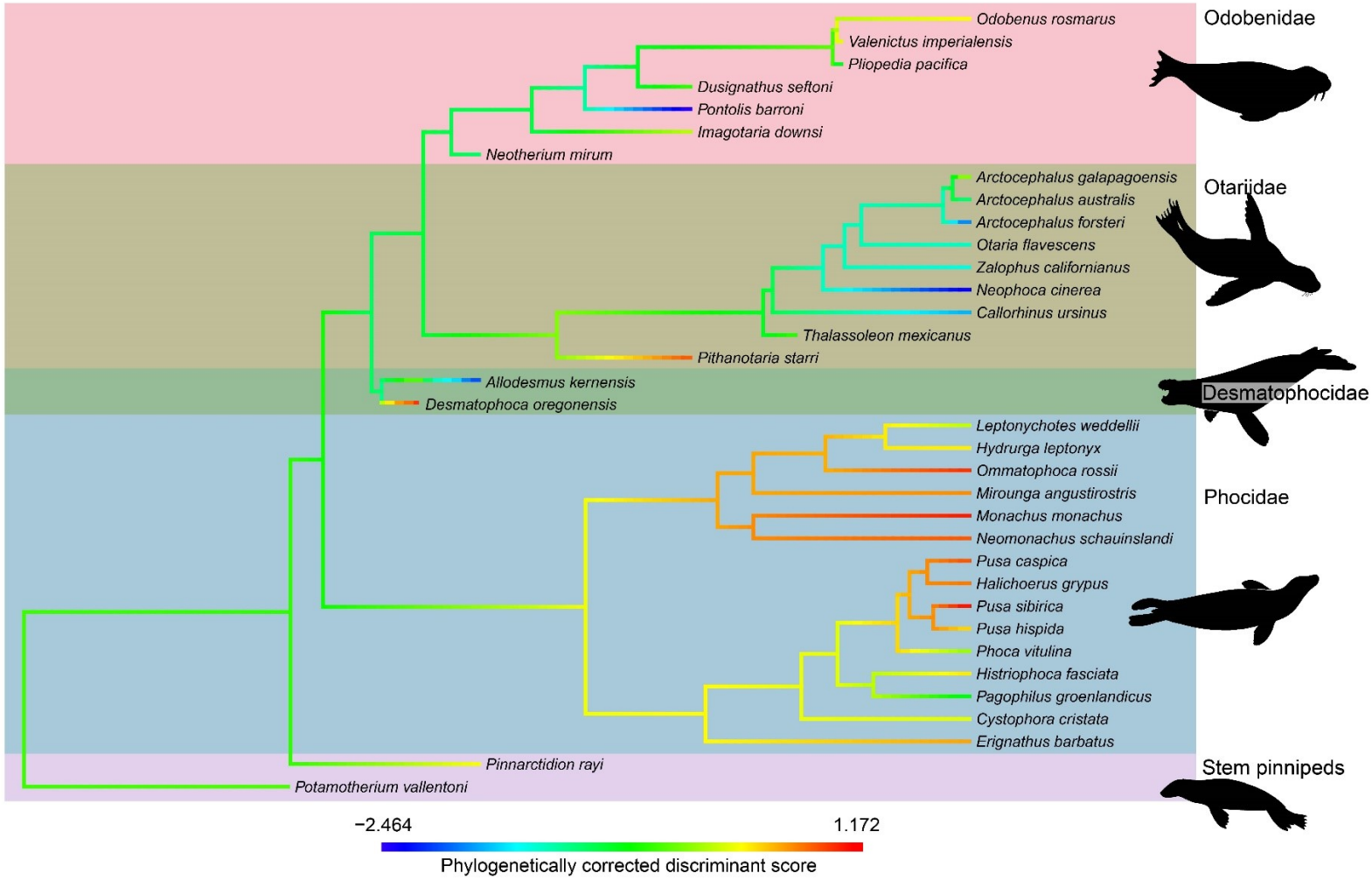

FIGURE 7. Discriminant scores from the phylogenetically corrected flexible discriminant analysis plotted across that phylogeny. Specimen-specific discriminant scores can be viewed in Table 3. Cool colors represent a forelimb-dominated swimming style and warm colors represent a hindlimb-dominated swimming style.

P. rayi as hindlimb-propelled swimmers is consistent with previous studies that recovered the plesiomorphy of hindlimb propulsion in pinnipeds (Bebej, 2009; Paterson, 2017; Hocking et al., 2018, 2021; Paterson et al., 2020). Additionally, the resolution of *P. valletoni*, *N. mirum*, *I. downsi*, *D. seftoni*, and *P. pacifica* as close to the mean discriminant score also supports their reliance on a more intermediate swimming mode than modern hindlimb swimmers. However, our recovery of early otarioids as hindlimb-propelled runs contrary to the hypothesis that forelimb swimming evolved at the base of Otarioidea with a partial reversal to hindlimb-dominated combination swimming at some point prior to the divergence of *O. rosmarus*. Instead, our results suggest that forelimb-dominated swimming actually evolved three different times in the otarioid lineage: once in an ancestor of desmatophocid *A. kernensis*, as previously recovered in Bebej (2009) and Furbish (2015); once in an ancestor of large-bodied odobenid *P. barroni*; and once either in an ancestor of crown Otariidae, as supported by the pFDA, or an ancestor of *T. mexicanus* and crown Otariidae, as supported by the npFDA. Notably I consider it possible that the pFDA misclassified *T. mexicanus* for several reasons. First, *T. mexicanus* possessed a humerus with long deltoid crest that runs parallel to the shaft, a prominent greater tubercle, and a protuberant medial epicondyle, all structures that correlated with forelimb-dominated propulsion. Furthermore, it misclassified the modern forelimb-dominated training taxa 33% of the time, and *T. mexicanus* had a posterior forelimb classification rate of 0.34. Given these circumstances, I consider it likely that *T. mexicanus* was an intermediate swimmer relying more on forelimb propulsion than its hindlimb-propelled ancestors but not yet as strongly adapted to forelimb propulsion as modern otariids.

Regardless of the true locomotor ecology of *T. mexicanus*, the evolution of forelimb-propelled swimming three separate times in Otarioidea raises questions about both why and how

this modality arose repeatedly in this lineage. As noted by Backhouse (1962), forelimb propulsion is highly unusual among marine mammals as the majority, including phocids and odobenids, produce most of their thrust with their hindlimbs. Cetaceans, sirenians, and the sea otter *E. lutris* all generate thrust via dorsoventral caudal propulsion; cetaceans and sirenians undulate their wide, flattened tails in the vertical plane while *E. lutris* undulates its tail and webbed hindlimbs (Fish, 1996). In the fossil record, both the Miocene desmostylian *Desmostylus hesperus* (Domning, 2002; Gingerich, 2005) and aquatic giant sloth *Thalassocnus natans* (Amson et al., 2015) appear to have primarily relied on alternating paddling strokes of the forelimb, similar to polar bears (*Ursus maritimus*), but this modality differs substantially from the bilateral pectoral oscillation used by otariids. The otariid mode of forelimb propulsion is indeed more similar to the "underwater flying" modality used in penguins and sea turtles (Feldkamp, 1987b; Gutarra and Rahman, 2022).

One possible driver for the evolution of forelimb-propelled swimming could be for counteracting torque. Torque increases as the distance increases between the source of the propulsive force and the center of mass of the object. Forelimb propulsion places the source of propulsive force closer to the center of mass, decreasing torque and therefore reducing energy expenditures for counteracting torque. Indeed, otariids have a remarkably high aerobic efficiency, the ratio of power expended to mechanical work accomplished, among marine mammals (Fish, 1996). Otariids are also the fastest and most aquatically agile of the pinnipeds, with California sea lion *Z. californianus* able to swim up to 30 miles per hour (Campagna et al., 2021). As suggested by English (1976), the higher swimming speed achievable by otariids compared to other pinnipeds grants access to faster prey items that slower predators cannot reliably capture. As discussed by Hocking et al. (2021), leopard seals rely more on forelimb

propulsion than any other modern phocid and their flippers converge on the otariid morphology; they also are able to achieve underwater speeds of up to 23 miles per hour and typically rely on speed, not stealth, to catch their fast-moving prey, including penguins (Muir et al., 2006). The ability to exploit this fast-swimming guild of prey species could have acted as a strong evolutionary attractor throughout pinniped evolution.

As I have previously noted, nearly all the fossil otarioids I examined in this study possess an elongated deltoid crest regardless of whether the FDAs classified them as hindlimb- or forelimb-propelled. *O. rosmarus*, which is primarily hindlimb-propelled, also possesses this trait, ostensibly to provide a long moment arm for forelimb adduction during the forward lunge in the terrestrial gait cycle (English, 1977; Gordon, 1983). Although otariid terrestrial locomotion differs from that of *O. rosmarus*, primarily in that they fully support their weight on their limbs whereas *O. rosmarus* rests its bulk on its venter, otariids still produce the majority of thrust during terrestrial locomotion from forelimb adduction (Beentjes, 1990). Given that a proximodistally long deltoid crest is not intrinsically indicative of forelimb-dominated aquatic propulsion and seems to have evolved prior to this locomotor ecology, I posit that this trait may have first arisen as an adaptation to accommodate terrestrial locomotion in a lineage whose forelimb morphology is constrained by the need to effectively locomote both on land and in the water. The prior availability of this structure thus provides a mechanism for the repeated evolution of forelimb-dominated propulsion.

Previous workers have posited that phocids are the most aquatically specialized of the pinnipeds as they lack external ears, are no longer able to walk on land, and generally spend more time at sea than their otarioid cousins (Howell, 1929; Ray, 1963; King, 1983; Berta et al., 2015). Our results present an alternative viewpoint: after diverging from a common aquatic

ancestor, phocids further specialized the ancestral hindlimb-dominated intermediate swimming style through a variety of skeletal changes, including the telescoping of the neck and the locking of their hindlimbs in the backwards position by a massively enlarged astragalar process and the resulting tension in the flexor hallucis longus muscle. Otariids, in turn, are not "less" aquatically adapted than phocids but have simply solved the same ecological problem in a different way, specializing in rapid, agile swimming in the marine environment while retaining the ability to move relatively quickly while on land. Odobenids are somewhat intermediate to these two conditions and appear to have largely maintained the ancestral combination swimming style with hindlimb domination at higher speeds. Together with observations that many phocid species also use forelimb propulsion to varying degrees (Backhouse, 1962; Hocking et al., 2018, 2021), this trait distribution demonstrates that forelimb-dominated propulsion and hindlimb-dominated propulsion form a continuum rather than two diametrically opposed conditions.

5 Conclusion

I tested the hypothesis that humeral morphology is diagnostic for swimming modality in pinnipeds using three-dimensional geometric morphometrics and then applied this methodology to predicting the swimming modes of fossil pinnipeds. Our results supported a hindlimb-dominated mode of aquatic propulsion as the plesiomorphic condition for all pinnipeds as well as otarioids, with three separate acquisitions of forelimb-dominated propulsion in desmatophocid *A. kernensis*, odobenid *P. barroni*, and in the Otariidae. The primary use of the forelimbs in aquatic locomotion seems to constrain humeral morphology and the range of other associated functional uses available to these taxa. As our analyses indicate that an elongated deltoid crest arose before

forelimb propulsion in otarioids, this condition seems to have predisposed otarioids to the evolution of forelimb propulsion. Overall, I find that when considering pinniped locomotion from the perspective of the fossil record as well as their modern ecology, the two main locomotor modes represent a continuum of swimming modalities.

6 Bridge

Understanding how pinniped locomotion has evolved provides critical insight into how their positionality within marine ecosystems has changed through time regarding factors from accessible prey items and predator avoidance to cooperative interactions with other predators and the particular marine and terrestrial environments they typically inhabit. However, locomotor abilities are only one of the dimensions influencing pinniped ecology. Abiotic environmental variables such as water temperature, coastal landforms, and presence or absence of ice also determine the geographic range and resources available to these marine mammals. As climate changes through time, so too does the biogeography of the organisms that live under those conditions. This coupling between the range of an organism and shifts in climate within evolutionary time provides a sort of paleoecological laboratory that conservation paleobiologists can use to better understand the fundamental niche of the organism in question, that is, the range of environmental conditions it is capable of tolerating as opposed to those it is currently known to inhabit. In the next chapter, I turn to the fossil record of the walrus *Odobenus rosmarus*, the last living odobenid, to investigate its paleobiogeography with respect to the availability of sea ice in order to model its response to the next hundred years of anthropogenic climate change.

CHAPTER IV

FOSSIL DATA INDICATE *ODOBENUS ROSMARUS*, THE LAST ODOBENID, CAN SURVIVE IN SEASONALLY ICE-FREE CONDITIONS

This chapter is planned for submission to *Frontiers of Biogeography*, co-authored with E. B. Davis. The project idea, data collection, coding and ecological niche modeling, and writing were all performed by M. K. Tate-Jones. Editorial assistance was provided by E. B. Davis.

1 Introduction

With the Arctic Circle warming two to four times faster than the rest of the planet, its constituent ecosystems are undergoing similarly rapid changes (Yletyinen 2019, Huntington et al. 2020, Turner et al. 2020, Jacobs et al. 2021, Rantanen et al. 2021). As anthropogenic climate change and polar amplification increase Arctic temperatures, the melting of sea ice is accelerating (Meehl et al. 2018, Diebold and Rudebusch 2021). Even conservative models predict a high likelihood of a seasonally ice-free Arctic by 2050 or earlier (Overland and Wang 2013, Jahn et al. 2016, Notz and Stroeve 2018, Guarino et al. 2020, Årthun et al. 2021, Diebold and Rudebusch 2021). As sea ice plays a critical role in Arctic marine ecosystems (Wassmann et al. 2011), its retreat will drastically alter their structuring and composition (Post et al. 2013). The loss of sea ice is particularly threatening for the wide diversity of pagophilic (ice-dependent) species from microscopic algae (Clarke and Peck 1991), bacteria (Amiraux et al. 2021), and zooplankton (Werner 1997) to seabirds (Divoky et al. 2015), polar bears (Rode et al. 2014), and pinnipeds, including six seal species and the walrus (Laidre et al. 2015). Understanding how the decline in sea ice availability will affect these organisms as well as the broader ecosystems with

which they interact is crucial for mitigating the impact of climate change on the Arctic environment.

One such ice-dependent organism is the walrus, *Odobenus rosmarus* (Fig. 1a, b; Linnaeus 1758). The only living member of the pinniped family Odobenidae, *O. rosmarus* is a large-bodied molluscivorous marine mammal easily identified by its prominent tusks and bristling whiskers, or vibrissae (Fay 1985). Today, the walrus has a discontinuous circumpolar distribution and consists of two genetically distinct subspecies, the Atlantic (*O. rosmarus rosmarus*) and Pacific (*O. rosmarus divergens*) walrus (Fay 1985, Lindqvist et al. 2009; Fig. 1c). Because of its

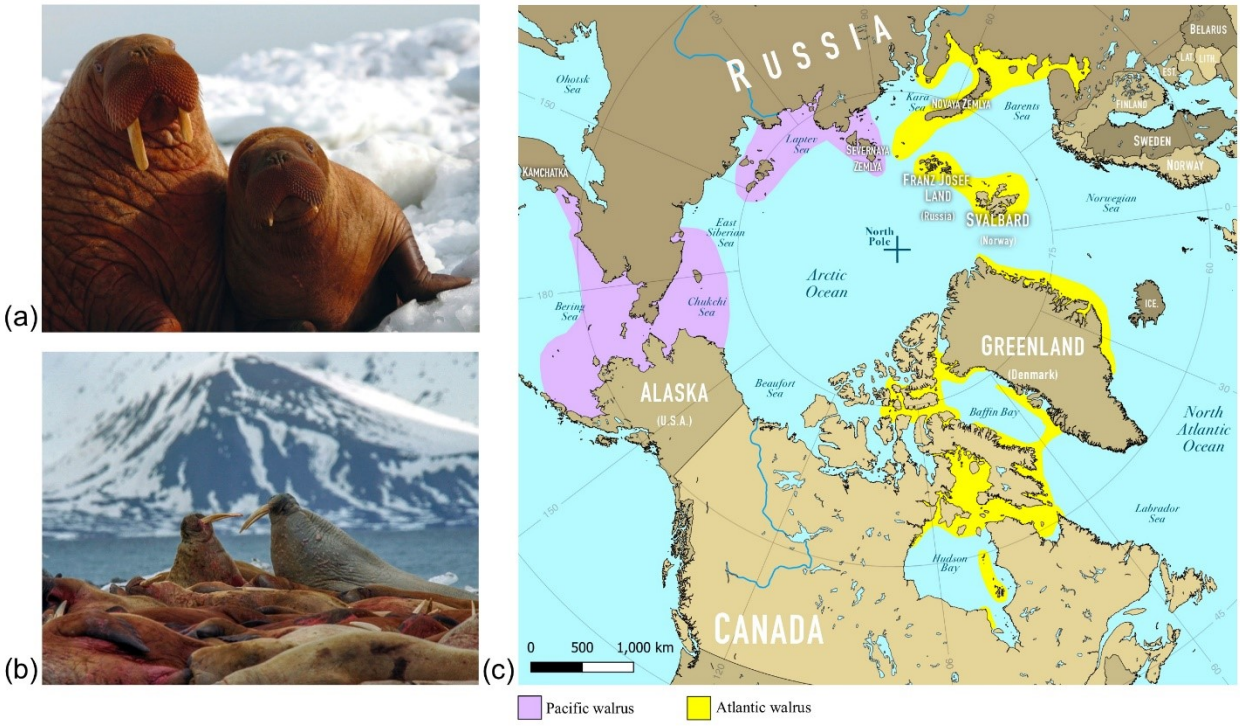

Figure 1. Walrus general appearance and typical habitat and map of known distribution of the modern walrus *Odobenus rosmarus*. a) Female Pacific walrus and calf on a summer ice floe; photograph taken by United States Fish and Wildlife Service, public domain. b) Atlantic walruses hauled out at a terrestrial rookery in Svalbard, Norway; photograph taken by Jerzy Strzelecki and provided under Creative Commons Attribution. Photographs were downloaded from Wikimedia Commons. c) Range of the two subspecies of walrus: the Atlantic walrus (yellow; *O. rosmarus rosmarus*) and the Pacific walrus (purple; *O. rosmarus divergens*) (Higdon and Stewart 2018).

unique feeding modality, *O. rosmarus* serves as an Arctic ecosystem engineer (Hocking et al. 2021). While foraging, walruses uncover infaunal bivalves by sweeping away sediment with their flippers or through oral hydraulic jetting. This sediment bioturbation restructures benthic communities over thousands of square kilometers of ocean seafloor and changes ocean productivity by redistributing nutrients within the water column (Ray et al. 2006). Furthermore, walruses serve as a critical food source for Alaskan and Siberian indigenous peoples; historical collapses of local walrus populations have led to famine and starvation in these communities (Metcalf and Robards 2008, Jay et al. 2011, Ray et al. 2016), demonstrating the importance of walruses for food security within the Arctic Circle.

The crucial position walruses hold within Arctic ecosystems and cultures necessitates a robust understanding of how sea ice loss will impact them. Currently, walrus dependence on sea ice varies seasonally and according to sex. In the winter, walruses gather in mixed herds in ice-free polynyas deep within the pack ice where they forage for bivalves in the shallow waters of the continental shelf (Fay 1982). In late spring, males typically remain in more southerly regions where they haul out at terrestrial rookeries. Alternately, females and calves follow the retreating sea ice northwards, using ice as a resting platform between foraging trips (Beatty et al. 2016). As a result, the overall decline in summer sea ice as well as its increasing distance from the bivalve beds where walruses typically forage raises the question of how and whether walruses will adapt to its total loss. Jay et al. (2017) found that when walruses lack access to sea ice during the summer, they spend significantly less time foraging or resting than when sea ice is available, diminishing their ability to develop endogenous fat stores. Models developed by Udevitz et al. (2017) predicted that by the second half of the 21st century, this relationship between sea ice loss and fat storage would lead female walruses to weigh 7–12% less by the end of the summer

foraging season than they do currently. Although the broader demographic impacts of such changes remain unknown, the impact of this predicted trend could be substantial, especially since walruses have the lowest reproductive rate of all pinnipeds, calving only every two years (Fay 1985). Already walrus behavior has been shifting. Increasingly, female walruses and their calves are hauling out in large numbers along coastlines and islands by late summer as sea ice becomes too distant and unreliable (Jay et al. 2012). This change increases their vulnerability not only to polar bear predation but also to trampling mortality as walruses tend to stampede when disturbed (Øren et al. 2018). Because trampling deaths disproportionately affect calves and young walruses, this trend could be particularly detrimental to walrus populations (Udevitz et al. 2013).

With the ambiguity surrounding the future of the walrus, turning to the past can offer new insights. Historically, extirpated walrus populations inhabited significantly warmer climes than current walrus populations (Boessenecker and Churchill 2021). Both the Canadian Maritimes *O. rosmarus*, hunted to extinction by the end of the 18th century (McLeod et al. 2014), and the recently identified Icelandic *O. rosmarus*, eradicated following Norse settlement in medieval times (Keighley et al. 2019), seemed to have thrived in seasonally ice-free conditions. The fossil record provides further evidence that modern walruses may indeed inhabit only a subset of the environmental conditions they are capable of tolerating. Paleontologists have identified Pleistocene fossils of *O. rosmarus* much further south than they range today, including in Tokyo (Harington 2008), San Francisco Bay (Jefferson 1991, Harington 2008), and Edisto Island off the southern coast of South Carolina (Roth and Laerm 1980). Even during the coldest periods of the Pleistocene, these areas were warmer than current walrus habitat and likely ice-free much or all of the year during both glacial and interglacial intervals (Batchelor et al. 2019).

While the historical and paleontological distribution of *O. rosmarus* suggests that walruses may indeed be capable of surviving warmer, more seasonally ice-free conditions than they do today, this hypothesis has yet to be quantitatively tested. Ecological niche models (ENMs) provide a robust methodology for predicting range shifts by correlating geographic occurrence data with environmental predictor variables (Elith et al. 2010). These models can then be projected to the conditions predicted by future climate simulations. Despite their utility, such models are limited by the difference between the realized niche and fundamental niche of an organism. Although a species may currently occupy a certain set of environmental parameters, known as its realized niche, these conditions do not necessarily reflect the total breadth of conditions within which the species can survive, its fundamental niche (Svenning et al. 2011). The inclusion of fossil occurrences of extant organisms can illuminate potential gaps between realized and fundamental niches (Davis et al. 2014, Dietl et al. 2015, Maguire et al. 2015, Myers et al. 2015, Lima-Ribeiro et al. 2017). For instance, Jarvie et al. (2021) used fossil occurrences of the tuatara, a New Zealand rhynchocephalian reptile, to identify areas of suitable habitat that fall outside the ecological limits of its current distribution. Even more notably, Mallorcan midwife toads, believed to be extinct until found in remote gorges on the island in 1980, have been successfully reintroduced to suitable areas as identified by EMNs generated using fossil occurrence data (Bloxam and Tonge 1995). Here, we are the first to apply these techniques to the walrus.

In this study, we test the hypothesis that the fundamental niche of *O. rosmarus* is broader than the range of conditions they currently occupy and that walrus fundamental niche in fact includes the seasonally ice-free conditions predicted to characterize the Arctic within the next two to three decades. First, we evaluate whether the environmental conditions inhabited by

walruses during the Pleistocene are significantly different from current conditions using two datasets of fossil and modern geographic occurrences, respectively. We then construct two sets of ENMs derived from these two datasets to quantify the current ecological and paleoecological niche of *O. rosmarus*. Finally, we extrapolate each of these ENMs to future climate scenarios and compare the level of threat to walrus survivorship implied by each set of projections. We conclude by exploring the implications of our results for further research into odobenid ecology as well as the development of conservation policy.

2 Materials and Methods

2.1 Input Data

2.1.1 Modern Occurrence Data— We compiled modern occurrence data both from online databases and literature sources for both walrus subspecies. Occurrence records for *O. rosmarus* were downloaded from the Global Biodiversity Information Facility (GBIF) on July 30, 2021, and from the Ocean Biodiversity Information System (OBIS) databases on November 30, 2021. Because occurrences from GBIF and OBIS were concentrated around North America and Svalbard, we supplemented these database occurrences with additional records drawn from the literature to represent walrus sightings from the northern coast of Norway (Gjertz et al. 1993) as well as populations from the Kara, Laptev, and Chukchi Seas (Zyryanov and Vorontsov 2009, Lydersen et al. 2012, Glazov et al. 2013). We then cleaned the data of duplicates, fossil occurrences, and points with latitude and longitude that fell out of the expected range (e.g., occurrences that fell well inland or in the Southern hemisphere). After cleaning, the dataset contained 4586 occurrence points for modern *O. rosmarus* (Fig. 2).

Because of geographic sampling bias, spatial autocorrelation is ubiquitous in databases like GBIF and OBIS (García-Roselló et al. 2015) as well as regional occurrences records from specific literature sources (Dennis and Thomas 2000, Kadmon et al. 2004). Such autocorrelation can overinflate measures of model performance, leading to overfitting and diminished model applicability (Veloz 2009). Several studies have demonstrated that thinning occurrences according to a spatial filter can reduce the effects of sampling bias (Pearson et al. 2007, Kramer-Schadt et al. 2013, Boria et al. 2014, Fourcade et al. 2014). Therefore we used the R package *spThin* (Aiello-Lammens et al. 2015) to spatially filter the modern occurrences so that no occurrence fell within 50 km of any other occurrence. The 50 km spatial filter reduced the density of well-sampled areas like the Bering Sea and Svalbard to approximate the distribution of occurrences in areas with fewer recorded occurrences like the coast of Siberia. Following thinning, 383 total modern occurrences remained in the modern dataset.

2.1.2 Fossil Occurrence Data—We downloaded fossil occurrence data from the Paleobiology Dabatase (PBDB; http://paleobiodb.org) on July 21, 2021, for *Odobenus rosmarus* from the Pleistocene and Holocene. Again, we cleaned this dataset of duplicate occurrences. None of the downloaded fossil occurrences fell outside of the expected latitude and longitude. Because most fossils are found on land as a result of collection bias, the majority of fossil occurrences in our dataset were located on terrestrial raster cells. Consequently, we manually moved fossil occurrence datapoints that fell on terrestrial cells to the closest laterally adjacent marine cell using QGIS (QGIS Development Team, 2022). Following cleaning, our fossil dataset contained 103 occurrences of *O. rosmarus*. We did not thin the fossil occurrences both because preliminary models performed poorly when using thinned fossil datasets and because the

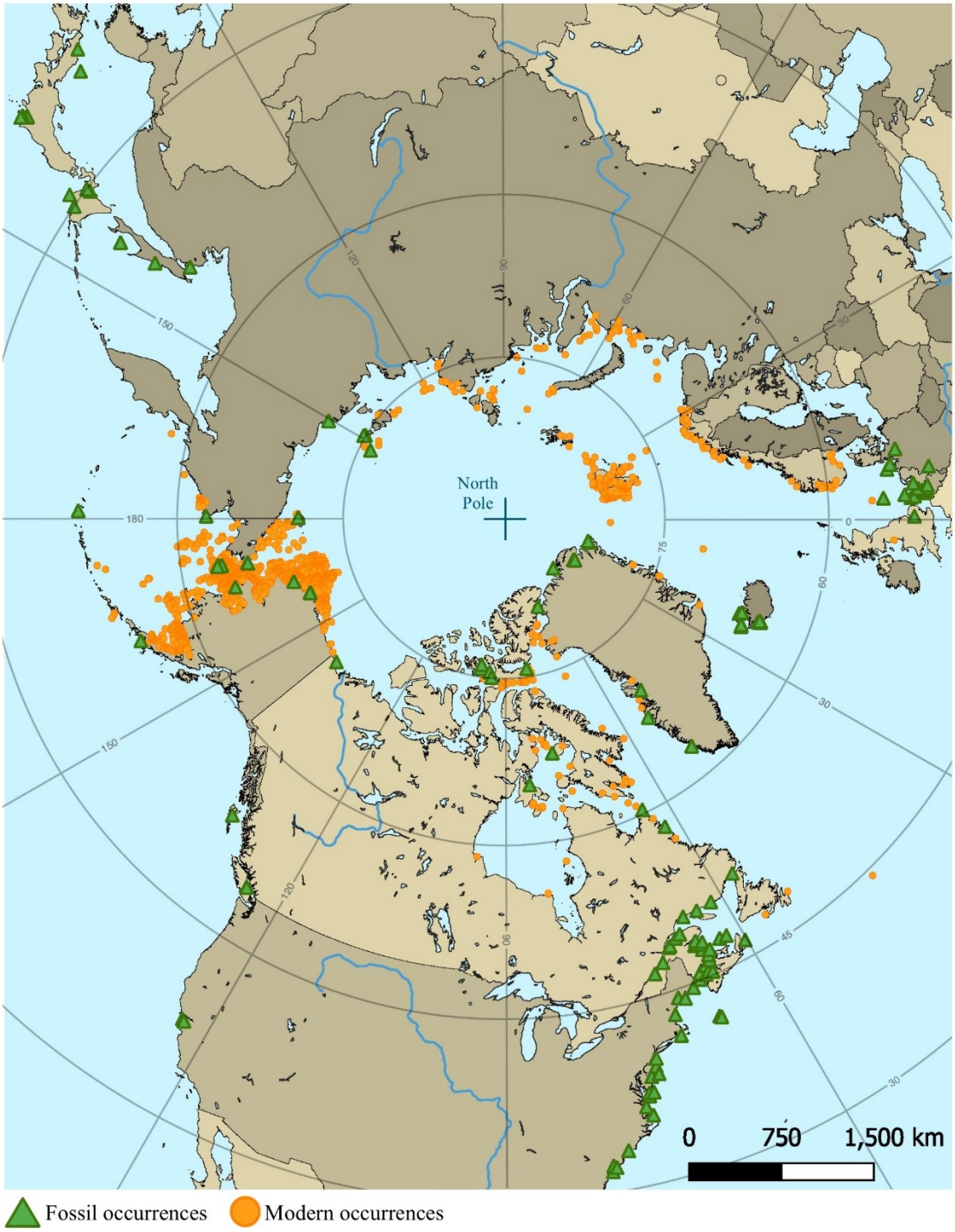

Figure 2. Occurrences of *O. rosmarus* from the dataset used in this study. Modern walrus occurrences are indicated by orange circles and were compiled from the Global Biodiversity Information Facility (GBIF), Ocean Biodiversity Information System (OBIS), Gjertz et al. (1993), Zyryanov and Vorontsov (2009), Lydersen et al. (2012), and Glazov et al. (2013). Fossil occurrences are indicated by green triangles and were downloaded from the Paleobiology Database (PBDB).

taphonomic biases inherently present in the fossil record have already naturally thinned the fossil sample.

Our fossil dataset exhibits relatively poor age constraint both because many of the specimens come from poorly dated Pleistocene terrace deposits and because the PBDB assigns fossil ages using North American Land Mammal Age rather than absolute dates (Peters and McClennen 2015). Additionally, we used paleoenvironmental raster data from the Last Glacial Maximum (LGM) because marine raster data were not available for other time periods and constructing them was outside the scope of this project. However, not all of our fossil occurrences have age ranges that include this time period. Despite these problems, we decided to include all of the available fossil occurrences for *O. rosmarus* for several reasons. First, we assume climatic conditions during the LGM are approximately equivalent to those of other glacial periods during the Pleistocene (Lisiecki and Raymo 2005, Zachos et al. 2008, Alonso-Garcia et al. 2011, Verbitsky et al. 2018, Batchelor et al. 2019). Second, although some number of these occurrences undoubtedly fall during warmer transitional or interglacial periods, considering them to all occur during the LGM allows for the most conservative temperature estimate of their fundamental ecological niche.

2.1.3 Environmental Predictors—To train our ENMs and quantify the realized ecological niche of walruses, we used three climatic variables: minimum annual sea surface temperature (SST_{min}), annual sea surface temperature range (SST_{rg}), and annual sea surface salinity range (SSS_{rg}). Although previous studies have found strong relationships between walrus presence and the distribution of sea ice (Beatty et al. 2016, Udevitz et al. 2017), layers directly quantifying the presence of sea ice are not available from paleo-MARSPEC and future predictions of such are considered overly uncertain for use in ENM construction (Bonan et al.

2021). Therefore we chose to use SST_{min}, SST_{rg}, and SSS_{rg} because together they mechanistically impact sea ice formation and distribution. When sea ice forms, the salinity of the remaining liquid water increases; when ice melts in the summer, seawater salinity decreases again. Additionally, the polynyas where walruses congregate in winter are associated with high winter salinity which prevents the water there from freezing (Winsor and Björk 2000). Because of these factors, areas with a larger relative SSS_{rg} likely correlate with the seasonal presence of sea ice. While the variance of sea surface salinity would be preferable to range, variance layers were not available for the LGM or for future projections and creating these layers is outside the scope of this project. Furthermore, Gebruk et al. (2021) demonstrated that walrus distribution also correlates with the location and biomass of bivalves, their main prey item, and both salinity and temperature influence the distribution and biomass of bivalves (Green 1973, Van Dolah et al. 1999, Feng and Papeş 2017, Pourmozaffar et al. 2020). Although previous studies have identified a correlation between walrus presence and water depth (Beatty et al. 2016), we did not include bathymetry as one of our predictor variables because our fossil dataset hails almost exclusively from the terrestrial environment, artificially biasing the fossil dataset towards shallow water. Instead, we incorporated bathymetry *post hoc* by cropping our final binary presence/absence projections to depths of 200 meters or less since walruses rarely forage in deeper waters (Born et al. 2005, Lowther et al. 2015, Garde et al. 2018) and because the wind-driven polynyas inhabited by walruses during the winter do not typically exceed 200 meters in depth (Winsor and Björk 2000). Finally, the calculated variable inflation factors (VIFs) for these three variables were less than 5, reducing the impact of multicollinearity on the models (Dormann et al. 2013). We calculated VIFs calculated using R package *usdm* (Naimi 2015).

We downloaded modern and future environmental raster data from bio-ORACLE 2.2 (Ocean Rasters for Analysis of CLimate and Environment; Tyberghein et al. 2012, Assis et al. 2018) and paleoclimatic data for the Last Glacial Maximum (LGM; 21 ka) from paleo-MARSPEC (MARine SPatial ECology; Sbrocco 2014) at a resolution of 5 arcmin using the R package *sdmpredictors* (Bosch et al. 2017). We chose predicted future raster layers for the years 2050 and 2100 based on Representative Concentration Pathway (RCP) 8.5 which represents a climate scenario for relatively high greenhouse gas emissions (Riahi et al. 2011, van Vuuren et al. 2011).

We took several steps to prepare the rasters for analysis. In the modern and future raster layers, SST_{min} did not extend lower than -1.94 °C, the approximate freezing temperature of water; however, SST_{min} for the LGM extended below -1.94 °C. To ensure comparability between the three climate scenarios, we changed all values for SST_{min} that were below -1.94 °C in the LGM raster to this value. We also recalculated SST_{rg} for the LGM by subtracting the new SST_{min} raster from an SST maximum layer so the SST_{rg} rasters would be comparable between the modern and LGM datasets. Raster manipulations were accomplished using the R package *raster* (Hijmans et al. 2015).

2.2 Analyses

All analyses were performed in R (R Core Team 2021) unless otherwise noted.

2.2.1 Comparing Niche Space— To compare the ecospace represented by the modern and fossil occurrence datasets for *O. rosmarus*, we first extracted the values of SST_{min}, SST_{rg}, and SSS_{rg} associated with each occurrence and calculated the mean and standard deviation for each of the sets of extracted environmental variables. Next, we visualized the variance between the environmental space occupied by each respective dataset using broken-stick principal

components analysis (PCA) (Legendre and Legendre, 1998). We then conducted a permutational multivariate analysis of variance (PERMANOVA; Anderson 2001) to quantitatively test the hypothesis that Pleistocene populations of *O. rosmarus* inhabited a significantly different niche space than modern populations. Because PERMANOVA assumes that the multivariate dispersion of the variables in question is roughly equal, we began by evaluating this assumption using the PERMDISP2 procedure of Anderson (2006) to assess for multivariate homogeneity of group dispersions using the "betadisper()" function in the R package *vegan* (Oksanen et al. 2018). This test demonstrated that the variance of the modern and fossil datasets was significantly different ($p = 0.001$). Although the results of PERMANOVA are robust to such heterogeneous group dispersions, this condition applies only when the compared groups are the same size (Anderson and Walsh 2013). To meet this criterion, we used a modified bootstrapping process to produce 1000 datasets of equal size to the fossil dataset by randomly sampling without replacement from the modern dataset. Next, we ran the PERMANOVA using *vegan* function "adonis()" with 9999 permutations using the Euclidean method for calculating pairwise distance between individuals on each of the 1000 modern sample datasets using a for-loop. We report the average p-value from this modified bootstrap as well as the effect size (R^2).

2.2.2 Ecological Niche Models—To estimate suitable habitat range for walruses, we implemented the maximum entropy (Maxent) algorithm using the R package *ENMeval* version 2.0 (Kass et al. 2021). Maxent uses a machine learning algorithm to identify the environmental variables that best discriminate between occurrence points and background points (Phillips et al. 2004, Elith et al. 2006). We chose to use Maxent for our ENMs because it performs well with small sample sizes (Hernandez et al. 2006, Pearson et al. 2007), requires relatively little computational power relative to other ENM methodologies (Kaky et al. 2020), outperforms

conventional methods when analyzing complex nonlinear relationships (Elith et al. 2006, Shoemaker et al. 2018), and balances overfitting and model complexity with overgeneralization when used in conjunction with species-specific model parameters (Radosavljevic and Anderson 2014).

Following the protocol of Simoes et al. (2020), we first built a buffer around the modern occurrence points using a radius of 3000 km based on the dispersal ability of walruses (Reeves et al. 1992). We then defined the calibration area by masking the modern environmental layers according to this buffer. Using the "randomPoints" function in R package *dismo* (Hijmans et al. 2017), we next generated 100,000 random background points. To calibrate the model, we tested four Maxent features classes (linear, linear quadratic, product, and linear quadratic product) and six regularization multipliers (0.1, 0.25, 0.5, 1, 2, and 4). Following Jarvie et al. (2021), we evaluated the appropriateness of the resulting models using the average area under the curve (AUC) and the omission rate of the minimum training presence value (OR_{MTP}). AUC measures predictive accuracy on a scale from 0 to 1 with a value of 0.5 equivalent to random predictive accuracy and a value of 1 denoting absolute accuracy. OR_{MTP} signifies goodness of fit on a scale of 0 to 1 with higher values indicating greater degrees of overfitting.

Out of the models generated under these parameters, we selected the model with the lowest Akaike Information Criterion corrected for small sample sizes (AICc) value, which optimizes model fit with model complexity (Warren and Seifert 2011, Muscarella et al. 2014). We chose this model selection criterion because previous studies have shown AICc provides the most conservative predictions and also outperforms other criteria in terms of selecting the true model as the best model in simulations (Katz and Zellmer 2018) and because AICc optimizes transferability across different time periods because of its penalization of model complexity

(Moreno-Amat et al. 2015). For the final model, we selected complementary log-log (cloglog) as the output format per the recommendation of Phillips et al. (2017) and evaluated the relative contribution of each of the three environmental variables using a jackknife approach. We then projected this final model to present environmental conditions and visually assessed how well it fit the current known distribution of walruses. Lastly, we projected this model to 2050 and 2100 for RCP 8.5 to evaluate how walrus distribution is predicted to shift according to walrus current ecological niche.

We then repeated this process for the fossil dataset. The optimal model generated from the fossil dataset was subsequently projected to modern conditions and visually compared to known walrus range and finally projected to future conditions for 2050 and 2100 under RCP 8.5.

2.2.3 Binary Maps and Centroid and Area Calculations—To assess the differences in the ranges predicted by the modern and fossil models, we calculated the area and centroid of the latitude of each of the projected ranges for current and future conditions from the two ENMs. To quantify these differences, projections were first restricted to the latitudes inhabited by walruses during historical times according to the range defined by Higdon and Stewart (2018) as we consider it unlikely walruses will establish new populations south of this range. We then restricted the projections to water depths of 200 meters or less as previously explained. We next converted these restricted ranges from continuous suitability indices ranging from 0 to 1 to binary predictions of presence or absence by rejecting cells with a suitability index less than 0.25. We then calculated the centroid latitude of the range and the area of the predicted range using R and QGIS (QGIS Development Team, 2022) respectively.

3 Results

3.1 Niche Space Comparisons

Extracting environmental variables revealed that modern occurrences were associated with an SST_{min} of -1.85 ± 0.55 °C, SST_{rg} of 10.84 ± 2.43 °C, and an SSS_{rg} range of 4.84 ± 1.88 PSS (Practical Salinity Scale) (mean ± standard deviation); fossil occurrences were associated with an SST_{min} of 0.57 ± 4.73 °C, SST_{rg} of 7.87 ± 5.00 °C, and an SSS_{rg} of 2.90 ± 2.92 PSS (mean ± standard deviation). Our broken-stick PCA identified principal components (PCs) 2 and 3 as significant, accounting for 32.02% and 22.09% of the variation, respectively (Fig. 3). Although PC1 accounted for 45.89% of the variation, it was nonsignificant according to this test

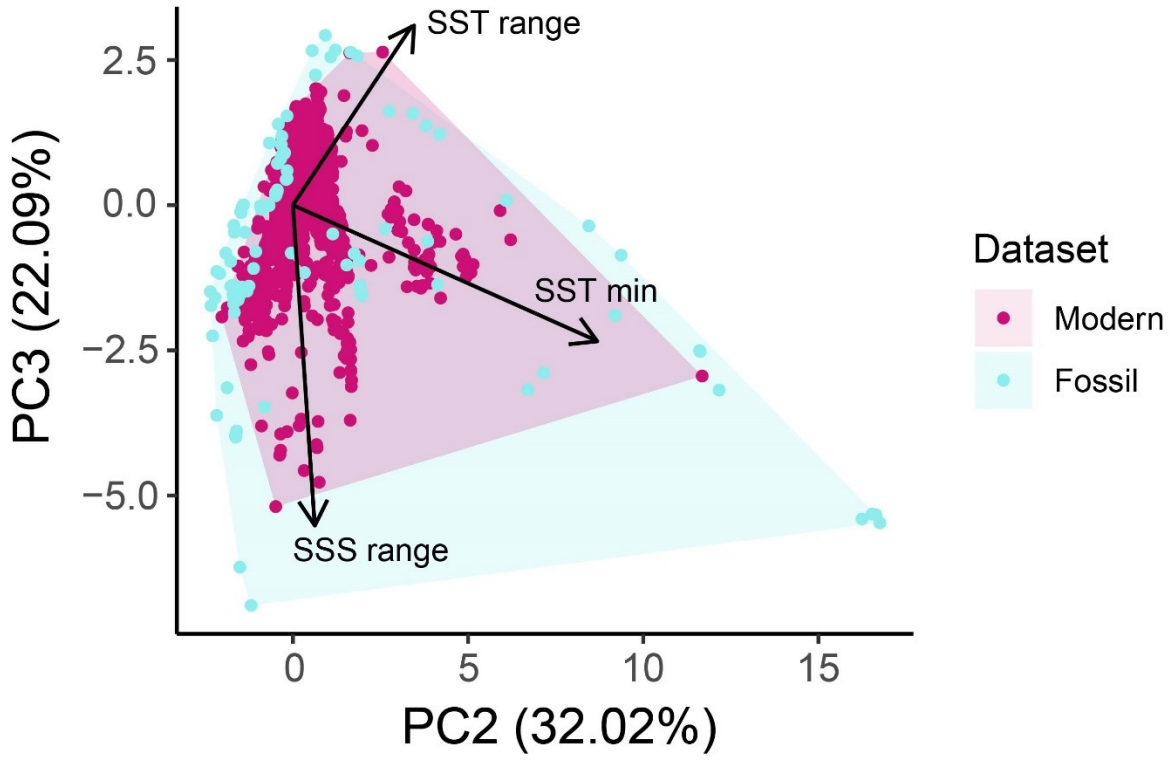

Figure 3. Projections of the ecospace for modern (maroon) and fossil (light blue) occurrences of *O. rosmarus* onto the significant axes of a broken stick principal component analysis (PCA). The arrows indicate how sea surface temperature minimum, sea surface temperature range, and sea surface salinity range are distributed along principal components 2 and 3. See Fig. S1 for plot of PC1 and PC2.

Table 1. Percent contribution of the environmental variables sea surface temperature minimum (SST_{min}), sea surface temperature range (SST_{rg}), and sea surface salinity range (SSS_{rg}) to each of the three principal components (PCs) from the broken-stick principal components analysis. The significant PCs are demarcated in grey.

Environmental variable	PC1	PC2	PC3
SST_{min}	23.85	60.27	18.80
SST_{rg}	35.67	35.45	37.27
SSS_{rg}	40.48	4.28	43.92

(Appendix D). The percent contribution of each environmental variable to the three PCs is summarized in Table 1. For the PERMANOVA comparing the fossil and modern ecospace, the average *p*-value for the 1000 bootstrapped sample runs was 0.0001 ± 0.0000 (mean ± standard deviation) with significance level $\alpha = 0.0005$. The average $R^2 = 0.125 \pm 0.010$ (mean ± standard deviation).

3.2 Ecological Niche Models

The predictive ability of both the modern and fossil models was excellent. The modern model produced an average AUC = 0.885 ± 0.011 (mean ± SE) and AUC range = 0.872–0.900, and the fossil model produced an average AUC = 0.849 ± 0.012 (mean ± SE) and AUC range = 0.829–0.865 (Appendix E). Neither model was overfit, with the modern model average OR_{MTP} = 0.010 ± 0.003 (mean ± SE) and range = 0.002–0.010 and the fossil model average OR_{MTP} = 0.017 ± 0.006 (mean ± SE) and range = 0.009–0.031 (Appendix E). In the modern ENM, the variable that contributed the most to the model was minimum SST followed by SST range and subsequently SSS range; for the fossil ENM, the minimum SST had the highest contribution followed by SSS range and finally SST range. For the modern model, the iteration with the lowest AICc (10343.94) used the linear quadratic function and 0.1 regularization multiplier; for

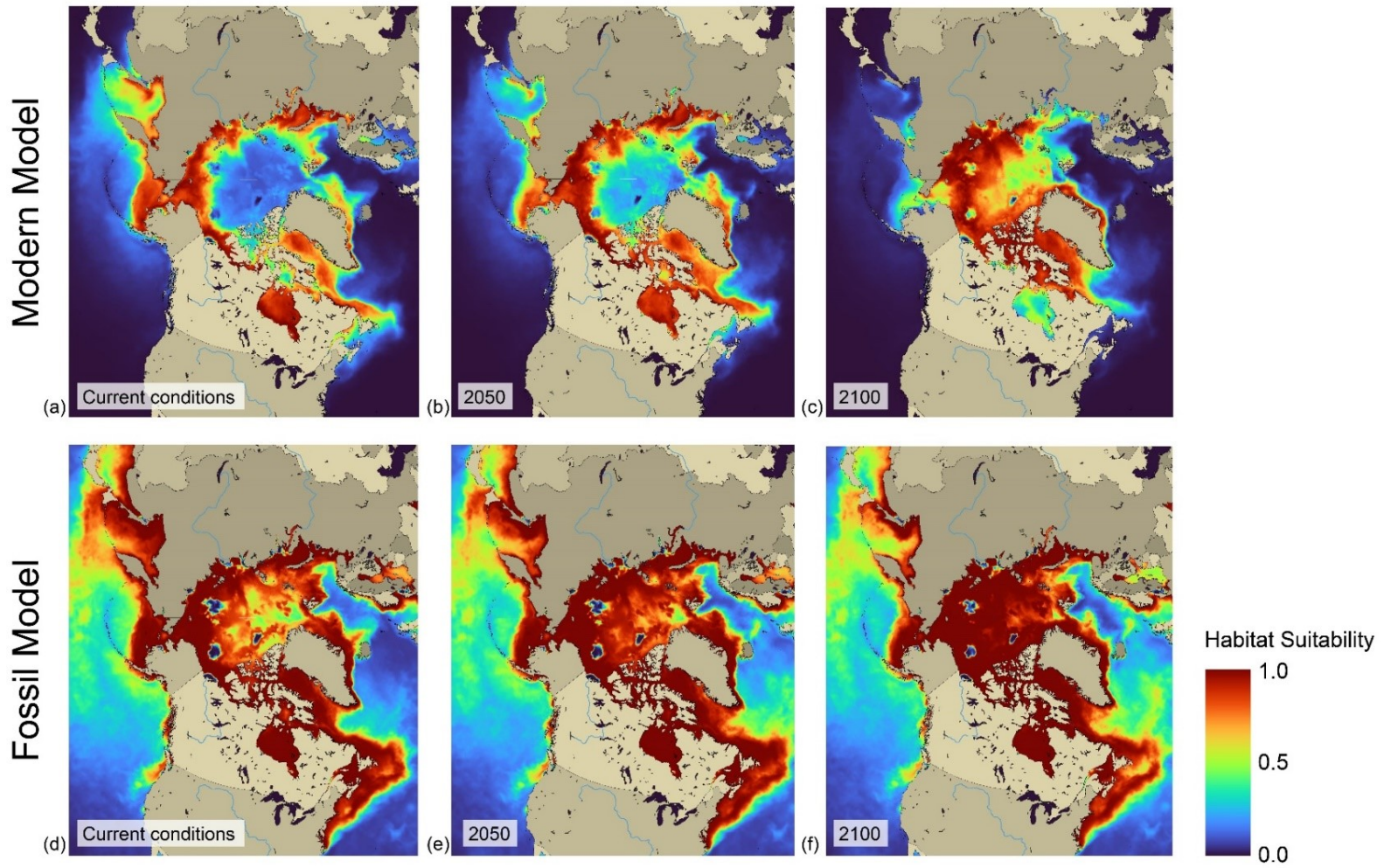

Figure 4. Maximum entropy (Maxent) models of environmental suitability derived from modern (a–c) and fossil (d–f) occurrences of *Odobenus rosmarus* as projected to current (a and d) and future (b, c, e, and f) climate scenarios. We constructed the fossil model using climate data from paleo-MARSPEC (Sbrocco 2014); for building the modern model and for the current and future projections of each model, we utilized climate data from Bio-ORACLE 2.0 (Assis et al. 2018). The future climate scenarios derive from Representative Concentration Pathway (RCP) 8.5. In general, the modern model predicts that suitable conditions for walruses will shift far northward by the end of the 21st century. In contrast, the fossil model predicts relatively little change in environmental suitability. Map scale and coordinate grid are the same as Figs. 1 and 2.

the fossil model, the lowest AICc (2770.164) was achieved with the same feature class and regularization multiplier as the modern model.

3.3 Projections to Current Conditions

When projected to current environmental conditions, the modern model explained the known range of walruses remarkably well overall, with some exceptions (Fig. 4a; for known range of walruses, see Born et al. 1995, Jay et al. 2011, Lydersen et al. 2012, Glazov et al. 2013, Higdon and Stewart 2018). This model did identify high suitability (> 0.8) in areas where walruses are not known currently or in recent historical times, such as the western East Siberian Sea, the Beaufort Sea, the western Canadian Arctic Archipelago, the eastern-central and southeastern coast of Kamchatka, and the Sea of Okhotsk. Interestingly, the waters around the Canadian Maritimes received a relatively low suitability index (< 0.25) except for the eastern extent of the Bay of Fundy (0.40–0.52). Additionally, while the majority of the area around Iceland displays a low suitability index (< 0.10 south of the island and < 0.20 north of the island), our model identified the ocean surrounding northwestern Iceland with medium suitability (< 0.5), the same area where Keighley et al. (2018) identified the highest density of the medieval Icelandic walrus population.

Conversely, when we projected the fossil model to current conditions, several discrepancies with the known range of walruses arise (Figure 4d). The fossil model predicts very high suitability (>0.90) in areas where walruses are not known to occur outside of individual vagrants, such as the western coast of Canada, the Sea of Japan, the Yellow Sea, the northeast coast of the United States, the southern coast of Norway, and the southern North Sea. However, the fossil model does predict extremely high suitability around the entirety of the Canadian Maritimes (<0.99) and also better predicts the distribution of walruses on the coast of Iceland as

mapped by Keighley et al. (2019) with a suitability index of up to 0.80 in the northwestern corner of the island, up to 0.73 in its northeastern extent, and up to 0.66 in the southwestern reaches.

3.4 Future Projections

According to the modern model, suitable conditions shift only slightly northwards by 2050 (Fig. 4b). The most noticeable change is the development of higher suitability around Svalbard, Franz Josef Land, and Severnaya Zemlya compared to modern conditions and decreased suitability off the eastern coast of Chukotka Province. However, by 2100, the suitability of much of the current range of walruses diminishes appreciably (Fig. 4c). The suitability of the Bering Sea drops precipitously, particularly along the eastern coast of Kamchatka and Chukotka in northeastern Russia. The southern Chukchi Sea, where female Pacific walruses and their calves migrate in the summer, becomes less suitable as well, albeit not as severely as the Bering Sea. Suitability also decreases sharply around Svalbard, Franz Josef Land, and in the Barents and Kara Seas, areas formerly characterized by high suitability. Hudson Bay suitability indices drop by more than 40% throughout most of its extent, especially in the southern reaches of the bay where only a small relict population of walruses remains today (Higdon and Stewart 2018). Notably, the Laptev Sea remains highly suitable by 2100. Conversely, the fossil model essentially indicates that the Arctic will, overall, become better suited for walruses over the next 80 years as the biome warms. No areas where walruses currently reside become less suitable from current conditions to 2050 or 2100 and in most cases these areas become more suitable (Fig. 4e, f).

3.5 Binary Maps and Area Calculations

Consistent with predictions of Arctic warming, our results predict decreasing ecological niche area and north-shifting latitudinal centroids for walruses by 2100 under both models (Table 2), although these trends are extremely small for the fossil model. For the modern model, the centroid of the current range has a latitude of 70.54 °N; by 2050, the centroid latitude is predicted to shift to 71.04 °N and by 2100 to 71.82 °N. The fossil model predicts little appreciable shift in the centroid latitude under the projected scenarios from 71.10 °N in current conditions to 71.17 °N by 2050 and 71.19 °N by 2100. The modern model predicts that current suitable habitat occupies approximately 6.77 x 10^6 km^2, and the fossil model predicts 7.10 x 10^6 km^2 of current suitable habitat (Fig. 5a, d). Under RCP 8.5, the modern model predicts that this range will grow by 1.26% by 2050 but shrink by 11.31% by 2100 (Fig. 5b, c). However, the fossil model predicts almost no change in suitable habitat, with an increase of 0.07% by 2050 and a decrease 0.001 % by 2100 (Fig. 5e, f).

4 Discussion

Our findings show that during the Pleistocene, *O. rosmarus* occupied a significantly wider ecospace than its current representatives inhabit, supporting our hypothesis that walrus fundamental niche does indeed include the relatively warm, seasonally ice-free conditions likely to characterize the Arctic in the near future. Below, we discuss how the outcomes of the PCA and PERMANOVA relate to our understanding of walrus fundamental niche. We then interpret the modern and future projections of both the modern and fossil ENMs regarding this understanding and predict how walrus populations will respond to climate change and the associated loss of sea ice. Finally, we recommend future research directions and consider the implications of our study for walrus conservation in the face of Arctic warming.

Table 2. Geographical changes in ecological niche space predicted by the modern ENM and fossil ENM.

Time Period	Centroid Latitude	Distance Shifted from Current Centroid Latitude	Binary Area	Percent Change from Projected Current Range
Modern model				
Current	70.54 °N	*n/a*	6.77 x 10^6 km^2	*n/a*
2050	71.04 °N	55.5 km north	6.85 x 10^6 km^2	1.26
2100	71.82 °N	142.08 km north	6.00 x 10^6 km^2	-11.31
Fossil model				
Current	71.18 °N	*n/a*	6.98 x 10^6 km^2	*n/a*
2050	71.17 °N	11.1 km south	6.95 x 10^6 km^2	-0.36
2100	71.19 °N	22.2 km north	6.95 x 10^6 km^2	-0.37

4.1 Niche Space Comparisons

Plotting our PCA shows that the ecospace inhabited by the fossil dataset is wider than that of the modern dataset with respect to both PC2 and PC3, the significant PCs according to the broken-stick criterion (Fig. 3). The results of our PERMANOVA, which support the hypothesis of a significantly different niche space between the two populations ($p = 0.0001$), demonstrate that the difference in ecospace shown in the PCA is statistically significant, if relatively small in terms of real-world impacts ($R^2 = 0.125$). Together, these analyses indicate that walrus fundamental niche is not fully realized by its current distribution and that this fundamental niche does in fact include seasonally ice-free condition.

Furthermore, our results probably still underestimate the true breadth of walrus fundamental niche because of biases within our analyses, particularly with regard towards warmer climates. Our fossil occurrence dataset is likely biased towards interglacial occurrences for a number of taphonomic reasons. Because sea level was often greater than 100 meters lower during glacial periods than it is today (Berends et al. 2021), many of the coastal facies likely to preserve walrus fossils from glacial periods are currently below sea level and thus largely

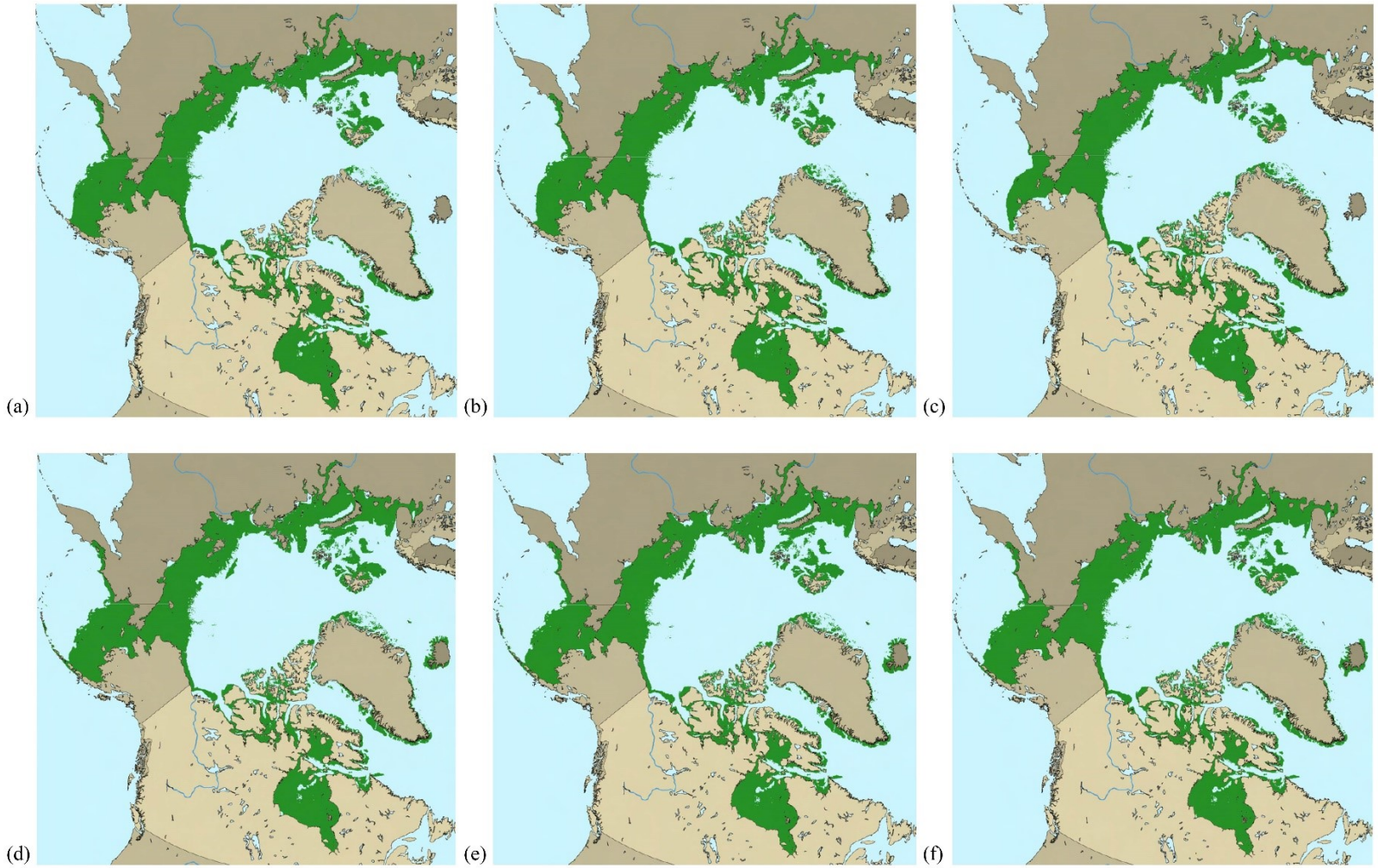

Figure 5. Binary maps showing optimal walrus habitat for current and future climate scenarios for the modern model (a–c) and fossil model (d–f). We generated these maps by constraining the optimal habitat to cells with a suitability index of 0.25 or greater and cropping the areas to water depths of 200 meters or less. Overall, neither model predicted a significant change in optimal habitat by 2050. In contrast, the predictions of the two models diverge substantially by 2100, with the modern model predicting a large northwards contraction of walrus range and the fossil model predicting little appreciable change. Map scale and coordinate grid are the same as Figs. 1 and 2.

inaccessible to fossil collectors. While some few specimens have been recovered through dredging (e.g., the San Francisco Bay specimens; Harington 2008), almost all of the *O. rosmarus* fossils included in our study have been recovered on land in areas that would have been coastal or underwater during past interglacial periods but far from the shore during glacial periods. For instance, the Edisto Island, South Carolina, specimen (Roth and Laerm 1980) was likely deposited during an interglacial period, as sea level would have been lower and the coastline nearly 100 miles further east during glacial periods (De Groeve et al. 2022). These taphonomic considerations strongly suggest that specimens from glacial periods are underrepresented while interglacial occurrence records are overrepresented in our fossil dataset. Additionally, we extracted environmental variables associated with fossil occurrence localities from rasters based on LGM climatic conditions both because interglacial raster data were not available and because we chose to take a conservative approach to our analyses. So even though the temperatures associated with the fossil dataset (average SST_{min} = 0.57 °C) are overall higher than those associated with the modern dataset (average SST_{min} = -1.85 °C), they are still likely cooler than the actual conditions in which many of these individuals lived. Improving age constraints for our fossil dataset and constructing raster layers for interglacial periods would offer clarity on these limitations.

4.2 Current Climate Projections

Current suitable habitat projected by the modern ENM and fossil ENM display several important differences. Overall, the geographical projection of the modern model covers a smaller, more northerly area than the much wider range projected by the fossil model. It also correlates more closely with the actual geographic range inhabited by modern walruses compared to the paleontological ENM, which predicts suitable habitat over a much wider area

than walruses actually occupy, congruent with the findings of our niche space comparisons. Notably, it also predicts moderately suitable habitat in areas where walruses do not currently reside but were historically present despite our decision not to include historical records in our modern dataset. It identified both northwestern Iceland and the Bay of Fundy as moderately suitable, both of which were home to walrus populations prior to extirpation 1,000 and 250 years ago, respectively (McLeod et al. 2014, Keighley et al. 2019).

However, several noteworthy inconsistencies exist between the modern ENM and actual current and historical walrus geographic range. Although the zooarchaeological record demonstrates that walruses were widely present throughout the Maritimes (McLeod et al. 2014), our model only identified the Bay of Fundy as moderately suitable. Similarly, although the greatest density of Icelandic walrus specimens identified by Keighley et al. (2019) fell in areas of moderate suitability according to the modern model, they also list specimens from areas our model identified as unsuitable. Notably, both the Icelandic and Maritimes walrus were genetically distinct from the modern Atlantic walrus (McLeod et al. 2014, Keighley et al. 2019) and the Maritimes walrus was morphologically distinct as well on the basis of their larger body size and more asymmetrical tusks. It is certainly possible that each of these populations were relicts of more warm-adapted Pleistocene walrus populations, as suggested by Boessenecker and Churchill (2021), and that these more heat-tolerant walruses did not survive the end-Pleistocene megafaunal extinction event, eliminating this variation from surviving populations. More precise dating of southerly fossil specimens could reveal the merit of this hypothesis. However, we consider it implausible that walruses have, on the whole, become more cold-adapted as average temperatures across their range have risen by 4–20 °C since the LGM (Osman et al. 2021). Instead, we find it more likely that other factors have constrained their range to its current

boundaries, where ice provides convenient haul-outs but is not a crucial element for their survival. Further investigation is needed to determine the identity and nature of these limiting factors.

An additional inconsistency between the modern model and documented walrus range is the identification by the modern ENM of the Sea of Okhotsk as highly suitable. Although paleontological and zooarchaeological evidence indicates that walruses were present in this region during the late Pleistocene and early Holocene (Borisiak 1930; Vasilevskii 1971), an exhaustive analysis of historical records and archeological material by Slobodin (2010) determined that walruses have been absent from the Sea of Okhotsk for at least the last 2,500 years. The fact that our modern model identifies this area as highly suitable for walruses raises the question of why they went extinct in this region. Investigating this quandary could lend further insight into the factors that determine walrus distribution.

Although on the whole, the southern extent of the fossil model projections reaches much further south than walruses usually range, summer and fall sightings of vagrant walruses around Britain, Ireland, and the northern coast of continental Europe appear to have been increasing according to numerous news articles reporting walrus sightings around Europe[1]. This pattern has not been thoroughly investigated, obfuscating the degree to which it is the result of true ecological change or simply alterations in reporting. However, while these nomads are far from self-sustaining populations, the relative health of these individuals, some of whom were observed for several months, does provide at least anecdotal evidence that walruses can survive in ice-free

[1] https://www.cornwalllive.com/news/cornwall-news/wally-walrus-could-latvia-year-7323451; https://www.politico.eu/article/wally-walrus-ireland-cork-coast/; https://www.bbc.com/news/uk-england-hampshire-63940472; https://www.nbcnews.com/news/world/freya-the-walrus-norway-sinking-boats-rcna40174; https://www.scotsman.com/arts-and-culture/arctic-walrus-rare-sighting-orkney-beach-328507; all accessed December 15, 2022; https://www.smithsonianmag.com/smart-news/the-unusual-european-journey-of-thor-the-walrus-180981734/; accessed April 18, 2023

and much warmer conditions than the majority currently do. So perhaps the predictions of suitable walrus habitat in the North Sea by the fossil model are less erroneous than they would appear on first inspection.

4.3 Future Climate Projections

The two sets of ENMs display considerably disparate outcomes for the walrus over the next seventy years. The modern model predicts a severe decrease in suitability by 2100 for several regions where walruses currently live, including the Bering Sea, Svalbard, the Laptev Sea, the southern Kara Sea, and the Barents Sea (Fig. 4c). Conversely, according to the fossil model projections, no areas currently inhabited by walruses display significant decreases in suitability and indeed many become even more suitable (Fig. 4f). Similarly, according to our binary maps, the modern ENM predicts that by 2100, suitable habitat for walruses will decrease by 18.47% and that the average latitude of suitable habitat will shift northwards by 1.09° or ~120 km (Table 2; Fig. 5c). However, the fossil model predicts no appreciable change either in the total area of suitable habitat or in the centroid latitude of suitable habitat before the end of the 21st century (Table 2; Fig. 5f).

Unfortunately, no species-wide demographic surveys of walruses have been undertaken in the last several decades, limiting our ability to assess which of these scenarios most closely aligns with current trends. Studies of individual walrus populations present a relatively equivocal picture of the current status of *O. rosmarus* and its response to ongoing Arctic warming (Fischbach et al. 2009, Jay and Fischbach 2010, Garlich-Miller et al. 2011, Jay et al. 2012, MacCracken 2012). Across the Arctic, female walruses and their calves have been increasingly utilizing terrestrial haul-outs in late summer and fall as sea ice becomes unavailable, demonstrating adaptive behavioral plasticity (Jay et al. 2012, Lydersen et al. 2012, Udevitz et al.

2017, Higdon and Stewart 2018). A study of changes in Kara Sea marine mammal distribution and density between 1996 and 2013 found little to no change in Atlantic walrus occurrences (Mäkinen and Vanhatalo 2018). Similarly, a study examining the energetic impacts of increasing distance between feeding grounds and haul-outs in the Chukchi Sea found that as long as walruses were able to rebuild their endogenous fat reserves while overwintering in the Bering Sea, the increased energetic costs of longer foraging trips would not likely alter walrus population dynamics (Jay et al. 2017). Less encouragingly, Zagrebelny and Kochnev (2017) reported that numerous historical terrestrial haul-outs in eastern Chukotka and Kamchatka have disappeared with their previous inhabitants apparently shifting to a smaller number of much larger haul-outs, increasing the risk of depleting benthic foraging grounds that are also being altered by climate change. Several mass-mortality events for walruses, particularly calves and juveniles, have also been reported in the last few decades with causes ranging from trampling to prolonged exposure to turbulent seas (Ovsyanikov et al. 2008; Fischbach et al. 2009, Goertz et al. 2017). Thus we consider a future intermediate to the highly optimistic fossil model and the direr situation presented by the modern model to be more likely than either endmember.

Although the retreat of sea ice is generally predicted to have a negative consequence on walrus populations, its seasonal disappearance from the high Arctic may open up new refugia for the species. For instance, both the modern and fossil ENMs predict that the northern reaches of Greenland and the Arctic Archipelago will be highly suitable for walruses by 2100 (Fig. 4c, f). These areas are not currently accessible to walruses as they are ice-locked year-round. However, with the northward retreat and eventual loss of the Arctic ice cap, these coastlines will open up as potential terrestrial haul-outs. The species has already demonstrated the ability to establish rookeries in novel locations within both the Atlantic and Pacific subpopulations (Kovacs et al.

2014; Zagrebelny and Kochnev 2017). Investigating how and why walruses establish new terrestrial haul-outs could reveal the likelihood of walrus dispersal to such previously inaccessible localities.

4.4 Future Research Directions and Walrus Conservation

Our study primarily tests the hypothesis that walruses can survive without the availability of year-round sea ice. While our results offer hope for the survival of walruses in the face of decreasing sea ice, multiple other environmental biotic and abiotic factors influence walrus distribution and health, including proximity to and condition of feeding grounds (Beatty et al. 2016), the presence and density of predators such as orcas and polar bears (Kryukova et al. 2012, Øren et al. 2018), frequency and intensity of storm events (Campagna et al. 2021), and increasing toxin exposure from harmful algae blooms (Lefebvre et al. 2022). As climate change will impact all of these variables, we recommend incorporating dynamic quantifications of these elements into future models. Furthermore, constructing ENMs from mechanistic rather than correlative patterns can improve their applicability by using knowledge of the critical maximum and minimum tolerable values for salient environmental variables (Shin et al. 2021). Research into the range of seawater temperatures, ambient air temperatures, and seawater salinity that walruses are physiologically capable of tolerating would allow for the construction of such mechanistic ENMs.

We also note that our models do not incorporate directly anthropogenic elements that are likely to impact walrus demographics. As sea ice melts, human activity in this region will also change and without concerted international conservation efforts, these changes will likely have negative consequences on the long term likelihood of walrus survival. Nation states are already vying for the rights to increasingly accessible Arctic shipping lanes that pass through critical

walrus habitat (Theocharis et al. 2018), increasing risk of collision-related mortality and contamination from fuel spillage as well as damage from ice-breaking ships to pupping platforms (Gross 2018, Wilson et al. 2020). Additionally, vast fossil fuel reserves have been identified in such crucial walrus and walrus prey habitats as the Kara, Pechora, Beaufort, and Barents Seas (Spencer et al. 2011). The overlap in undeveloped fossil fuel reserves and walrus range highlights the need to transition to a cleaner energy future not only to reduce carbon emissions but also to preserve the ecosystems where these resources are located. Given the status of *O. rosmarus* as an Arctic keystone species and ecosystem engineer (Ray et al. 2006, Hocking et al. 2021), policies guiding Arctic resource development should include robust plans for protecting walrus haul-outs, migration corridors, and feeding grounds in order to maintain overall ecosystem health.

5 Conclusion

In essence, our models support the hypothesis that walrus fundamental niche encompasses the seasonally ice-free conditions that will characterize the Arctic in the coming decades. While the acceleration of polar warming and sea ice loss will continue to alter Arctic ecosystems, the results presented here demonstrate that if humans protect walruses from other sources of anthropogenic environmental degradation, they are likely to adapt to the next century of climate change.

CHAPTER V

DISSERTATION SUMMARY

The goals of this dissertation were to a) expand our knowledge of the early evolution of the extinct pinniped family Desmatophocidae through the description of new basal species *Eodesmus condoni*, b) investigate the locomotor evolution of otarioid pinnipeds by exploring the utility of humerus morphology for diagnosing swimming mode in modern and fossil taxa, and c) quantify and compare the modern and paleoecological niches of the walrus *Odobenus rosmarus* in order to model its response to the next 70 years of climate change. First, I described new fossil cranium UOMNCH F-68583 from the Iron Mountain Bed of the Astoria Formation where it outcrops at Moolack Beach on the Oregon coast. After determining that the specimen represented a desmatophocid pinniped based on the morphology of its mortised jugal-squamosal suture, I identified it as a new species after comparing it to other known species of desmatophocid and performing a phylogenetic analysis to resolve its placement within the Desmatophocidae. New species *Eodesmus condoni* nests at the base of the desmatophocid phylogeny and is the earliest diverging desmatophocid yet identified. The identification of another desmatophocid species at the already pinniped-rich Iron Mountain Bed suggests that the approximately synchronous mid-Miocene Climatic Optimum played a role in this increase in pinnipedimorph species diversity.

Next, I found that humeral morphology is discriminatory for aquatic locomotor mode and recovered a hindlimb-propelled as the ancestral condition for Pinnipedia as a whole as well as subclade Otarioidea (eared seals, walruses, and desmatophocid seals). Using three-dimensional geometric morphometrics, I landmarked the humeri of modern phocids, otariids, and O. rosmarus

as well as fossil stem pinnipeds and otarioids. Following data collection, I performed a Procrustes superimposition and principal components analysis (PCA) to explore the between-group variation; I then used the principal components to construct two flexible discriminant analyses (FDAs), one with phylogenetic correction and one without, to classify the fossil taxa according to their predicted aquatic locomotor mode. As the literature suggested, the humeral structures that most distinguished between the hindlimb- and forelimb-propelled swimming were the deltoid crest, greater tubercle, lesser tubercle, and lateral and medial epicondyles, as identified by the PCA. The FDAs classified all the fossil pinnipeds as hindlimb-propelled with the exception of desmatophocid *Allodesmus kernensis* and odobenid *Pontolis barroni*, and otariid *Thalassoleon* mexicanus in the nonphylogenetic FDA, strongly suggesting that the otarioid ancestor was hindlimb-propelled like the stem pinnipeds. The presence of a proximodistally elongated deltoid crest in hindlimb-propelled species like *O. rosmarus* as well other earlier otarioids raises the possibility that this trait first arose as an adaptation for the peculiar lunging gait modern otariids and odobenids use on land before its exaptation for forelimb-propelled swimming in these three lineages, implying that terrestrial and aquatic locomotor modes are evolutionarily coupled in otarioids.

Finally, I found that modern walrus populations indeed inhabit only a portion of their past ecospace, including the ice-free conditions likely to characterize the Arctic in the upcoming decades. The permutational multivariate analysis of variance (PERMANOVA) supported a significant difference between the ecospace inhabited by modern and fossil walrus populations and the PCA showed that during the Pleistocene, walruses inhabited a wider range of environmental conditions with a higher temperature maximum than they do today. Furthermore, while the future projections derived from the modern ecological niche model predict an 18%

decrease in suitable walrus habitat by 2100, the fossil model projections predict no appreciable change in range over the next century. Although we consider an intermediate scenario more realistic than either endmember, our results nonetheless present encouraging evidence that with the enactment of conservation policies addressing other sources of anthropogenic environmental degradation, walruses may survive and adapt to a seasonally ice-free Arctic climate. These findings contrast the widespread narrative of probable walrus population collapse with the loss of summer sea ice, inviting further investigation into how conservation strategies can enhance *O. rosmarus* survivorship in an increasingly ice-free Arctic Ocean.

In conclusion, this dissertation advances our knowledge of early desmatophocid diversification, the locomotor evolution of otarioid pinnipeds, and the fundamental ecological niche of *O. rosmarus* with respect to predicting their response to climate change in the Arctic. This provides a framework for further exploration of how pinniped fauna have evolved with respect to taxonomic and locomotor ecology as well as the range of environmental parameters within which pinnipeds can survive. As human exploitation continues to deteriorate global and marine and coastal ecosystems, understanding the paleoecology of disproportionately threatened tertiary consumers like pinnipeds will provide a critical baseline for the establishment of evidence-based conservation policies.

APPENDIX A

DESCRIPTION OF CHARACTERS USED IN THE PHYLOGENETIC ANALYSIS OF CHAPTER II

1. Rostrum, premaxilla-nasal contact. Boessenecker and Churchill (2018: character 1) Deméré and Berta (2002: character 1), Kohno (1996: character 2).
0 = extensive along lateral border of nasal; ~50% or greater of total nasal length.
1 = reduced along lateral border of nasal; ~25%-50% of total nasal length
2 = reduced; does not contact lateral border of nasal and only contacts anterior margin

2. Rostrum, nasal-frontal suture. Boessenecker and Churchill (2018: character 2), Deméré and Berta (2002: character 2), Kohno (1996: character 3, 6).
0 = transverse
1 = v-shaped
2 = w-shaped

3. Rostrum, prenarial shelf. Boessenecker and Churchill (2018: character 3), Kohno (1996: character 1).
0 = absent
1 = present
2 = present and transversely expanded anteriorly

4. Rostrum, alveolar margin of maxilla in lateral view. Boessenecker and Churchill (2018: character 4).
0 = straight or slightly concave
1 = distinctly concave leading to posteroventrally inclined maxillary root of zygomatic arch
2 = strongly concave, but leading to no change in the orientation of the maxillary root of the zygomatic arch

5. Nasals, anterior margin. Boessenecker and Churchill (2018: character 5).
0 = at level of canine or P
1 = well posterior

6. Premaxilla, prenarial process. Boessenecker and Churchill (2018: character 6), Berta and Wyss (1994: character 3), Kohno et al. (2007: character 1), Boessenecker and Churchill (2013: character 1).
0 = absent or indistinct
1 = present

7. Premaxilla, posterior termination. Boessenecker and Churchill (2018: character 7).
0 = well anterior to level of infraorbital foramen
1 = extends posteriorly to level of infraorbital foramen

8. Pterygoid process of the maxilla. Boessenecker and Churchill (2018: character 8), Berta and Wyss (1994: character 6), Deméré and Berta (2002: character 3), Kohno (1996: character 16).
0 = does not form anteromedial floor to orbit
1 = posterolaterally expanded as corner-like shelf below orbit

9. Infraorbital foramen. Boessenecker and Churchill (2018: character 9), Berta and Wyss (1994: character 11), Deméré and Berta (2002: character 17).
0 = large and broad, visible in anterior view
1 = narrow, not visible in anterior view

10. Antorbital process. Boessenecker and Churchill (2018: character 10), Deméré (1994: character 6), Kohno (1996: character 7).
0 = present
1 = absent
2 = prominent

11. Maxilla, nasolabialis fossa. Boessenecker and Churchill (2018: character 11), Berta and Wyss (1994: character 7), Boessenecker and Churchill (2015: 12).
0 = present
1 = absent

12. Palate arching. Boessenecker and Churchill (2018: character 12), Deméré and Berta (2002: character 4), Kohno (1996: character 9).
0 = relatively flat (palatal arch approximately 0.18-0.19)
1 = transversely arched (palatal arch greater than 0.25)

13. Palate: Incisive foramina. Boessenecker and Churchill (2018: character 13), Deméré and Berta (2002: character 7), Kohno (1996: character 4).
0 = divided by medial septum
1 = medial septum absent
2 = foramina reduced

14. Palate, toothrows. Boessenecker and Churchill (2018: character 14), Berta and Wyss (1994: character 13), Kohno (1996: character 8).
0 = slightly divergent
1 = strongly divergent
2 = parallel

15. Supraorbital process of frontals. Boessenecker and Churchill (2018: character 15), Berta and Wyss (1994: character 17), Deméré and Berta (2002: character 8), Kohno (1996: characters 11, 12).
0 = low but distinct ridge
1 = polymorphic for states 0 and 2
2 = absent or indistinct
3 = small and posteriorly positioned along intertemporal bar
4 = strongly developed rectangular or triangular supraorbital shelf

16. Orbit size. Boessenecker and Churchill (2018: character 16).
0 = Large (18-21% BL)
1 = Very Large (+21% BL)
2 = Small (< 18%)

17. Orbit, orbital vacuity. Boessenecker and Churchill (2018: character 17), Berta and Wyss (1994: character 12), Kohno (1996, character 13).
0 = absent
1 = present

18. Orbit, optic foramen. Boessenecker and Churchill (2018: character 18), Kohno (1996: character 17).
0 = located anterodorsally
1 = positioned posteroventrally anterior to braincase

19. Orbit, optic foramina. Boessenecker and Churchill (2018: character 19), Kohno (1996: character 19).
0 = bilateral and separated
1 = merged at sagittal plane

20. Lateral wall of alisphenoid canal. Boessenecker and Churchill (2018: character 20), Berta and Wyss (1994: character 20); Furbish (2015: character 22).
0 = thick and well-developed
1 = thin
2 = absent

21. Zygomatic arch: dorsal margin of maxillary root. Boessenecker and Churchill (2018: character 21), Deméré and Berta (2002: character 6), Kohno (1996: character 10).
0 = not retracted dorsal to infraorbital foramen
1 = retracted dorsal to infraorbital foramen

22. Zygomatic arch: squamosal-jugal articulation. Boessenecker and Churchill (2018: character 22), Berta and Wyss (1994: character 39), Deméré and Berta (2002: character 11), Kohno (1996: character 15).
0 = splint like

1 = mortised, zygomatic process of squamosal exhibits minimal dorsoventral expansion
2 = mortised, zygomatic process of squamosal greatly expanded dorsoventrally

23. Zygomatic arch: jugal-maxillary suture. Boessenecker and Churchill (2018: character 23), Deméré and Berta (2002: character 12), Kohno (1996: character 14).
0 = jugal with anterodorsal and anteroventral splints
1 = polymorphic for states 0 and 2
2 = jugal with anterodorsal splint only
3 = elongate anteroventral splint extends anteriorly to level of M1

24. Zygomatic arch, ventral tuberosity of anterior zygomatic root. Boessenecker and Churchill (2018: character 24), Kohno et al. (2007: character 7).
0 = absent
1 = present

25. Zygomatic arch, postorbital process. Boessenecker and Churchill (2018: character 25).
0 = well developed and triangular
1 = indistinct, dorsal surface smooth and flush with zygomatic process

26. Zygomatic arch, transverse width. Boessenecker and Churchill (2018: character 26).
0 = widest point at approximate level of anterior border of the glenoid fossa
1 = anterior to glenoid fossa

27. Braincase, pseudosylvian sulcus. Boessenecker and Churchill (2018: character 27), Kohno (1996, character 25).
0 = visible externally on braincase
1 = absent, lateral wall of braincase smoothly convex

28. Braincase, anterolateral margin in dorsal view. Boessenecker and Churchill (2018: character 28), Boessenecker and Churchill (2015: character 58).
0 = forms a corner
1 = smoothly convex

29. Braincase, squamosal fossa. Boessenecker and Churchill (2018: character 29), Deméré and Berta (2002: character 18).
0 = undivided
1 = divided, posterior and anterior portions of approximately equal in size
2 = divided, posterior portion smaller than anterior

30. Basicranium, paroccipital process. Boessenecker and Churchill (2018: character 30), Berta and Wyss (1994: character 45). Deméré and Berta (2002: character 9), Kohno (1996: character 29).

0 = small and blunt
1 = large and excavated
2 = large and not excavated
3 = small and crest-like

31. Basicranium, tympanic bulla. Boessenecker and Churchill (2018: character 31), Deméré and Berta (2002: character 10).
0 = only ectotympanic inflated
1 = ectotympanic flat with minimal inflation
2 = entotympanic and ectotympanic greatly inflated and bulbous

32. Styloid process of tympanic bulla. Boessenecker and Churchill (2018: character 32), Berta and Wyss (1994: character 41), Deméré and Berta (2002: character 13).
0 = present
1 = absent, anterior corner of entotympanic retracted posteriorly
2 =absent, ectotympanic reduced

33. Stylomastoid foramen. Boessenecker and Churchill (2018: character 33), Deméré and Berta (2002: character 14).
0 = in common fossa with tympanohyal pit
1 = separated from tympanohyal by a raised strut or ridge

34. Basicranium, pterygoid strut. Boessenecker and Churchill (2018: character 34), Deméré (1994: character 13), Kohno (1996: character 18).
0= slender
1= dorsoventrally and laterally projected
2= dorsoventrally thick and transversely broad
3= transversely thin and "rolled"

35. Basicranium, shape of basioccipital. Boessenecker and Churchill (2018: character 35), Berta and Wyss (1994: character 42), Kohno (1996, character 26).
0 = parallel sided
1 = pentagonal in shape, gradually but noticeably narrows anteriorly

36. Basicranium, posterior lacerate foramen. Boessenecker and Churchill (2018: character 36), Berta and Wyss (1994: character 43), Kohno (1996, character 28).
0 = anteroposteriorly expanded
1 = transversely expanded
2 = fissure

37. Mandible, angular process. Boessenecker and Churchill (2018: character 37), Berta and Wyss (1994: character 21).
0 = well developed
1 = polymorphic for states 0 and 2
2 = reduced or absent

38. Mandible, digastric insertion. Boessenecker and Churchill (2018: character 38), Berta and Wyss (1994: character 52), Deméré (1994: character 44), Deméré and Berta (2002: character 22), Kohno (1996: character 30).
0 = small and indistinct
1 = well developed

39. Mandible: depth of horizontal ramus. Boessenecker and Churchill (2018: character 39), Boessenecker and Churchill (2013: 43).
0 = deepest part of horizontal ramus posterior to mandibular symphysis
1 = deepest part of horizontal ramus at posteroventral terminus of symphysis

40. Mandible: mandibular condyle. Boessenecker and Churchill (2018: character 40), Berta and Wyss (1994: character 53).
0 = at or slightly above level of tooth row
1 = elevated above tooth row

41. Mandible, genial tuberosity. Boessenecker and Churchill (2018: character 41), Boessenecker and Churchill (2013: character 37).
0 = absent or indistinct
1 = present; developed as small tubercle or process on anterior portion of ramus
2 = present and well developed; extends well below ventral margin of ramus

42. Symphyseal angle of mandible (angle between longest axis of symphysis and alveolar margin of mandible in medial view). Boessenecker and Churchill (2018: character 43).
0 = >50°
1 = 40-50°
2 = <40°

43. Mandible: length of lower postcanine tooth row length. Boessenecker and Churchill (2018: character 43), Berta and Wyss (1994: character 69), Boessenecker and Churchill (2013: character 65).
0 = long (length of tooth row greater than 40% of the mandible length).
1 = short (length of tooth row less than or equal to 40% of the mandible length).

44. Dentition, I3 orientation. Boessenecker and Churchill (2018: character 44), Deméré and Berta (2002: character 23), Kohno (1996: character 31).
0 = vertical or subvertical
1 = procumbent and laterally directed

45. I3 size and shape. Boessenecker and Churchill (2018: character 45).
0 = same size or only slightly larger than I1-2
1 = greatly larger than I1-2 and canine-like
2 = similar in morphology to premolars

46. C1, carinae. Boessenecker and Churchill (2018: character 46), Deméré and Berta (2002: character 24), Kohno (1996: character 32).
0 = posterior and medial carinae present
1 = posterior and medial carinae absent

47. Upper postcanine tooth roots orientation. Boessenecker and Churchill (2018: character 47), Deméré and Berta (2002: character 28)
0 = vertical
1 = anteriorly inclined

48. P1-3 crowns, cingulum. Boessenecker and Churchill (2018: character 48), Berta and Wyss (1994: character 67), Boessenecker and Churchill (2013: character 71; 2015: character 82).
0 = narrow, smooth lingual cingulum
1 = well-developed cuspate cingulum
2 = no cingulum

49. P2-P3 rooting. Boessenecker and Churchill (2018: character 49), Berta and Wyss (1994: character 62), Boessenecker and Churchill (2013: character 74; 2015: character 82)
0 = double
1 = polymorphic for states 0 and 2
2 = single

50. P4 rooting. Boessenecker and Churchill (2018: character 50), Berta and Wyss (1994: character 64), Boessenecker and Churchill (2013: character 76; 2015: character 82)
0 = Triple
1 = polymorphic for states 0 and 2
2 = Double
3 = Single

51. P4, metacone. Boessenecker and Churchill (2018: character 51), Deméré and Berta (2001: character 16).
0 = distinct
1 = reduced or absent

52. P4, protocone shelf. Boessenecker and Churchill (2018: character 52), Berta and Wyss (1994: character 63), Boessenecker and Churchill (2013: character 75), Deméré (1994: character 36), Kohno et al. (2007: character 47).
0 = anteromedially placed
1 = posteromedially placed with small cuspules
2 = reduced or absent

53. Dentition, size of M1 relative to premolars. Boessenecker and Churchill (2018: character 53), Berta and Wyss (1994: character 66), Kohno (1996: character 40).

0 = equal in size
1 = reduced in size

54. M1 rooting. Boessenecker and Churchill (2018: character 54), Berta and Wyss (1994: character 65), Boessenecker and Churchill (2013: character 77; 2015: character 82).
0 = Triple
1 = polymorphic for state 0 and 2
2 = Double
3 = polymorphic for state 2 and 4
4 = Single

55. M2. Boessenecker and Churchill (2018: character 55), Berta and Wyss (1994: character 68), Kohno (1996: character 39).
0 = present
1 = polymorphic for states 0 and 2
2 = absent

56. M1, metacone. Boessenecker and Churchill (2018: character 56).
0 = distinct, prominent cusp
1 = absent or indistinct

57. M1, protocone. Boessenecker and Churchill (2018: character 57).
0 = distinct, prominent and posteromedially positioned, resulting in a triangular-shaped M1
1 = indistinct or absent, resulting in a largely round or square M1

58. Dentition, lower cheek teeth, size. Boessenecker and Churchill (2018: character 58), Berta and Wyss (1994: character 66), Kohno (1996: character 40).
0 = p4-m1 larger than p2-3
1 = p2-m1 all approximately equal size
2 = m1 distinctly smaller than p2-4

59. Dentition, orientation of lower cheek teeth. Boessenecker and Churchill (2018: character 59).
0 = teeth parallel to adjacent cheek teeth, oriented dorsoventrally
1 = cheektooth orientation is divergent, with p1 directed anterodorsally and posterior teeth posterodorsally

60. Lower postcanines, crowns. Boessenecker and Churchill (2018: character 60), Berta and Wyss (1994: character 75), Boessenecker and Churchill (2013, character 63; 2015: character 74).
0 = transversely narrow
1 = round and bulbous

61. Lower postcanines, cingulum. Boessenecker and Churchill (2018: character 61), Boessenecker and Churchill (2013: character 67).
0 = present lingually and labially
1 = present lingually only
2 = absent

62. p2-4 rooting. Boessenecker and Churchill (2018: character 62), Boessenecker and Churchill (2013: 72, 73; 2015: character 92).
0 = double rooted
1 = polymorphic for states 0 and 2
2 = single rooted

63. p2-4 crowns, paraconid and hypoconid cusps. Boessenecker and Churchill (2018: character 63), Berta and Wyss (1994: character 70); Boessenecker and Churchill (2013: character 66, 68; 2015: 93).
0 = trenchant
1 = conical
2 = absent or reduced

64. m1 rooting. Boessenecker and Churchill (2018: character 64), Boessenecker and Churchill (2013: 79; 2015: 92).
0 = double
1 = polymorphic for states 0 and 2
2 = single

65. m1, talonid basin. Boessenecker and Churchill (2018: character 65), Berta and Wyss (1994: character 71), Boessenecker and Churchill (2013: 69).
0 = present as slight concavity or small shelf
1 = absent

66. m1, metaconid. Boessenecker and Churchill (2018: character 66), Berta and Wyss (1994: character 72), Boessenecker and Churchill (2013: 70).
0 = present
1 = reduced
2 = absent

67. m2. Boessenecker and Churchill (2018: character 67), Berta (1995: character 31), Berta (1994: character 19), Berta and Wyss (1994: character 85), Churchill et al. (2014: character 83), Boessenecker and Churchill (2015: character 98)
0 = present
1 = polymorphic for states 0 and 2
2 = absent

68. Manubrium, proportions. Boessenecker and Churchill (2018: character 68).
0 = anterior and posterior halves similar in transverse diameter
1 = anterior portion transversely wider

69. Scapula, supraspinous fossa. Boessenecker and Churchill (2018: character 69), Berta and Wyss (1994: character 85).
0 = slightly larger than infraspinous fossa.
1 = much larger than infraspinous fossa.

70. Scapula, acromion process. Boessenecker and Churchill (2018: character 70), Berta and Wyss (1994: character 83).
0 = knoblike
1 = reduced

71. Scapula, hook-like process for teres major. Boessenecker and Churchill (2018: character 71), Berta and Wyss (1994: character 82).
0 = present
1 = absent

72. Scapula, secondary spine. Boessenecker and Churchill (2018: character 72), Berta and Wyss (1994: character 86), Boessenecker and Churchill 2015: character 103).
0 = absent
1 = absent, but a scapular undulation is present
2 = present

73. Humerus, greater tuberosity. Boessenecker and Churchill (2018: character 73).
0 = at level of humeral head
1 = extends far proximal to humeral head and lesser tuberosity

74. Humerus, length of deltopectoral crest. Boessenecker and Churchill (2018: character 74), Berta and Wyss (1994: character 88).
0 = less than or equal to 1/2 humerus length
1 = 1/2 to 3/4 humerus length

75. Humerus, distal termination of deltopectoral crest. Boessenecker and Churchill (2018: character 75), Berta and Wyss (1994: character 88).
0 = gradual
1 = abrupt

76. Humerus, supinator ridge. Boessenecker and Churchill (2018: character 76), Berta and Wyss (1994: character 89).
0 = well developed
1 = absent or reduced

77. Humerus, diameter of humeral trochlea. Boessenecker and Churchill (2018: character 77), Berta and Wyss (1994: character 93), Deméré (1994: character 47).
0 = medial and lateral edges equal
1 = medial edge much larger

78. Humerus, deltoid tubercle. Boessenecker and Churchill (2018: character 78), Deméré (1994: character 45).
0 = on deltopectoral crest
1 = separated from deltopectoral crest

79. Humerus, posterior margin in lateral view. Boessenecker and Churchill (2018: character 79).
0 = straight to concave
1 = strongly sinuous owing to anteriorly prominent supinator ridge

80. Ulna, olecranon process. Boessenecker and Churchill (2018: character 80), Berta and Wyss (1994: character 94).
0 = knoblike and unexpanded
1 = transversely flattened and posteriorly expanded

81. Radius, shape in lateral view. Boessenecker and Churchill (2018: character 81), Berta and Wyss (1994: character 95).
0 = convexly arched and distal end similar in anteroposterior width to proximal end
1 = distal end expanded and approximately twice as wide as proximal end

82. Radius, distal end. Boessenecker and Churchill (2018: character 82), Deméré (1994: character 48).
0 = unexpanded
1 = expanded, with small radial process
2 = expanded, with large radial process

83. Radius, pronator teres process. Boessenecker and Churchill (2018: character 83), Berta and Wyss (1994: character 96).
0 = positioned at midpoint or on distal 1/2 of shaft
1 = positioned on proximal 1/2 of shaft

84. Scapholunar, pit for magnum. Boessenecker and Churchill (2018: character 84), Deméré (1994: character, 50).
0 = absent
1 = present

85. Metacarpal 1, pit or rugosity. Boessenecker and Churchill (2018: character 85), Berta and Wyss (1994: character 99).
0 = absent
1 = present

86. Ungual phalanges. Boessenecker and Churchill (2018: character 86), Berta and Wyss (1994: character 102).
0=small claw core present
1=distal end blocky and rugose for cartilaginous extension of digit

87. Innominate, foramen for obturator nerve. Boessenecker and Churchill (2018: character 87), Berta and Wyss (1994: character 113).
0 = obturator foramen absent
1 = obturator foramen present

88. Innominate, ischial spine. Boessenecker and Churchill (2018: character 88), Berta and Wyss (1994: character 114).
0 = small
1 = large and triangular

89. Femur, fovea for teres femoris ligament. Boessenecker and Churchill (2018: character 89), Berta and Wyss (1994: character 115).
0 = present
1 = absent

90. Femur, lesser trochanter. Boessenecker and Churchill (2018: character 90), Berta and Wyss (1994: character 116).
0 = present
1 = absent

91. Femur, greater trochanter. Boessenecker and Churchill (2018: character 91), Berta and Wyss (1994: character 117).
0 = small and rounded
1 = large and anteroposteriorly flattened

92. Astragalus, calcaneal process. Boessenecker and Churchill (2018: character 92), Berta and Wyss (1994: character 126).
0 = absent
1 = present
2 = elongated

93. Calcaneum, calcaneal tuber. Boessenecker and Churchill (2018: character 93), Berta and Wyss (1994: character 125).
0 = straight
1 = medially prominent

94. Calcaneum, secondary sustentacular shelf. Boessenecker and Churchill (2018: character 94), Berta and Wyss (1994: character 123).
0 = absent
1 = present

95. Tarsals, entocuneiform/mesocuneiform articulation. Boessenecker and Churchill (2018: character 95), Deméré (1994: character 53).
0 = abutting
1 = overlapping

96. Anterior narial opening. Tonomori et al. (2018: character 3).
0 = large, thin margin, and rounded
1= large, thick margin, and dorsoventrally elliptical

97. Epitympanic recess. Tonomori et al. (2018: character 28).
0= small
1= large
2= very large

98. Jugal, postorbital process. Tonomori et al. (2018: character 22).
0 = small
1 = dorsally projecting

APPENDIX B

NEXUS FORMATTED MORPHOLOGICAL CHARACTER MATRIX FOR CHAPTER II

#NEXUS
[written Thu Dec 19 17:47:40 PST 2019 by Mesquite version 3.51 (build 898) at LAPTOP-2ALJS32L/10.0.0.48]

BEGIN TAXA;
	TITLE Taxa;
	DIMENSIONS NTAX=26;
	TAXLABELS
		Enaliarctos_spp. Pteronarctos_goedertae Pinnarctidion_bishopi Pinnarctidion_rayi Desmatophoca_oregonensis Desmatophoca_brachycephala Allodesmus_kernensis Atopotarus_courseni Allodesmus_packardi Allodesmus_naorai Allodesmus_demerei Allodesmus_uraiporensis Allodesmus_sinanoensis Thalassoleon_mexicanus Callorhinus_ursinus Zalophus_californianus Proneotherium_repenningi Neotherium_mirum Imagotaria_spp. Gomphotaria_pugnax Odobenus_rosmarus Devinophoca_claytoni Monachus_monachus Erignathus_barbatus USNM_335445 UOMNCH_F_68583
	;

END;

BEGIN CHARACTERS;
	TITLE Character_Matrix;
	DIMENSIONS NCHAR=98;
	FORMAT DATATYPE = STANDARD GAP = - MISSING = ? SYMBOLS = " 0 1 2 3 4";
	MATRIX
	Enaliarctos_spp.
00000000000000000000000000000000000000000000000000020000000000000?100000000000000?01000000000000
	Pteronarctos_goedertae
00000110000000000000000000000010000000?000110000002010200000000000000?10100??????????????????????000
	Pinnarctidion_bishopi
???0???10000?02?0100000001000100010 1???????0??00000?02000?????????????????????????????????10

Pinnarctidion_rayi
00000101000000010100000001002 10?01010110 2?10000002010200010010101001?1000010000
1?????????001????010
Desmatophoca_oregonensis
11000001001010010100013000002210110011112111100102111310110110101001?10100101?00
1???????????????021
Desmatophoca_brachycephala
??00??010010000101000131010012101100???????1?00?02???4001????????????????????????
??????????????21
Allodesmus_kernensis
11211011101120311111123010112211111121102211111223121411121122211101101101110001
111001101110101121
Atopotarus_courseni
??0?01????1??0???????2?000??2??0????2110211111????1??????11120?0?121101101110001111
?01?????????1?1
Allodesmus_packardi
11101?010110?13?11001230110021111101????11??11?23??040?1????????????????????????
?????????????121
Allodesmus_naorai
1110101?1110?13?1???1?00??00??????????????????10223??04????????????????????????????
???????????1??
Allodesmus_demerei
1121101?111???31????123001?122111111211012 1?1?1?03??040???????????01????0111000???
?????????????121
Allodesmus_uraiporensis
111?1?111111200 1????123?01?????????????????1??1?23???40?????????????1??11???????????
??101010101 1?1
Allodesmus_sinanoensis
1?2?101??01120????????3????1221?????????21??111?23???4?????1?2???1??101101110001111
??100?1?010?1??
Thalassoleon_mexicanus
02000100021002401010000000100110000000102110100002120201110010201 12?1012110100
11111001101010000 0?0
Callorhinus_ursinus
02000100021002411010000000100110000000102010100023120311110012121120101211010 0
11111001101010010000
Zalophus_californianus
02000100021002411010000000100110000000102110100123120411110012121 12?1012110100
11111001101010010000
Proneotherium_repenningi
00000101001000001000000000000110021000100110100001010100010010001 00????????????
?????????0?111010?0
Neotherium_mirum
0000?10100100000?00?0000001101100210001001101000020101 0??10010201 10?????101100
?100???11??1110?010

Imagotaria_spp.
0000010002100200010000000011011002100110201010011211020?110111101111?10?01101100
112011???1011101110
Gomphotaria_pugnax
0100010002101200110000000011O??0?21001100?111102231204 2?11012222112?????1101100
112011??11011101111
Odobenus_rosmarus
2000010102110202110000000111011002100010 1?1?21022?12???2??01222?1120101011011 10
1120111111011101111
Devinophoca_claytoni
01000?000000012?????00?0?1110322??0220110?10??000202002 00?000000?????????????????
??????????????021
Monachus_monachus
1100000002100121110202200100132203102111111000010212122111000000102001100011 00
1110000011112000021
Erignathus_barbatus
1102000000100111102021?000003220302010111100000021202201100 0?01?2?01000011001
1100000111120000 21
USNM_335445
2110000100000000 00?0020000?0121?111001012100110102 12???2??10110201 00?????????????
??????????????0?1
UOMNCH_F_68583
2110000101000020?000020000112111111 0??????????0102121 40????????????????????????????
?????????????0?1

;

END;
ctype ord : 15 23 37 49 50 54 55 62 64 67;

END;
BEGIN ASSUMPTIONS;
TYPESET * UNTITLED = unord: 1- 98;

END;

BEGIN MESQUITECHARMODELS;
ProbModelSet * UNTITLED = 'Mk1 (est.)': 1- 98;
END;

Begin MESQUITE;
MESQUITESCRIPTVERSION 2;
TITLE AUTO;
tell ProjectCoordinator;
timeSaved 1576806460323;
getEmployee #mesquite.minimal.ManageTaxa.ManageTaxa;

```
		tell It;
			setID 0 421770968555457424;
		endTell;
		getEmployee #mesquite.charMatrices.ManageCharacters.ManageCharacters;
		tell It;
			setID 0 3333749591159525760;
			mqVersion 351;
			checksumv 0 3 2067079459 null  getNumChars 98 numChars 98
getNumTaxa 26 numTaxa 26   short true   bits 31   states 31   sumSquaresStatesOnly 11630.0
sumSquares 11630.0 longCompressibleToShort false usingShortMatrix true   NumFiles 1
NumMatrices 1;
			mqVersion;
		endTell;
		getWindow;
		tell It;
			suppress;
			setResourcesState false false 141;
			setPopoutState 300;
			setExplanationSize 0;
			setAnnotationSize 0;
			setFontIncAnnot 0;
			setFontIncExp 0;
			setSize 2091 1174;
			setLocation 1510 150;
			setFont SanSerif;
			setFontSize 10;
			getToolPalette;
			tell It;
			endTell;
			desuppress;
		endTell;
		getEmployee  #mesquite.trees.BasicTreeWindowCoord.BasicTreeWindowCoord;
		tell It;
			makeTreeWindow #421770968555457424
#mesquite.trees.BasicTreeWindowMaker.BasicTreeWindowMaker;
			tell It;
				suppressEPCResponse;
				setTreeSourceEditMode #mesquite.trees.StoredTrees.StoredTrees;
				tell It;
					laxMode;
					setTreeBlock -2147483647;
					toggleUseWeights off;
				endTell;
				setAssignedID 985.1576714518141.3785034216871739372;
				getTreeWindow;
				tell It;
```

```
                                        setExplanationSize 30;
                                        setAnnotationSize 20;
                                        setFontIncAnnot 0;
                                        setFontIncExp 0;
                                        setSize 1950 1102;
                                        setLocation 1510 150;
                                        setFont SanSerif;
                                        setFontSize 10;
                                        getToolPalette;
                                        tell It;
                                                setTool
mesquite.trees.BasicTreeWindowMaker.BasicTreeWindow.interchange;
                                        endTell;
                                        getTreeDrawCoordinator
#mesquite.trees.BasicTreeDrawCoordinator.BasicTreeDrawCoordinator;
                                    tell It;
                                        suppress;
                                        setTreeDrawer
#mesquite.trees.SquareLineTree.SquareLineTree;
                                        tell It;
                                                setNodeLocs
#mesquite.trees.NodeLocsStandard.NodeLocsStandard;
                                                tell It;
                                                        branchLengthsToggle off;
                                                        toggleScale on;
                                                        toggleBroadScale off;
                                                        toggleCenter on;
                                                        toggleEven on;
                                                        setFixedTaxonDistance 0;
                                                endTell;
                                                setEdgeWidth 4;
                                                showEdgeLines on;
                                                orientRight;
                                        endTell;
                                        setBackground White;
                                        setBranchColor Black;
                                        showNodeNumbers off;
                                        showBranchColors on;
                                        labelBranchLengths off;
                                        centerBrLenLabels on;
                                        showBrLensUnspecified on;
                                        showBrLenLabelsOnTerminals on;
                                        setBrLenLabelColor 0 0 255;
                                        setNumBrLenDecimals 6;
                                        desuppress;
```

```
                                        getEmployee
#mesquite.trees.BasicDrawTaxonNames.BasicDrawTaxonNames;
                                        tell It;
                                                setFontSize 24;
                                                setColor Black;
                                                toggleColorPartition off;
                                                toggleColorAssigned on;
                                                toggleShadePartition off;
                                                toggleShowFootnotes on;
                                                toggleNodeLabels on;
                                                toggleCenterNodeNames off;
                                                toggleShowNames on;
                                                namesAngle ?;
                                        endTell;
                                endTell;
                                        setTreeNumber 1;
                                        setTree
'(((((((25,26),((5,6),((7,(8,9)),((10,11),(12,13))))),(24,(23,22))),(14,(15,16)),((20,21),19),(18,17)),
(3,4)),2),1);';
                                        setDrawingSizeMode 0;
                                        toggleLegendFloat on;
                                        scale 0;
                                        toggleTextOnTree off;
                                        togglePrintName off;
                                        showWindow;
                                endTell;
                                setEditMode 'Edited, based on Untitled Tree   [Stored Trees]';
                                desuppressEPCResponseNORESET;
                                getEmployee #mesquite.trees.ColorBranches.ColorBranches;
                                tell It;
                                        setColor Red;
                                        removeColor off;
                                endTell;
                                getEmployee #mesquite.ornamental.BranchNotes.BranchNotes;
                                tell It;
                                        setAlwaysOn off;
                                endTell;
                                getEmployee
#mesquite.ornamental.ColorTreeByPartition.ColorTreeByPartition;
                                tell It;
                                        colorByPartition off;
                                endTell;
                                getEmployee
#mesquite.ornamental.DrawTreeAssocDoubles.DrawTreeAssocDoubles;
                                tell It;
                                        setOn on;
```

```
                                        toggleShow consensusFrequency;
                                        toggleShow posteriorProbability;
                                        toggleShow bootstrapFrequency;
                                        toggleShow consensusFrequency;
                                        toggleShow posteriorProbability;
                                        toggleShow bootstrapFrequency;
                                        setDigits 4;
                                        setThreshold ?;
                                        writeAsPercentage off;
                                        toggleCentred off;
                                        toggleHorizontal on;
                                        toggleWhiteEdges on;
                                        toggleShowOnTerminals on;
                                        setFontSize 10;
                                        setOffset 0  0;
                                endTell;
                                getEmployee
#mesquite.ornamental.DrawTreeAssocStrings.DrawTreeAssocStrings;
                                tell It;
                                        setOn on;
                                        toggleCentred on;
                                        toggleHorizontal on;
                                        setFontSize 10;
                                        setOffset 0  0;
                                        toggleShowOnTerminals on;
                                endTell;
                                getEmployee #mesquite.trees.TreeInfoValues.TreeInfoValues;
                                tell It;
                                        panelOpen false;
                                endTell;
                        endTell;
                endTell;
                getEmployee
#mesquite.charMatrices.BasicDataWindowCoord.BasicDataWindowCoord;
                tell It;
                        showDataWindow #3333749591159525760
#mesquite.charMatrices.BasicDataWindowMaker.BasicDataWindowMaker;
                        tell It;
                                getWindow;
                                tell It;
                                        setExplanationSize 30;
                                        setAnnotationSize 20;
                                        setFontIncAnnot 0;
                                        setFontIncExp 0;
                                        setSize 1950 1102;
                                        setLocation 1510 150;
```

```
                    setFont SanSerif;
                    setFontSize 10;
                    getToolPalette;
                    tell It;
                            setTool
mesquite.charMatrices.BasicDataWindowMaker.BasicDataWindow.ibeam;
                    endTell;
                    setActive;
                    setTool
mesquite.charMatrices.BasicDataWindowMaker.BasicDataWindow.ibeam;
                    colorCells  #mesquite.charMatrices.NoColor.NoColor;
                    colorRowNames
#mesquite.charMatrices.TaxonGroupColor.TaxonGroupColor;
                    colorColumnNames
#mesquite.charMatrices.CharGroupColor.CharGroupColor;
                    colorText  #mesquite.charMatrices.NoColor.NoColor;
                    setBackground White;
                    toggleShowNames on;
                    toggleShowTaxonNames on;
                    toggleTight off;
                    toggleThinRows off;
                    toggleShowChanges on;
                    toggleSeparateLines off;
                    toggleShowStates on;
                    toggleAutoWCharNames on;
                    toggleAutoTaxonNames off;
                    toggleShowDefaultCharNames off;
                    toggleConstrainCW on;
                    toggleBirdsEye off;
                    toggleShowPaleGrid off;
                    toggleShowPaleCellColors off;
                    toggleShowPaleExcluded off;
                    togglePaleInapplicable on;
                    toggleShowBoldCellText off;
                    toggleAllowAutosize on;
                    toggleColorsPanel off;
                    toggleDiagonal on;
                    setDiagonalHeight 80;
                    toggleLinkedScrolling on;
                    toggleScrollLinkedTables off;
            endTell;
            showWindow;
            getWindow;
            tell It;
                    forceAutosize;
            endTell;
```

```
                    getEmployee #mesquite.charMatrices.AlterData.AlterData;
                    tell It;
                        toggleBySubmenus off;
                    endTell;
                    getEmployee #mesquite.charMatrices.ColorByState.ColorByState;
                    tell It;
                        setStateLimit 9;
                        toggleUniformMaximum on;
                    endTell;
                    getEmployee #mesquite.charMatrices.ColorCells.ColorCells;
                    tell It;
                        setColor Red;
                        removeColor off;
                    endTell;
                    getEmployee #mesquite.categ.StateNamesStrip.StateNamesStrip;
                    tell It;
                        showStrip off;
                    endTell;
                    getEmployee #mesquite.charMatrices.AnnotPanel.AnnotPanel;
                    tell It;
                        togglePanel off;
                    endTell;
                    getEmployee
#mesquite.charMatrices.CharReferenceStrip.CharReferenceStrip;
                    tell It;
                        showStrip off;
                    endTell;
                    getEmployee
#mesquite.charMatrices.QuickKeySelector.QuickKeySelector;
                    tell It;
                        autotabOff;
                    endTell;
                    getEmployee
#mesquite.charMatrices.SelSummaryStrip.SelSummaryStrip;
                    tell It;
                        showStrip off;
                    endTell;
                    getEmployee
#mesquite.categ.SmallStateNamesEditor.SmallStateNamesEditor;
                    tell It;
                        panelOpen true;
                    endTell;
                endTell;
            endTell;
            endTell;
end;
```

APPENDIX C

FIRST AND LAST APPEARANCE DATA FOR TAXA IN CHAPTER II

First appearance datum (FAD) and last appearance datum (LAD) in millions of years ago for each of the taxa used to timescale the phylogeny in Figure 4 of Chapter II after Boessenecker and Churchill (2018) and Poust and Boessenecker (2018).

Taxon Name	FAD	LAD
Enaliarctos spp.	30.6	16.6
Pteronarctos goedertae	20.2	16.6
Pinnarctidion bishopi	24	21.5
Pinnarctidion rayi	24.7	19.1
Desmatophoca oregonensis	20.2	16.6
Desmatophoca brachycephala	22.9	19
Allodesmus kernensis	15.85	15.15
Atopotarus courseni	15.7	14
Allodesmus packardi	14.8	11.6
Allodesmus naorai	13.5	11.8
Allodesmus demerei	10.5	9.1
Allodesmus uraiporensis	16.3	13.5
Allodesmus sinanoensis	13.5	12.5
Thalassoleon mexicanus	6	4.9
Callorhinus ursinus	1.81	0
Zalophus californianus	0.78	0
Proneotherium repenningi	17.3	16.6
Neotherium mirum	15.85	15.15
Imagotaria downsi	10	7
Gomphotaria pugnax	7.1	4.9
Odobenus rosmarus	2.7	0
Devinophoca claytoni	16.3	12.82
Monachus monachus	0.98	0
Erignathus barbatus	1.81	0
Eodesmus condoni	17.3	16.6
USNM 335445	17.3	16.6

APPENDIX D

TIME-SCALED PHYLOGENY IN NEWICK FORMAT USED IN CHAPTER III

(((((((Devinophoca_claytoni:3.68,(((Erignathus_barbatus:0.5,Erignathus_barbatus1:0.5):10.5,((Cystophora_cristata1:0.5,Cystophora_cristata:0.5):6.5,(((Histriophoca_fasciata1:0.5,Histriophoca_fasciata:0.5):3.5,(Pagophilus_groenlandicus:0.5,Pagophilus_groenlandicus1:0.5):3.5):1.5,((Phoca_vitulina:0.5,Phoca_vitulina1:0.5,Phoca_vitulina2:0.5):2.5,(((Pusa_hispida:0.5,Pusa_hispida1:0.5):1,(Pusa_sibirica2:0.5,Pusa_sibirica3:0.5,Pusa_sibirica1:0.5,Pusa_sibirica:0.5):1):1,(Pusa_caspica:1.75,(Halichoerus_grypus1:0.5,Halichoerus_grypus:0.5):1.25):0.75):0.5):2.5):1.5):4):5,((Homiphoca_capensis:3.504,Piscophoca_pacifica:3.504):2,(((Neomonachus_schauinslandi1:0.5,Neomonachus_schauinslandi2:0.5,Neomonachus_schauinslandi:0.5):8.5,Monachus_monachus:9):1.5,((Mirounga_angustirostris:0.5,Mirounga_angustirostris1:0.5):8.5,((Ommatophoca_rossii:0.5,Ommatophoca_rossii1:0.5):5.5,((Leptonychotes_weddellii:0.5,Leptonychotes_weddellii1:0.5):3,(Hydrurga_leptonyx1:0.5,Hydrurga_leptonyx:0.5):3):2.5):3):1.5):2.25):3.25):1.5):9.44,(((Eodesmus_condoni:1.06,Eodesmus_sp.:1.06):3.25,(Allodesmus_kernensis:1.47,(Desmatophoca_brachycephala:0.97,Desmatophoca_oregonensis:3.56):0.5):0.25):0.17,((Neotherium_mirum:1.16,(Imagotaria_downsi:6.615,(Pontolis_barroni:4.41,(Dusignathus:2.205,(Pliopedia_pacifica:0.367,(Valenictus_imperialensis:0.1835,(Odobenus_rosmarus:0.5,Odobenus_rosmarus1:0.5,Odobenus_rosmarus2:0.5,Odobenus_rosmarus3:0.5,Odobenus_rosmarus4:0.5,Odobenus_rosmarus5:0.5,Odobenus_rosmarus8:0.5,Odobenus_rosmarus9:0.5,Odobenus_rosmarus6:0.5,Odobenus_rosmarus7:0.5):5.0165):0.1835):8.125):2.205):2.205):3.365):1.16,(((((((((Arctocephalus_australis:0.5,Arctocephalus_australis1:0.5):0.2,(Arctocephalus_galapagoensis1:0.5,Arctocephalus_galapagoensis:0.5):0.2):0.4,(Arctocephalus_forsteri:0.5,Arctocephalus_forsteri1:0.5):0.6):3.4,(Otaria_bryonia:0.5,Otaria_bryonia1:0.5):4):0.7,((Eumetopias_jubatus:0.5,Eumetopias_jubatus1:0.5,Eumetopias_jubatus2:0.5):4,(Zalophus_californianus:0.5,Zalophus_californianus1:0.5):4):0.7):0.9,(Neophoca_cinerea1:0.5,Neophoca_cinerea:0.5):5.6):2.1,(Callorhinus_ursinus:0.5,Callorhinus_ursinus1:0.5):7.7):0.4,Thalassoleon_mexicanus:1.354):8.59,Pithanotaria_starri:5.57):5.57):2.16):2.02):1.36,Pinnarctidion_rayi:7.86):1.2,Pteronarctos_goedertae:9.06):2.5,Enaliarctos_emlongi:3.9):1,Enaliarctos_tedfordi:4.9):2.5,Enaliarctos_mealsi:7.4):3.91,Potamotherium_vallentoni:11.01);

APPENDIX E

PRINCIPAL COMPONENTS USED TO TRAIN THE FLEXIBLE DISCRIMINANT ANALYSES IN CHAPTER III

Table 1. First 13 principal components from principal components analysis in Chapter III. Specimen numbers are after Table 1. Continues onto subsequent page.

	Taxon Name	PC1	PC2	PC3	PC4	PC5	PC6	PC7	PC8	PC9	PC10	PC11	PC12	PC13
1.	*Potamotherium valletoni*	0.0386	0.0562	0.0284	0.0034	0.0371	-0.0075	-0.0169	0.0459	0.0310	0.0094	0.0086	0.0159	0.0242
2.	*Pinnarctidion rayi*	0.0067	0.0446	0.0128	0.0008	-0.0050	0.0062	0.0060	0.0336	0.0634	-0.0346	-0.0411	0.0153	0.0051
3.	*Desmatophoca oregonensis*	-0.0270	-0.0073	-0.0270	0.0199	0.0155	-0.0234	-0.0287	0.0449	0.0452	-0.0131	-0.0256	0.0167	-0.0116
4.	*Allodesmus kernensis*	-0.0799	0.0124	-0.0220	0.0194	0.0242	-0.0319	0.0032	0.0080	0.0236	-0.0282	-0.0211	0.0148	0.0098
5.	*Pithanotaria starri*	-0.0133	0.0412	0.0079	0.0097	0.0389	-0.0326	-0.0160	0.0325	0.0454	-0.0245	-0.0307	0.0103	-0.0124
6.	*Thalassoleon mexicanus*	-0.0852	0.0312	-0.0107	0.0079	0.0129	-0.0002	-0.0096	0.0197	0.0025	0.0007	-0.0017	-0.0093	0.0095
7.	*Neotherium mirum*	-0.0199	0.0726	-0.0110	0.0543	0.0060	0.0190	-0.0333	0.0143	0.0201	-0.0024	-0.0506	0.0119	0.0121
8.	*Imagotaria downsi*	-0.0133	0.0374	-0.0058	0.0256	-0.0046	0.0157	-0.0267	0.0039	0.0150	-0.0114	-0.0327	0.0265	-0.0154
9.	*Pontolis barroni*	-0.0886	0.0395	0.0002	0.0352	0.0156	-0.0077	-0.0192	0.0309	0.0052	-0.0021	-0.0231	0.0085	-0.0042
10.	*Dusignathus seftoni*	-0.0690	0.0063	-0.0310	0.0018	-0.0070	0.0141	0.0305	0.0204	0.0271	-0.0097	0.0059	0.0137	0.0266
11.	*Pliopedia pacifica*	-0.0843	-0.0301	-0.0472	0.0192	-0.0516	0.0293	0.0001	-0.0304	0.0334	-0.0119	-0.0602	-0.0062	-0.0037
12.	*Valenictus imperialensis*	-0.0436	0.0005	-0.0574	0.0479	-0.0130	0.0345	-0.0117	0.0310	0.0264	0.0211	-0.0181	0.0214	0.0267
13.	*Odobenus rosmarus*	-0.1051	-0.0078	-0.0428	-0.0279	-0.0677	-0.0458	-0.0236	0.0018	-0.0046	-0.0054	0.0314	0.0051	-0.0035
14.		-0.0641	0.0208	-0.0457	-0.0216	-0.0622	-0.0574	0.0217	-0.0197	0.0080	0.0149	-0.0518	-0.0021	-0.0251
15.		-0.0772	0.0295	-0.0566	-0.0244	-0.0205	-0.0342	-0.0041	0.0232	-0.0018	0.0249	0.0139	-0.0031	0.0098
16.	*Arctocephalus australis*	-0.0720	0.0223	0.0332	-0.0188	0.0101	-0.0147	0.0204	-0.0049	0.0312	-0.0018	0.0025	0.0295	-0.0023
17.		-0.1019	0.0087	0.0327	-0.0070	0.0109	0.0153	-0.0023	0.0101	-0.0182	0.0050	0.0297	0.0200	0.0056
18.	*Arctocephalus forsteri*	-0.1063	0.0105	0.0047	-0.0394	0.0282	0.0442	-0.0253	0.0030	-0.0140	0.0288	-0.0106	0.0000	0.0251
19.		-0.0886	0.0336	0.0288	-0.0236	0.0175	0.0301	0.0041	-0.0152	-0.0035	0.0114	-0.0227	0.0326	0.0062
20.	*Arctocephalus galapagoensis*	-0.0708	0.0364	0.0195	0.0036	0.0107	-0.0263	0.0165	0.0128	0.0393	0.0213	-0.0043	0.0065	0.0013
21.	*Callorhinus ursinus*	-0.1084	-0.0221	0.0406	-0.0141	0.0113	0.0112	-0.0086	0.0150	-0.0174	-0.0352	0.0296	-0.0108	-0.0073
22.		-0.1009	0.0141	0.0466	-0.0182	0.0007	-0.0103	0.0017	-0.0037	0.0242	0.0020	0.0175	0.0088	-0.0067
23.	*Neophoca cinerea*	-0.1372	-0.0054	-0.0187	0.2112	0.0076	0.0108	-0.0364	-0.0200	0.0175	0.0025	-0.0068	-0.0075	-0.0050
24.	*Otaria flavescens*	-0.0727	-0.0357	0.0338	-0.0074	-0.0065	0.0057	-0.0216	0.0051	-0.0264	0.0039	-0.0113	-0.0368	0.0065
25.		-0.0902	-0.0313	0.0365	0.0036	-0.0012	-0.0007	0.0263	-0.0054	-0.0409	0.0024	-0.0158	-0.0199	-0.0092
26.	*Zalophus californianus*	-0.0816	-0.0139	0.0384	-0.0202	0.0045	-0.0023	0.0114	0.0081	0.0020	-0.0112	-0.0127	-0.0128	-0.0049
27.		-0.0819	-0.0018	0.0464	-0.0338	0.0084	0.0020	0.0021	-0.0269	-0.0231	-0.0213	-0.0065	-0.0061	0.0110
28.	*Cystophora cristata*	0.0788	0.0438	0.0259	-0.0095	0.0142	0.0169	-0.0241	0.0076	0.0072	0.0196	-0.0010	0.0038	0.0054
29.		0.0636	0.0001	0.0208	0.0149	-0.0275	0.0005	-0.0119	0.0026	-0.0040	-0.0029	-0.0010	-0.0021	-0.0113
30.	*Erignathus barbatus*	0.0634	0.0530	-0.0059	-0.0362	0.0101	-0.0209	-0.0300	-0.0154	0.0221	-0.0018	0.0051	-0.0500	-0.0093

Table 1. Continued from previous page.

	Taxon Name	PC1	PC2	PC3	PC4	PC5	PC6	PC7	PC8	PC9	PC10	PC11	PC12	PC13
1.		0.0474	0.0597	0.0043	-0.0175	0.0200	0.0049	-0.0173	0.0119	0.0169	0.0087	0.0044	-0.0333	-0.0180
2.	*Halichoerus grypus*	0.0528	0.0593	-0.0270	0.0148	-0.0541	0.0019	-0.0434	0.0474	-0.0238	-0.0269	-0.0115	0.0222	-0.0031
3.		0.0713	0.0489	-0.0010	-0.0040	-0.0120	0.0278	-0.0164	-0.0217	-0.0232	0.0082	-0.0081	0.0234	-0.0065
4.	*Histriophoca fasciata*	0.0854	-0.0133	0.0233	-0.0072	-0.0103	0.0094	-0.0233	-0.0318	0.0200	-0.0079	0.0094	-0.0196	0.0196
5.		0.0672	-0.0098	0.0221	-0.0097	-0.0246	0.0012	0.0015	-0.0322	0.0062	0.0005	0.0048	0.0065	0.0108
6.	*Hydrurga leptonyx*	0.0486	-0.1142	0.0085	-0.0055	-0.0457	0.0377	-0.0053	0.0450	0.0380	-0.0016	-0.0317	-0.0074	0.0424
7.	*Leptonychotes weddellii*	0.0418	-0.0608	0.0181	0.0326	-0.0103	0.0129	0.0522	0.0277	-0.0127	0.0089	-0.0049	-0.0058	-0.0198
8.		0.0403	-0.0273	0.0193	-0.0060	-0.0117	0.0081	0.0191	0.0401	0.0268	0.0253	0.0301	-0.0028	-0.0026
9.	*Mirounga angustirostris*	0.0124	-0.0315	-0.0277	0.0137	-0.0088	0.0022	0.0284	-0.0044	0.0371	-0.0216	0.0245	0.0067	-0.0117
10.	*Monachus monachus*	0.0055	-0.0142	-0.0709	-0.0250	0.0138	-0.0149	-0.0173	0.0110	-0.0053	-0.0528	-0.0103	0.0020	0.0040
11.	*Neomonachus schauinslandi*	0.0087	-0.0418	-0.1078	-0.0076	0.0455	0.0138	0.0153	-0.0229	-0.0044	0.0186	0.0256	-0.0057	-0.0010
12.		-0.0227	-0.0057	-0.1061	-0.0238	0.0405	0.0245	0.0083	-0.0003	0.0118	0.0061	-0.0138	-0.0035	0.0092
13.		-0.0190	-0.0144	-0.1191	-0.0037	0.0249	0.0248	0.0189	-0.0003	-0.0077	-0.0180	-0.0023	0.0080	0.0010
14.	*Ommatophoca rossii*	0.0820	-0.1174	0.0377	-0.0023	0.0972	-0.0881	-0.0398	0.0136	-0.0031	0.0023	-0.0167	0.0243	-0.0105
15.		0.0904	-0.1109	-0.0079	-0.0080	-0.0575	0.0086	-0.0135	-0.0465	-0.0282	0.0302	0.0135	0.0105	-0.0174
16.	*Pagophilus groenlandicus*	0.0581	0.0078	0.0392	0.0010	0.0060	0.0252	0.0294	-0.0222	0.0151	-0.0363	0.0000	0.0071	-0.0145
17.		0.0404	0.0018	0.0274	-0.0062	-0.0081	0.0076	-0.0030	-0.0443	0.0273	-0.0147	-0.0021	0.0066	0.0082
18.	*Phoca vitulina*	0.0482	0.0215	0.0180	0.0371	-0.0157	0.0000	0.0322	0.0298	-0.0066	-0.0045	0.0012	0.0051	0.0004
19.	*Pusa caspica*	0.0908	0.0404	0.0051	0.0567	0.0028	-0.0573	0.0289	-0.0020	-0.0378	0.0034	0.0254	-0.0030	0.0518
20.	*Pusa hispida*	0.0675	0.0212	0.0078	0.0051	0.0265	0.0274	0.0191	0.0217	-0.0275	0.0053	-0.0005	-0.0134	-0.0389
21.		0.0729	0.0263	-0.0042	0.0010	0.0034	0.0193	-0.0180	0.0025	-0.0121	0.0044	0.0002	0.0192	-0.0004
22.	*Pusa sibirica*	0.0891	0.0598	-0.0009	0.0155	0.0141	0.0051	-0.0204	0.0134	0.0082	0.0093	-0.0023	0.0087	-0.0156

APPENDIX F

PLOT OF PRINCIPAL COMPONENTS 1 AND 2 FROM PRINCIPAL COMPONENT ANALYSIS OF ENVIRONMENTAL PARAMETERS FROM CHAPTER IV

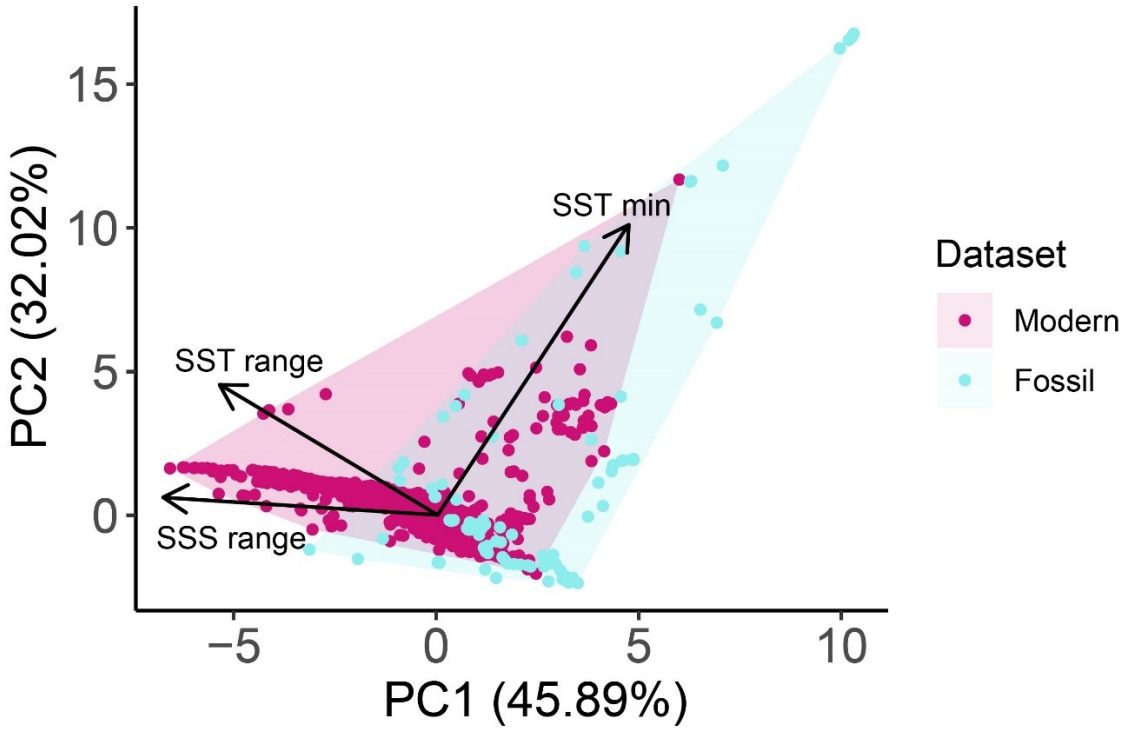

Projections of the ecospace for modern (maroon) and fossil (light blue) occurrences of *O. rosmarus* onto the first two axes of a principal component analysis (PCA). According to the broken stick criterion, principal component (PC1) is non-significant and PC2 is significant. The arrows indicate how sea surface temperature minimum, sea surface temperature range, and sea surface salinity range each influence PCs 1 and 2.

APPENDIX G

ECOLOGICAL NICHE MODEL SUMMARY STATISTICS

Table 1. Evaluation summary statistics for the modern ecological niche models from ENMevaluate object (Kass et al., 2021). Tr = training dataset, AUC = area under the curve, CBI = Boyce Index (an index measuring the quality of the ecological niche model predictions for the presence of the relevant species; Boyce et al. 2002), Mean AUC.diff = the average difference between the training and testing AUC across *k* bins (indicates degree of model overfitting; Warren and Seifert, 2011), SD = standard deviation, AUC.val = AUC calculated on the validation training sets (the data withheld during cross-validation), CBI.val = CBI calculated on the validation training sets, OR_{MTP} = omission rate with threshold as the minimum suitability value across occurrence records, OR_{10P} = omission rate with threshold as the minimum suitability value across occurrence records after removing the lowest 10 percent, AICc = Akaike criterion corrected for small sample sizes, AICc.delt = highest AIC value across all models subtracted from this model's AICc, where lower values mean higher performance, NC = number of model coefficients, fc = function class, L = linear, LQ = linear-quadratic, LQP = linear-quadratic-product, rm = regularization multiplier. Continued onto the subsequent page.

Run	Tuning Arguments	AUC_{Tr}	CBI_{Tr}	Mean AUC.diff	SD AUC.diff	Mean AUC.val	SD AUC.val	Mean CBI.val
1	fc.L_rm.0.1	0.8726	0.890	0.00181	0.00110	0.872	0.00088	0.882
2	fc.LQ_rm.0.1	0.8933	0.942	0.00776	0.00282	0.892	0.00582	0.900
3	fc.P_rm.0.1	0.8773	0.898	0.00184	0.00078	0.877	0.00157	0.901
4	fc.LQP_rm.0.1	0.9014	0.970	0.00753	0.00203	0.900	0.00566	0.919
5	fc.L_rm.0.25	0.8725	0.888	0.00180	0.00110	0.872	0.00089	0.886
6	fc.LQ_rm.0.25	0.8931	0.948	0.00757	0.00270	0.892	0.00552	0.909
7	fc.P_rm.0.25	0.8772	0.898	0.00192	0.00076	0.877	0.00162	0.903
8	fc.LQP_rm.0.25	0.9013	0.971	0.00745	0.00203	0.900	0.00554	0.920
9	fc.L_rm.0.5	0.8725	0.889	0.00178	0.00110	0.872	0.00090	0.884
10	fc.LQ_rm.0.5	0.8930	0.950	0.00718	0.00252	0.892	0.00495	0.913
11	fc.P_rm.0.5	0.8769	0.902	0.00205	0.00067	0.877	0.00165	0.903
12	fc.LQP_rm.0.5	0.9010	0.973	0.00727	0.00202	0.900	0.00539	0.924
13	fc.L_rm.1	0.8724	0.890	0.00175	0.00110	0.872	0.00093	0.878
14	fc.LQ_rm.1	0.8927	0.947	0.00654	0.00217	0.892	0.00422	0.913
15	fc.P_rm.1	0.8764	0.914	0.00218	0.00056	0.876	0.00157	0.910
16	fc.LQP_rm.1	0.8997	0.958	0.00700	0.00187	0.899	0.00496	0.927
17	fc.L_rm.2	0.8723	0.883	0.00169	0.00111	0.872	0.00097	0.882
18	fc.LQ_rm.2	0.8924	0.929	0.00573	0.00147	0.892	0.00328	0.899
19	fc.P_rm.2	0.8764	0.911	0.00214	0.00058	0.876	0.00153	0.908
20	fc.LQP_rm.2	0.8985	0.951	0.00626	0.00161	0.898	0.00374	0.926
21	fc.L_rm.4	0.8721	0.881	0.00162	0.00113	0.872	0.00107	0.879
22	fc.LQ_rm.4	0.8918	0.896	0.00462	0.00037	0.892	0.00176	0.883
23	fc.P_rm.4	0.8764	0.915	0.00207	0.00060	0.876	0.00148	0.912
24	fc.LQP_rm.4	0.8956	0.932	0.00489	0.00106	0.895	0.00255	0.906

Table 1. Continued.

Run	SD CBI.val	Tuning Arguments	Mean OR_{MTP}	SD OR_{MTP}	AICc	AICc.delt	NC
1	0.0035	fc.L_rm.0.1	0.00245	0.00347	10833	488.65	3
2	0.0750	fc.LQ_rm.0.1	0.00490	0.00693	10344	0.00	6
3	0.0120	fc.P_rm.0.1	0.00245	0.00347	10810	466.17	3
4	0.0566	fc.LQP_rm.0.1	0.00980	0.01386	10473	129.35	8
5	0.0057	fc.L_rm.0.25	0.00245	0.00347	10833	489.36	3
6	0.0728	fc.LQ_rm.0.25	0.00490	0.00693	10351	6.76	6
7	0.0134	fc.P_rm.0.25	0.00245	0.00347	10807	463.40	3
8	0.0559	fc.LQP_rm.0.25	0.00980	0.01386	10476	132.17	8
9	0.0000	fc.L_rm.0.5	0.00245	0.00347	10834	490.51	3
10	0.0686	fc.LQ_rm.0.5	0.00490	0.00693	10363	18.93	5
11	0.0120	fc.P_rm.0.5	0.00245	0.00347	10807	463.14	3
12	0.0580	fc.LQP_rm.0.5	0.00980	0.01386	10478	134.41	7
13	0.0028	fc.L_rm.1	0.00245	0.00347	10837	492.94	3
14	0.0559	fc.LQ_rm.1	0.00490	0.00693	10390	46.22	5
15	0.0191	fc.P_rm.1	0.00245	0.00347	10809	464.62	2
16	0.0566	fc.LQP_rm.1	0.00735	0.01040	10487	142.63	6
17	0.0092	fc.L_rm.2	0.00245	0.00347	10842	498.07	3
18	0.0382	fc.LQ_rm.2	0.00490	0.00693	10450	106.26	5
19	0.0226	fc.P_rm.2	0.00245	0.00347	10816	471.62	2
20	0.0481	fc.LQP_rm.2	0.00490	0.00693	10531	186.79	6
21	0.0092	fc.L_rm.4	0.00245	0.00347	10853	509.27	3
22	0.0601	fc.LQ_rm.4	0.00490	0.00693	10580	236.10	5
23	0.0247	fc.P_rm.4	0.00245	0.00347	10830	485.56	2
24	0.0757	fc.LQP_rm.4	0.00245	0.00347	10626	281.84	6

Table 2. Evaluation summary statistics for the fossil ecological niche models from ENMevaluate object (Kass et al., 2021). Abbreviations are the same as in Table 1. Continued onto the subsequent page.

Run	Tuning Arguments	AUC_{Tr}	CBI_{Tr}	Mean AUC.diff	SD AUC.diff	Mean AUC.val	SD AUC.val	Mean CBI.val	SD CBI.val
1	fc.L_rm.0.1	0.8470	0.966	0.00448	0.00221	0.846	0.00129	0.897	0.0163
2	fc.LQ_rm.0.1	0.8568	0.882	0.01462	0.00312	0.857	0.00859	0.762	0.0460
3	fc.P_rm.0.1	0.8293	0.959	0.01293	0.00312	0.829	0.00959	0.936	0.0021
4	fc.LQP_rm.0.1	0.8649	0.929	0.01072	0.00839	0.862	0.00794	0.878	0.0672
5	fc.L_rm.0.25	0.8470	0.967	0.00453	0.00227	0.846	0.00131	0.891	0.0014
6	fc.LQ_rm.0.25	0.8571	0.881	0.01538	0.00413	0.856	0.00937	0.771	0.0431
7	fc.P_rm.0.25	0.8293	0.96	0.01329	0.00264	0.829	0.00986	0.940	0.0035
8	fc.LQP_rm.0.25	0.8651	0.923	0.01100	0.00733	0.864	0.00735	0.875	0.0516
9	fc.L_rm.0.5	0.8470	0.967	0.00459	0.00235	0.846	0.00135	0.894	0.0141
10	fc.LQ_rm.0.5	0.8576	0.891	0.01461	0.00368	0.857	0.00846	0.780	0.0283
11	fc.P_rm.0.5	0.8292	0.96	0.01391	0.00176	0.830	0.01027	0.937	0.0035
12	fc.LQP_rm.0.5	0.8655	0.923	0.00902	0.00682	0.865	0.00372	0.872	0.0403
13	fc.L_rm.1	0.8470	0.966	0.00471	0.00249	0.846	0.00141	0.896	0.0156
14	fc.LQ_rm.1	0.8581	0.885	0.01432	0.00425	0.858	0.00811	0.794	0.0651
15	fc.P_rm.1	0.8291	0.964	0.01515	0.00025	0.831	0.01051	0.943	0.0092
16	fc.LQP_rm.1	0.8663	0.921	0.00760	0.00523	0.862	0.00349	0.897	0.0502
17	fc.L_rm.2	0.8470	0.969	0.00498	0.00276	0.846	0.00156	0.886	0.0000
18	fc.LQ_rm.2	0.8584	0.844	0.01089	0.00504	0.856	0.00393	0.746	0.1718
19	fc.P_rm.2	0.8288	0.957	0.01562	0.00008	0.832	0.01069	0.936	0.0071
20	fc.LQP_rm.2	0.8670	0.926	0.00584	0.00008	0.861	0.00790	0.921	0.0219
21	fc.L_rm.4	0.8471	0.962	0.00563	0.00327	0.847	0.00178	0.889	0.0134
22	fc.LQ_rm.4	0.8588	0.827	0.00622	0.00339	0.847	0.00202	0.880	0.0127
23	fc.P_rm.4	0.8291	0.962	0.01589	0.00006	0.835	0.01027	0.887	0.0247
24	fc.LQP_rm.4	0.8671	0.919	0.01076	0.00633	0.863	0.00289	0.906	0.0163

Table 2. Continued.

Run	Tuning Arguments	Mean OR_{MTP}	SD OR_{MTP}	AICc	AICc.delt	NC
2	fc.LQ_rm.0.1	0.00943	0.01334	2770	0.00	6
3	fc.P_rm.0.1	0.01087	0.01537	2949	179.13	3
4	fc.LQP_rm.0.1	0.00943	0.01334	2800	30.27	9
5	fc.L_rm.0.25	0.02174	0.03074	2857	86.59	3
6	fc.LQ_rm.0.25	0.02030	0.00203	2771	1.18	6
7	fc.P_rm.0.25	0.01087	0.01537	2949	179.18	3
8	fc.LQP_rm.0.25	0.00943	0.01334	2802	31.59	9
9	fc.L_rm.0.5	0.02174	0.03074	2857	86.90	3
10	fc.LQ_rm.0.5	0.03117	0.01740	2773	2.88	6
11	fc.P_rm.0.5	0.01087	0.01537	2949	179.28	3
12	fc.LQP_rm.0.5	0.00943	0.01334	2804	33.80	9
13	fc.L_rm.1	0.02174	0.03074	2858	87.52	3
14	fc.LQ_rm.1	0.02174	0.03074	2777	7.10	6
15	fc.P_rm.1	0.01087	0.01537	2950	179.52	3
16	fc.LQP_rm.1	0.02174	0.03074	2809	38.53	9
17	fc.L_rm.2	0.02174	0.03074	2859	88.71	3
18	fc.LQ_rm.2	0.02174	0.03074	2787	16.77	6
19	fc.P_rm.2	0.01087	0.01537	2950	180.14	3
20	fc.LQP_rm.2	0.02174	0.03074	2811	40.97	7
21	fc.L_rm.4	0.02174	0.03074	2861	91.26	3
22	fc.LQ_rm.4	0.02174	0.03074	2809	39.12	5
23	fc.P_rm.4	0.01087	0.01537	2949	179.03	2
24	fc.LQP_rm.4	0.02174	0.03074	2816	45.93	5

REFERENCES CITED

Chapter I

Barnes, L. G. 1987. A new Miocene pinniped of the genus *Desmatophoca* (Mammalia: Otariidae) from Washington. Contributions in Science, Natural History Museum of Los Angeles County 382:1–20.

Bebej, R. M. 2009. Swimming mode inferred from skeletal proportions in the fossil pinnipeds *Enaliarctos* and *Allodesmus* (Mammalia, Carnivora). Journal of Mammalian Evolution 16:77–97.

Berta, A., M. Churchill, and R. W. Boessenecker. 2018. The origin and evolutionary biology of pinnipeds: seals, sea lions, and walruses. Annual Review of Earth and Planetary Sciences 46:203–228.

Boessenecker, R. W., and M. Churchill. 2013. A reevaluation of the morphology, paleoecology, and phylogenetic relationships of the enigmatic walrus *Pelagiarctos*. PLoS ONE 8.

Böhme, M. 2003. The Miocene Climatic Optimum: evidence from ectothermic vertebrates of Central Europe. Palaeogeography, Palaeoclimatology, Palaeoecology 195:389–401.

Bowen, W. D. 1997. Role of marine mammals in aquatic ecosystems. Marine Ecology Progress Series 158:267–274.

Cammen, K. M., D. B. Rasher, and R. S. Steneck. 2019. Predator recovery, shifting baselines, and the adaptive management challenges they create. Ecosphere 10.

Condon, T. A. 1906. A new fossil pinniped from the Miocene of the Oregon coast. University of Oregon Bulletin 3:5–14.

Deméré, T. A., and A. Berta. 2002. The Miocene pinniped *Desmatophoca oregonensis* Condon, 1906 (Mammalia: Carnivora), from the Astoria Formation, Oregon. Smithsonian Contributions to Paleobiology 93:113–147.

Diebold, F. X., and G. D. Rudebusch. 2021. Probability assessments of an ice-free Arctic: comparing statistical and climate model projections. Journal of Econometrics.

Dietl, G. P., and K. W. Flessa. 2011. Conservation paleobiology: putting the dead to work. Trends in Ecology & Evolution 26:30–37.

Dietl, G. P., S. M. Kidwell, M. Brenner, D. A. Burney, K. W. Flessa, S. T. Jackson, and P. L. Koch. 2015. Conservation paleobiology: leveraging knowledge of the past to inform conservation and restoration. Annual Review of Earth and Planetary Sciences 43:79–103.

Estes, J. A., J. Terborgh, J. S. Brashares, M. E. Power, J. Berger, W. J. Bond, S. R. Carpenter, T. E. Essington, R. D. Holt, J. B. C. Jackson, R. J. Marquis, L. Oksanen, T. Oksanen, R. T. Paine, E. K. Pikitch, W. J. Ripple, S. A. Sandin, M. Scheffer, T. W. Schoener, J. B. Shurin, A. R. E. Sinclair, M. E. Soulé, R. Virtanen, and D. A. Wardle. 2011. Trophic downgrading of planet Earth. Science 333:301–306.

Estes, J. A., R. S. Steneck, and D. R. Lindberg. 2013. Exploring the consequences of species interactions through the assembly and disassembly of food webs: a Pacific-Atlantic comparison. Bulletin of Marine Science 89:11–29.

Fay, F. H. 1982. Ecology and biology of the Pacific walrus, *Odobenus rosmarus divergens* (Illiger). North American Fauna 74:1–279.

Flower, B. P., and J. P. Kennett. 1993. Middle Miocene ocean-climate transition: high resolution oxygen and carbon isotopic records from Deep Sea Drilling Project Site 588A, southwest Pacific. Integration The Vlsi Journal 8:811–843.

Furbish, R. 2015. Something old, something new, something swimming in the blue: an analysis of the pinniped family Desmatophocidae, its phylogenetic position and swimming mode. 75 pp.

Hammerschlag, N., R. A. Martin, and C. Fallows. 2006. Effects of environmental conditions on predator-prey interactions between white sharks (*Carcharodon carcharias*) and Cape fur seals (*Arctocephalus pusillus pusillus*) at Seal Island, South Africa. Environmental Biology of Fishes 76:341–350.

Heithaus, M. R., A. Frid, A. J. Wirsing, and B. Worm. 2008. Predicting ecological consequences of marine top predator declines. Trends in Ecology and Evolution 23:202–210.

Hocking, D. P., F. G. Marx, S. Wang, D. Burton, M. Thompson, T. Park, B. Burville, H. L. Richards, R. Sattler, J. Robbins, R. P. Miguez, E. M. G. Fitzgerald, D. J. Slip, and A. R. Evans. 2021. Convergent evolution of forelimb-propelled swimming in seals. Current Biology 31:2404-2409.e2.

Huntington, H. P., S. L. Danielson, F. K. Wiese, M. Baker, P. Boveng, J. J. Citta, A. De Robertis, D. M. S. Dickson, E. Farley, J. C. George, K. Iken, D. G. Kimmel, K. Kuletz, C. Ladd, R. Levine, L. Quakenbush, P. Stabeno, K. M. Stafford, D. Stockwell, and C. Wilson. 2020. Evidence suggests potential transformation of the Pacific Arctic ecosystem is underway. Nature Climate Change 10:342–348.

IUCN. 2022. The IUCN Red List of Threatened Species. Version 2022-2. https://www.iucnredlist.org. Accessed on 4 March 2023.

Jablonski, D., and J. J. Sepkoski. 1996. Paleobiology, community ecology, and scales of ecological pattern. Ecology 77:1367–1378.

Jacobs, P., N. Lenssen, G. Schmidt, and R. Rohde. 2021. The Arctic is now warming four times as fast as the rest of the globe. AGU Fall Meeting.

Jahn, A., J. E. Kay, M. M. Holland, and D. M. Hall. 2016. How predictable is the timing of a summer ice-free Arctic? Geophysical Research Letters 43:9113–9120.

King, J. E. 1983. Seals of the World. Cornell University Press, Ithaca, New York, 240. pp.

Kohno, N. 1992. An Early Miocene enaliarctine pinniped (Carnivora: Otariidae) from the western North Pacific. Bulletin of the Mizunami Fossil Museum 19:273–292.

Kovacs, K. M., A. Aguilar, D. Aurioles, V. Burkanov, C. Campagna, N. Gales, T. Gelatt, S. D. Goldsworthy, S. J. Goodman, G. J. G. Hofmeyr, T. Härkönen, L. Lowry, C. Lydersen, J. Schipper, T. Sipilä, C. Southwell, S. Stuart, D. Thompson, and F. Trillmich. 2012. Global threats to pinnipeds. Marine Mammal Science.

Lipps, J. H., and E. Mitchell. 1976. Trophic model for the adaptive radiations and extinctions of pelagic marine mammals. Paleontological Society 2:147–155.

McCauley, D. J., M. L. Pinsky, S. R. Palumbi, J. A. Estes, F. H. Joyce, and R. R. Warner. 2015. Marine defaunation: animal loss in the global ocean. Science 347.

Notz, D., and J. Stroeve. 2018. The trajectory towards a seasonally ice-free Arctic Ocean. Current Climate Change Reports 4:407–416.

Overland, J. E., and M. Wang. 2013. When will the summer Arctic be nearly sea ice free? Geophysical Research Letters 40:2097–2101.

Paterson, R. 2017. Evidence for independent acquisition of aquatic specializations in pinnipeds (seals, sea lions, and walruses): insights from study of the phylogenetic position, locomotor behaviour and description of the stem pinniped, *Puijila darwini*.

Paterson, R. S., N. Rybczynski, N. Kohno, and H. C. Maddin. 2020. A total evidence phylogenetic analysis of pinniped phylogeny and the possibility of parallel evolution within a monophyletic framework. Frontiers in Ecology and Evolution 7:1–16.

Pyenson, N. D., R. B. Irmis, J. H. Lipps, L. G. Barnes, E. D. Mitchell, and S. A. McLeod. 2009. Origin of a widespread marine bonebed deposited during the middle Miocene Climatic Optimum. Geology 37:519–522.

Rantanen, M., A. Y. Karpechko, A. Lipponen, K. Ruosteenoja, T. Vihma, A. Laaksonen, K. Nordling, and O. Hyvärinen. 2021. The Arctic has warmed nearly four times faster than the globe since 1979. Communication 3:1–10.

Ray, G. C., J. McCormick-Ray, P. Berg, and H. E. Epstein. 2006. Pacific walrus: benthic bioturbator of Beringia. Journal of Experimental Marine Biology and Ecology 330:403–419.

Riedman, M. 1990. The Pinnipeds: Seals, Sea Lions, and Walruses. University of California Press, Berkeley. 1990, 149 pp.

Rule, J. P., J. W. Adams, F. G. Marx, A. R. Evans, A. J. D. Tennyson, R. P. Scofield, and E. M. G. Fitzgerald. 2020. First monk seal from the Southern Hemisphere rewrites the evolutionary history of true seals. Proceedings of Biological Sciences 287:20202318.

Springer, A. M., J. A. Estes, G. B. van Vliet, T. M. Williams, D. F. Doak, E. M. Danner, K. A. Forney, and B. Pfister. 2003. Sequential megafaunal collapse in the North Pacific Ocean: an ongoing legacy of industrial whaling? PNAS 100:12223–12228.

Theobald, M. R., P. D. Crittenden, A. P. Hunt, Y. S. Tang, U. Dragosits. 2006. Ammonia emissions from a Cape fur seal colony, Cape Cross, Namibia. Geophysical Research Letters 33: 1–4.

Tonomori, W., and H. Taru. 2022. Tarsals of early pinnipedimorphs (Mammalia: Carnivora) from the Lower Miocene, Japan, and their early diversity in the western North Pacific. Paleontological Research 26:314–326.

Tonomori, W., H. Sawamura, T. Sato, and N. Kohno. 2018. A new Miocene pinniped *Allodesmus* (Mammalia: Carnivora) from Hokkaido, Northern Japan. Royal Society Open Science 5.

Tsuchi, R. 1992. Neogene events in Japan and on the Pacific coast of South America. Revista Geológica de Chile: An International Journal on Andean Geology 19:67–73.

Turner, M. G., W. J. Calder, G. S. Cumming, T. P. Hughes, A. Jentsch, S. L. LaDeau, T. M. Lenton, B. N. Shuman, M. R. Turetsky, Z. Ratajczak, J. W. Williams, A. P. Williams, and S. R. Carpenter. 2020. Climate change, ecosystems and abrupt change: science priorities. Philosophical Transactions of the Royal Society B: Biological Sciences 375.

Valenzuela-Toro, A., and N. D. Pyenson. 2019. What do we know about the fossil record of pinnipeds? A historiographical investigation. Royal Society Open Science 6.

Yletyinen, J. 2019. Arctic climate resilience. Nature Climate Change 9:805–806.

Chapter II

Armentrout, J. M. 1981. Correlation and ages of Cenozoic stratigraphic units in Oregon and Washington; pp. 137–148 in J. M. Armentrout (ed.), Pacific Northwest Cenozoic Biostratigraphy. Geological Society of America, Boulder, Colorado.

Barnes, L. G. 1972. Miocene Desmatophocinae (Mammalia: Carnivora) from California. University of California Publications in Geological Sciences 89:1–69.

Barnes, L. G. 1979. Fossil enaliarctine pinnipeds (Mammalia: Otariidae) from Pyramid Hill, Kern County, California. Contributions in Science (Los Angeles) 318:1–41.

Barnes L. G. 1987. A new Miocene pinniped of the genus *Desmatophoca* (Mammalia: Otariidae) from Washington. Contributions in Science, Natural History Museum of Los Angeles County 382:1–20.

Barnes L. G. 1989. A new enaliarctine pinniped from the Astoria Formation, Oregon, and a classification of the Otariidae (Mammalia: Carnivora). Contributions in Science, Natural History Museum of Los Angeles County 403:1–26.

Barnes L. G. 1990. A new Miocene enaliarctine pinniped of the genus *Pteronarctos* (Mammalia: Otariidae) from the Astoria Formation, Oregon. Contributions in Science, Natural History Museum of Los Angeles County 442:1–20.

Barnes, L. G. 1992. A new genus and species of Middle Miocene enaliarctine pinniped (Mammalia, Carnivora, Otariidae) from the Astoria Formation in coastal Oregon. Contributions in Science (Natural History Museum of Los Angeles County) 431:1–27.

Barnes, L. G., and K. Hirota. 1994. Miocene pinnipeds of the otariid subfamily Allodesminae in the North Pacific Ocean: systematics and relationships. The Island Arc 3:329–360.

Bell, M. A, and G. T. Lloyd. 2015. Strap: an R package for plotting phylogenies against stratigraphy and assessing their stratigraphic congruence. Palaeontology 58:379–389.

Berta, A. 1991. New *Enaliarctos* (Pinnipedimorpha) from the Oligocene and Miocene of Oregon and the role of "enaliarctids" in pinniped phylogeny. Smithsonian Contributions to Paleobiology 69:1–33.

Berta, A. 1994. A new species of phocoid pinniped *Pinnarctidion* from the Early Miocene of Oregon. Journal of Vertebrate Paleontology 14:405–413.

Berta, A., M. Churchill, and R. W. Boessenecker. 2018. The origin and evolutionary biology of pinnipeds: seals, sea lions, and walruses. Annual Review of Earth and Planetary Sciences 46:203–228.

Boessenecker, R. W., and M. Churchill. 2018. The last of the desmatophocid seals: a new species of *Allodesmus* from the upper Miocene of Washington, USA, and a revision of the taxonomy of Desmatophocidae. Zoological Journal of the Linnaean Society XX:1–25.

Böhme, M. 2003. The Miocene Climatic Optimum: evidence from ectothermic vertebrates of Central Europe. Palaeogeography, Palaeoclimatology, Palaeoecology 195:389–401.

Bowditch, T.E. 1821. An Analysis of the Natural Classifications of Mammalia for the Use of Students and Travelers. J. Smith, Paris, 115 pp.

Churchill, M., M. T. Clementz, and N. Kohno. 2015. Cope's rule and the evolution of body size in Pinnipedimorpha (Mammalia: Carnivora). *Evolution* 69:201–215.

Colbath, S. L. 1985. Gastropod predation and depositional environments of two molluscan communities from the Miocene Astoria Formation at Beverly Beach State Park, Oregon. Journal of Paleontology 59:849–869.

Condon, T. A. 1906. A new fossil pinniped from the Miocene of the Oregon coast. University of Oregon Bulletin 3:5–14.

Coombs, M. C. 1979. *Tylocephalonyx*, a new genus of North American dome-skulled chalicotheres. Bulletin of the American Museum of Natural History 164:1–68.

Deméré, T. A., and A. Berta. 2002. The Miocene pinniped *Desmatophoca oregonensis* Condon, 1906 (Mammalia: Carnivora), from the Astoria Formation, Oregon. Smithsonian Contributions to Paleobiology 93:113–147.

Dewaele, L., O. Lambert, and S. Louwye. 2017. On *Prophoca* and *Leptophoca* (Pinnipedia, Phocidae) from the Miocene of the North Atlantic realm: redescription, phylogenetic affinities and paleobiogeographic implications. PeerJ 5:e3024.

Dewaele, L., O. Lambert, and S. Louwye. 2018. A critical revision of the fossil record, stratigraphy and diversity of the Neogene seal genus *Monotherium* (Carnivora, Phocidae). Royal Society Open Science 5:171669.

Downs, T. 1956. A new pinniped from the Miocene of Southern California: with remarks on the Otariidae. Journal of Paleontology 30:115–131.

Drehmer, C. J., D. Sanfelice, and C. Loch. 2015. Dental anomalies in pinnipeds (Carnivora: Otariidae and Phocidae): occurrence and evolutionary implications. Zoomorphology 134:325–338.

Domning, D. P. 2008. Desmostylia; pp. 640-645 in C. M. Janis, G. F. Gunnell, and M. D. Uhen (eds.), Evolution of Tertiary Mammals of North America, Volume II. Cambridge University Press, Cambridge, Massachusetts.

Flower, B. P., and J. P. Kennett. 1993. Middle Miocene ocean-climate transition: high resolution oxygen and carbon isotopic records from Deep Sea Drilling Project Site 588A, southwest Pacific. Integration The Vlsi Journal 8:811–843.

Goloboff, P. A., S. A. Catalano. 2016. TNT version 1.5, including a full implementation of phylogenetic morphometrics. Cladistics 32:221–238.

Illiger, C. 1811. Prodromus systematis mammalium et avium. Salfeld, Berlin, 304 pp.

Kellogg, R. 1922. Pinnipeds from Miocene and Pliocene deposits of California and a résumé of current theories regarding the origin of Pinnipedia. University of California Publications in Geological Sciences 13:23–132.

Kohno, N. 1996. Miocene pinniped *Allodesmus* (Mammalia: Carnivora); with special reference to the “Mito seal” from Ibaraki Prefecture, Central Japan. Transactions of the Proceedings of the Paleontological Society of Japan 181:388–404.

Kohno, N., L. G. Barnes, and K. Hirota. 1994. Miocene fossil pinnipeds of the genera *Prototaria* and *Neotherium* (Carnivora; Otariidae; Imagotariinae) in the North Pacific Ocean: evolution, relationships and distribution. The Island Arc 3:285–308.

Koretsky, I. A., and P. Holec. 2002. A primitive seal (Mammalia: Phocidae) from the Early Middle Miocene of Central Paratethys. Smithsonian Contributions to Paleobiology 93:163–178.

Linnaeus, C. 1758. Systema Naturae per Regna Tria Naturae, secundum Classes, Ordines, Genera, Species, cum Characteribus, Differentiis, Synonymis, Locis. Tomus I. Laurentii Salvii, Holmiae, Stockholm, 824 pp.

Lipps, J. H., and E. Mitchell. 1976. Trophic model for the adaptive radiations and extinctions of pelagic marine mammals. Paleontological Society 2:147–155.

Maddison, W.P., and D. R. Maddison. 2018 Mesquite: a modular system for evolutionary analysis. Version 3.51. Available at http://www.mesquiteproject.org. Accessed September 22, 2018.

Mitchell, E. 1966. The Miocene pinniped *Allodesmus*. University of California Publications in Geological Sciences 61:1–105.

Mitchell, E. 1968. The Mio-Pliocene pinniped *Imagotaria*. Journal of Fisheries Research Board of Canada 25:1843–1900.

Munthe, J., and M. C. Coombs. 1979. Miocene dome-skulled chalicotheres (Mammalia, Perissodactyla) from the western United States: a preliminary discussion of a bizarre structure. Journal of Paleon 53:77–91.

Nagao, T. 1941. An occurrence of a fossil sea lion in the Miocene deposits of Sinano, Japan. Journal of the Faculty of Science, Hokkaido Imperial University 6:75–84.

Packard, E. L., and R. Kellogg. 1934. A new cetothere from the Miocene Astoria Formation of Newport, Oregon. Contributions to Paleontology of the Carnegie Institution of Washington 447:1–62.

Poust, A., and R. W. Boessenecker. 2018. Expanding the geographic and geochronologic range of early pinnipeds: new specimens of *Enaliarctos* from Northern California and Oregon. Acta Palaeontologica Polonica 63: 25–40.

Prothero, D.R., C. Z. Bitboul, G. W. Moore, and E. J. Moore. 2001. Magnetic stratigraphy of the lower and middle Miocene Astoria Formation, Lincoln County, Oregon. Pacific Section SEPM Special Publication 91: 272–283.

Pyenson, N. D., R. B. Irmis, J. H. Lipps, L. G. Barnes, E. D. Mitchell, and S. A. McLeod. 2009. Origin of a widespread marine bonebed deposited during the middle Miocene Climatic Optimum. Geology 37:519–522.

R Core Team. 2019. R: a language and environment for statistical computing. R Foundation for Statistical Computing. Available at http://www.R-project.org/. Accessed December 18, 2018.

Rohlf, F.J. 2016. tpsDig 2, digitize landmarks and outlines. Version 2.31. Department of Ecology and Evolution, State University of New York at Stony Brook. Available at http://life.bio.sunysb.edu/morph/index.html. Accessed June 1, 2019.

Siversten, E. 1954. A survey of the eared seals (Family Otariidae) with remarks on the Antarctic seals collected by M/K <<Norvegia>> in 1928-1929. Det Norske Videnskaps-Akademi I Oslo 36:5–86.

Tonomori, W.H., H. Sawamura, T. Sato, and N. Kohno. 2018. A new Miocene pinniped *Allodesmus* (Mammalia: Carnivora) from Hokkaido, Northern Japan. Royal Society Open Science 5:172440.

Tsuchi, R. 1992. Neogene events in Japan and on the Pacific coast of South America. Revista Geológica de Chile: An International Journal on Andean Geology 19:67–73.

Valenzuela-Toro, A., and N. D. Pyenson. 2019. What do we know about the fossil record of pinnipeds? A historiographical investigation. Royal Society Open Science 6:1–18.

Winer, J. N., B. Arzi, D. M. Leale, P. H. Kass, and F. J. M. Verstraete. 2016. Dental and temporomandibular joint pathology of the walrus (*Odobenus rosmarus*). Journal of Comparative Pathology 155:242–253.

Chapter III

Adams, D., M. Collyer, A. Kaliontzopoulou, E. Baken. 2022. Geomorph: Software for geometric morphometric analyses. R package version 4.0.4. https://cran.r-project.org/package=geomorph

Allen, J. A. 1880. History of North American pinnipeds. US Geological and Geographical Survey of the Territories, Miscellaneous Publications 12:1–785

Amson, E., C. Argot, H. G. McDonald, and C. de Muizon. 2015. Osteology and functional morphology of the axial postcranium of the marine sloth *Thalassocnus* (Mammalia, Tardigrada) with paleobiological implications. Journal of Mammalian Evolution 473–518 pp.

Andersson, K. 2004. Elbow-joint morphology as a guide to forearm function and foraging behaviour in mammalian carnivores. Zoological Journal of the Linnean Society 142:91–104.

Arnason, U., A. Gullberg, A. Janke, M. Kullberg, N. Lehman, E. A. Petrov, and R. Väinölä. 2006. Pinniped phylogeny and a new hypothesis for their origin and dispersal. Molecular Phylogenetics and Evolution 41:345–354.

Backhouse, K. M. 1962. Locomotion of seals with particular reference to the forelimb. Symposia of the Zoological Society of London 5:59–75.

Baken, E., M. Collyer, A. Kaliontzopoulou, D. Adams. 2021. geomorph v4.0 and gmShiny: enhanced analytics and a new graphical interface for a comprehensive morphometric experience.

Bapst, D. W. 2012. Paleotree: An R package for paleontological and phylogenetic analyses of evolution. Methods in Ecology and Evolution 3:803–807.

Barnes, L. G. 1989. A new enaliarctine pinniped from the Astoria Formation, Oregon, and a classification of the Otariidae (Mammalia: Carnivora). Contributions in Science 403:1–26.

Barnes, L. G., and K. Hirota. 1994. Miocene pinnipeds of the otariid subfamily Allodesminae in the North Pacific Ocean: systematics and relationships. The Island Arc 3:329–360.

Bebej, R. M. 2009. Swimming mode inferred from skeletal proportions in the fossil pinnipeds *Enaliarctos* and *Allodesmus* (Mammalia, Carnivora). Journal of Mammalian Evolution 16:77–97.

Beentjes, M. P. 1990. Comparative terrestrial locomotion of the Hooker's sea lion (*Phocarctos hookeri*) and the New Zealand fur seal (*Arctocephalus forsteri*) and the evolutionary and ecological implications. Zoological Journal of the Linnean Society 98:307–325.

Bell, M. A., and G. T. Lloyd. 2015. Strap: an R package for plotting phylogenies against stratigraphy and assessing their stratigraphic congruence.

Berta, A. 1994. A new species of phocoid pinniped *Pinnarctidion* from the Early Miocene of Oregon. Journal of Vertebrate Paleontology 14:405–413.

Berta, A., and C. E. Ray. 1990. Skeletal morphology and locomotor capabilities of the archaic pinniped *Enaliarctos mealsi*. Journal of Vertebrate Paleontology 10:141–157.

Berta, A., and A. R. Wyss. 1994. Pinniped phylogeny. Contributions in Marine Mammal Paleontology Honoring Frank C. Whitmore, Jr.: Proceedings of the San Diego Society of Natural History 29:33–56.

Berta, A., and P. J. Adam. 2001. Evolutionary biology of pinnipeds; pp. 235–260 in J.-M. Mazin and V. de Buffrénil (eds.), Secondary Adaptation of Tetrapods to Life in Water. Verlag Dr. Friedrich Pfeil, Munich, Germany.

Berta, A., C. E. Ray, and A. R. Wyss. 1989. Skeleton of the oldest known pinniped, *Enaliarctos mealsi.* Science 244:60–92.

Berta, A., J. L. Sumich, K. M. Kovacs. 2015. Marine Mammals: Evolutionary Biology, 3rd ed. Academic Press, San Diego, California.

Berta, A., M. Churchill, and R. W. Boessenecker. 2018. The origin and evolutionary biology of pinnipeds: seals, sea lions, and walruses. Annual Review of Earth and Planetary Sciences 46:203–228.

Biewer, J. N., J. Velez-Juarbe, and J. F. Parham. 2020. Insights on the dental evolution of walruses based on new fossil specimens from California. Journal of Vertebrate Paleontology 40:1–42.

Boessenecker, R. W., and M. Churchill. 2015. The oldest known fur seal. Biology Letters 11.

Boessenecker, R. W., and M. Churchill. 2018. The last of the desmatophocid seals: a new species of *Allodesmus* from the upper Miocene of Washington, USA, and a revision of the taxonomy of Desmatophocidae. Zoological Journal of the Linnean Society XX:1–25.

Botton-Divet, L., R. Cornette, A. C. Fabre, A. Herrel, and A. Houssaye. 2016. Morphological analysis of long bones in semi-aquatic mustelids and their terrestrial relatives. Integrative and Comparative Biology 56:1298–1309.

Brusatte, S. L., M. J. Benton, M. Ruta, and G. T. Lloyd. 2008. Superiority, competition, and opportunism in the evolutionary radiation of dinosaurs. Science 321:1485–1488.

Campagna, C., R. Harcourt, R. Gentry, D. Costa, A. Valenzuela-Toro, M. Sepúlveda, T. Jeanniard-du-Dot, C. Guinet, D. Hocking, T. Park, J. Rule, F. Marx, M. Cassini, M. Kiyota, B. Le Boeuf, C. Bisioli, S. Ryazanov, C. Bonin, V. Franco-Trecu, J. Kingston Sinclair, S. Goldsworthy, I. Charrier, F. Hanke, C. Reichmuth, P. Cook, Z. Schakner, D. Blumstein, E. DeRango, J. Schwarz, C. Llamazares-Martín, E. Palagi, D. Rodríguez, G. Giardino, M. Mandiola, J. Gana, M. De León, J. Bastida, S. Morón, P. Denuncio, R. Bastida, E. Miller, A. Kochnev, A. Trites, E. Crespo, B. L. Chilvers, R. McIntosh, B. Pitcher, R. Kirkwood, F. Elorriaga-Verplancken, K. Acevedo-Whitehouse, T. Norris, A. Gutiérrez-Gutiérrez, M. José Amador-Capitanachi, A. Juárez-Ruiz, J. Sandoval-Sierra, C. Gálvez, X. Moreno-Sánchez, D. Naya, P. Inchausti, M. Riofrío-Lazo, and D. Páez-Rosas. 2021. Ethology and Behavioral Ecology of Otariids and the Odobenid. 667 pp.

Churchill, M., R. W. Boessenecker, and M. T. Clementz. 2014. Colonization of the Southern Hemisphere by fur seals and sea lions (Carnivora: Otariidae) revealed by combined evidence phylogenetic and Bayesian biogeographical analysis. Zoological Journal of the Linnean Society 172:200–225.

De Muizon, C. 1982. Phocid phylogeny and dispersal. Annals of the South African Museum 89: 175–213.

Deméré, T. A. 1994. Two new species of fossil walruses (Pinnipedia: Odobenidae) from the Upper Pliocene San Diego Formation, California. Proceedings of the San Diego Society of Natural History 29:77–98.

Deméré, T. A., and A. Berta. 2002. The Miocene pinniped *Desmatophoca oregonensis* Condon, 1906 (Mammalia: Carnivora), from the Astoria Formation, Oregon. Smithsonian Contributions to Paleobiology 93:113–147.

Dewaele, L., O. Lambert, and S. Louwye. 2017a. On *Prophoca* and *Leptophoca* (Pinnipedia, Phocidae) from the Miocene of the North Atlantic realm: Redescription, phylogenetic affinities and paleobiogeographic implications. PeerJ 2017:1–56.

Dewaele, L., E. Amson, O. Lambert, and S. Louwye. 2017b. Reappraisal of the extinct seal *"Phoca" vitulinoides* from the Neogene of the North Sea Basin, with bearing on its geological age, phylogenetic affinities, and locomotion. PeerJ 5:e3316:1–79.

Domning, D. P. 2002. The terrestrial posture of desmostylians; pp. 99–111 in R. J. Emry (ed.), Cenozoic Mammals of Land and Sea: Tributes to the Career of Clayon E. Ray. Smithsonian Contributions to Paleobiology 93.

English, A. W. 1976. Limb movements and locomotor function in the California sea lion (*Zalophus californianus*). Journal of Zoology 178:341–364.

English, A. W. M. 1977. Structural correlates of forelimb function in fur seals and sea lions. Journal of Morphology 151:325–352.

Fabre, A. C., A. Goswami, S. Peigné, and R. Cornette. 2014. Morphological integration in the forelimb of musteloid carnivorans. Journal of Anatomy 225:19–30.

Fabre, A. C., R. Cornette, A. Goswami, and S. Peigné. 2015. Do constraints associated with the locomotor habitat drive the evolution of forelimb shape? A case study in musteloid carnivorans. Journal of Anatomy 226:596–610.

Fay, F. H. 1982. Ecology and biology of the Pacific walrus, *Odobenus rosmarus divergens* Illiger. North American Fauna 74:1–279.

Feldkamp, S. D. 1987a. Foreflipper propulsion in the California sea lion, *Zalophus californianus*. Journal of Zoology 212:43–57.

Feldkamp, S. D. 1987b. Swimming in the California sea lion: morphometrics, drag and energetics. The Journal of Experimental Biology 131:117–135.

Finarelli, J. A. 2008. A total evidence phylogeny of the Arctoidea (Carnivora: Mammalia): Relationships among basal taxa. Journal of Mammalian Evolution 15:231–259.

Fish, F. E. 1994. Associatin of propulsive swimming mode with behavior in river otters (*Lutra canadensis*). Journal of Mammalogy 75:989–997.

Fish, F. E. 1996. Transitions from drag-based to lift-based propulsion in mammalian swimming. American Zoologist 36:628–641.

Fish, F. E. 2016. Secondary evolution of aquatic propulsion in higher vertebrates: validation and prospect. Integrative and Comparative Biology 56:1285–1297.

Fulton, T. L., C. Strobeck, and A. Crame. 2010. Multiple fossil calibrations, nuclear loci and mitochondrial genomes provide new insight into biogeography and divergence timing for true seals (Phocidae, Pinnipedia). Journal of Biogeography 37:814–829.

Furbish, R. 2015. Something old, something new, something swimming in the blue: an analysis of the pinniped family Desmatophocidae, its phylogenetic position and swimming mode. 75 pp.

Giffin, E. B. 1992. Functional implications of neural canal anatomy in recent and fossil marine carnivores. Journal of Morphology 214:357–374.

Gingerich, P. D. 2003. Land-to-sea transition in early whales: evolution of Eocene Archaeoceti (Cetacea) in relation to skeletal proportions and locomotion of living semiaquatic mammals. Paleobiology 29:429–454.

Gingerich, P. D. 2005. Aquatic adaptation and swimming mode inferred from skeletal proportions in the Miocene desmostylian *Desmostylus*. Journal of Mammalian Evolution 12:183–194.

Gordon, K. R. 1979. The analysis of locomotor behavior and functional morphology of the limbs of the walrus. University of California Press, Davis, California.

Gordon, K. R. 1981. Locomotor behaviour of the walrus. Journal of Zoology 195:349–367.

Gordon, K. R. 1983. Mechanics of the limbs of the walrus (*Odobenus rosmarus*) and the California sea lion (*Zalophus californianus*). Journal of Morphology 175:73–90.

Gray, J. E. 1821. On the natural arrangement of vertebrose animals. The London Medical Repository Monthly Journal and Review 15:296–310.

Gray, J. E. 1825. An outline of an attempt at the disposition of Mammalia into tribes and families, with a list of genera apparently appertaining to each tribe. Annals of Philosophy: New Series 10:337–344.

Gutarra, S., and I. A. Rahman. 2022. The locomotion of extinct secondarily aquatic tetrapods. Biological Reviews 97:67–98.

Hastie, T., R. Tibshirani, and A. Buja. 1994. Flexible discriminant analysis by optimal scoring. Journal of the American Statistical Association 89:1255.

Hay, O. P. 1930. Second bibliography and catalogue of the fossil Vertebrata of North America. Carnegie Institute of Washington Publication 390:1–1074.

Helle, E., H. Hyvärinen, and T. Sipilä. 1984. Breeding habitat and lair structure of the Saimaa ringed seal *Phoca hispida saimensis* in Finland. Acta Zoologica Fennica, 172:125–127.

Higdon, J. W., O. R. P. Bininda-Emonds, R. M. D. Beck, and S. H. Ferguson. 2007. Phylogeny and divergence of the pinnipeds (Carnivora: Mammalia) assessed using a multigene dataset. BMC Evolutionary Biology 7.

Hocking, D. P., F. G. Marx, S. Wang, D. Burton, M. Thompson, T. Park, B. Burville, H. L. Richards, R. Sattler, J. Robbins, R. P. Miguez, E. M. G. Fitzgerald, D. J. Slip, and A. R. Evans. 2021. Convergent evolution of forelimb-propelled swimming in seals. Current Biology 31:2404-2409.e2.

Hocking, D. P., M. A. Ladds, D. J. Slip, E. M. G. Fitzgerald, and A. R. Evans. 2017. Chew, shake, and tear: prey processing in Australian sea lions (*Neophoca cinerea*). Marine Mammal Science 33:541–557.

Hocking, D. P., B. Burville, W. M. G. Parker, A. R. Evans, T. Park, and F. G. Marx. 2020. Percussive underwater signaling in wild gray seals. Marine Mammal Science 36:728–732.

Hocking, D. P., F. G. Marx, R. Sattler, R. N. Harris, T. I. Pollock, K. J. Sorrell, E. M. G. Fitzgerald, M. R. McCurry, and A. R. Evans. 2018. Clawed forelimbs allow northern seals to eat like their ancient ancestors. Royal Society Open Science 5.

Howell, A. B. 1929. Contribution to the comparative anatomy of the eared and earless seals (genera *Zalophus* and *Phoca*). Proceedings of the United States National Museum 73:1–142.

Illiger, C. 1811. Prodromus systematis mammalium et avium. Salfeld, Berlin, 304 pp.

Jones, B., A. Martín-Serra, E. J. Rayfield, and C. M. Janis. 2022. Distal humeral morphology indicates locomotory divergence in extinct giant kangaroos. Journal of Mammalian Evolution 29:27–41.

Kellogg, A. R. 1922. Pinnipeds from Miocene and Pleistocene deposits of California. Bulletin of the Department of Geological Sciences, 13(4):23–132.

King, J. E. 1983. Seals of the World. Cornell University Press, Ithaca, New York, 240. pp.

Koretsky, I. A., and P. Holec. 2002. A primitive seal (Mammalia: Phocidae) from the Early Middle Miocene of Central Paratethys. Smithsonian Contributions to Paleobiology 93:163–178.

Koretsky, I. A., L. G. Barnes, and S. J. Rahmat. 2016. Re-evaluation of morphological characters questions current views of pinniped origins. Vestnik Zoologii 50:327–354.

Kuhn, C., and E. Frey. 2012. Walking like caterpillars, flying like bats--pinniped locomotion. Palaeobiodiversity and Palaeoenvironments 92:197–210.

Laakkonen, J., and H. Nihtilä. 2021. Comparison of the musculoskeletal forelimb anatomy of the Saimaa (*Pusa hispida saimensis*) and Baltic ringed seals (*Pusa hispida botnica*). Marine Mammal Science 37:1552–1563.

Linnaeus, C. 1758. Systema Naturae per Regna Tria Naturae, secundum Classes, Ordines, Genera, Species, cum Characteribus, Differentiis, Synonymis, Locis. Tomus I. Laurentii Salvii, Holmiae, Stockholm, 824 pp

Lone, K., K. M. Kovacs, C. Lydersen, M. Fedak, M. Andersen, P. Lovell, and J. Aars. 2018. Aquatic behaviour of polar bears (*Ursus maritimus*) in an increasingly ice-free Arctic. Scientific Reports 8:1–12.

Luan, P., O. A. Ryder, H. Davis, Y. Zhang, and L. Yu. 2013. Incorporating indels as phylogenetic characters: Impact for interfamilial relationships within Arctoidea (Mammalia: Carnivora). Molecular Phylogenetics and Evolution 66:748–756.

Lydersen, C., and I. Gjertz. 1986. Studies of the ringed seal (*Phoca hispida* Schreber 1775) in its breeding habitat in Kongsfjorden, Svalbard. Polar Research 4:57–63.

MacLaren, J. A., and S. Nauwelaerts. 2016. A three-dimensional morphometric analysis of upper forelimb morphology in the enigmatic tapir (Perissodactyla: Tapirus) hints at subtle variations in locomotor ecology. Journal of Morphology 277:1469–1485.

Magallanes, I., J. F. Parham, G. Santos, and J. Velez-Juarbe. 2018. A new tuskless walrus from the Miocene of Orange County, California, with comments on the diversity and taxonomy of odobenids. PeerJ 6:e5708:1–52.

Marramà, G., and J. Kriwet. 2017. Principal component and discriminant analyses as powerful tools to support taxonomic identification and their use for functional and phylogenetic signal detection of isolated fossil shark teeth. PLoS ONE 12:1–22.

Milne, N., S. F. Vizcaíno, and J. C. Fernicola. 2009. A 3D geometric morphometric analysis of digging ability in the extant and fossil cingulate humerus. Journal of Zoology 278:48–56.

Mitchell, E. 1966. The Miocene pinniped *Allodesmus*. University of California Publications in Geological Sciences 61:1–105.

Mitchell, E. 1968. The Mio-Pliocene pinniped *Imagotaria*. Journal of Fisheries Research Board of Canada 25:1843–1900.

Mongiardino Koch, N., R. J. Garwood, and L. A. Parry. 2021. Fossils improve phylogenetic analyses of morphological characters. Proceedings of the Royal Society B: Biological Sciences 288.

Morales-García, N. M., P. G. Gill, C. M. Janis, and E. J. Rayfield. 2021. Jaw shape and mechanical advantage are indicative of diet in Mesozoic mammals. Communications Biology 4:1–14.

Mori, K., S. Suzuki, D. Koyabu, J. Kimura, S. Y. Han, and H. Endo. 2015. Comparative functional anatomy of hindlimb muscles and bones with reference to aquatic adaptation of the sea otter. Journal of Veterinary Medical Science 77:571–578.

Motani, R., and L. Schmitz. 2011. Phylogenetic versus functional signals in the evolution of form-function relationships in terrestrial vision. Evolution 65:2245–2257.

Muir, S. F., D. K. A. Barnes, and K. Reid. 2006. Interactions between humans and leopard seals. Antarctic Science 18:61–74.

Muñoz, N. A. 2021. Locomotion in rodents and small carnivorans: are they so different? Journal of Mammalian Evolution 28:87–98.

Murie, J. 1870. Researches upon the anatomy of the Pinnipedia--Part I. On the walrus (*Trichechus rosmarus*, Linn.). The Transactions of the Zoological Society of London 7:411–463.

Nyakatura, K., and O. R. P. Bininda-Emonds. 2012. Updating the evolutionary history of Carnivora (Mammalia): A new species-level supertree complete with divergence time estimates. BMC Biology 10.

O'Reilly, J. E., M. N. Puttick, D. Pisani, and P. C. J. Donoghue. 2018. Probabilistic methods surpass parsimony when assessing clade support in phylogenetic analyses of discrete morphological data. Palaeontology 61:105–118.

Pagel, M. 1999. Inferring the historical patterns of biological evolution. Nature 401:877–884.

Paterson, R. 2017. Evidence for independent acquisition of aquatic specializations in pinnipeds (seals, sea lions, and walruses): insights from study of the phylogenetic position, locomotor behaviour and description of the stem pinniped, *Puijila darwini*.

Paterson, R. S., N. Rybczynski, N. Kohno, and H. C. Maddin. 2020. A total evidence phylogenetic analysis of pinniped phylogeny and the possibility of parallel evolution within a monophyletic framework. Frontiers in Ecology and Evolution 7:1–16.

Puttick, M. N., J. E. O'Reilly, D. Pisani, and P. C. J. Donoghue. 2019. Probabilistic methods outperform parsimony in the phylogenetic analysis of data simulated without a probabilistic model. Palaeontology 62:1–17.

R Core Team. 2021. R: a language and environment for statistical computing. R Foundation for Statistical Computing. Available at www.R- project.org. Accessed December 19, 2022.

R Project Team. 2017. mda: Mixture and flexible discriminant analysis. v.0.5-2.

Ray, G. C. 1963. Locomotion in pinnipeds. Natural History. 72:10–21.

Revell, L. J. 2012. phytools: an R package for phylogenetic comparative biology (and other things). Methods in Ecology and Evolution 3:217–223.

Richards, H. L., D. S. Rovinsky, J. W. Adams, and A. R. Evans. 2022. Inferring the palaeobiology of palorchestid marsupials through analysis of mammalian humeral and femoral shape. Journal of Mammalian Evolution.

Rohlf, F. J., and D. Slice. 1990. Extensions of the Procrustes method for the optimal superimposition of landmarks. Systematic Zoology 39:40–59.

Rule, J. P., J. W. Adams, F. G. Marx, A. R. Evans, A. J. D. Tennyson, R. P. Scofield, and E. M. G. Fitzgerald. 2020. First monk seal from the Southern Hemisphere rewrites the evolutionary history of true seals. Proceedings. Biological Sciences 287:20202318.

Samuels, J. X., J. A. Meachen, and S. A. Sakai. 2013. Postcranial morphology and the locomotor habits of living and extinct carnivorans. Journal of Morphology 274:121–146.

Savage, R. J. G. 1957. The anatomy of *Potamotherium* an Oligocene lutrine. Journal of Zoology 129:151–244.

Schutz, H., and R. P. Guralnick. 2007. Postcranial element shape and function: assessing locomotor mode in extant and extinct mustelid carnivorans. Zoological Journal of the Linnean Society 150:895–914.

Simpson, G. G. 1945. The principles of classification and a classification of mammals. American Museum of Natural History, 85.

Smith, M. R. 2019. Bayesian and parsimony approaches reconstruct informative trees from simulated morphological datasets. Biology Letters 15.

Stirling, I. 1977. Adaptations of Weddell and ringed seals to exploit the polar fast ice habitat in the absence or presence of surface predators. In G. A. Llano (ed.), Adaptations within Antarctic ecosystems (pp. 741–748). Proceedings of the 3rd Scientific Committee on Antarctic Research Symposium on Antarctic Biology, Washington, DC.

Tanaka, Y., and N. Kohno. 2015. A new late Miocene odobenid (Mammalia: Carnivora) from Hokkaido, Japan suggests rapid diversification of basal Miocene odobenids. PLoS ONE 10.

Tarasoff, F. J., A. Bisaillon, J. Piérard, and A. P. Whitt. 2008. Locomotory patterns and external morphology of the river otter, sea otter, and harp seal (Mammalia). Canadian Journal of Zoology 50:915–929.

Tate-Jones, M. K., C. M. Peredo, C. D. Marshall, and S. S. B. Hopkins. 2020. The dawn of Desmatophocidae: a new species of basal desmatophocid seal (Mammalia, Carnivora) from the Miocene of Oregon, U.S.A. Journal of Vertebrate Paleontology 40:1–11.

Tonomori, W., H. Sawamura, T. Sato, and N. Kohno. 2018. A new Miocene pinniped *Allodesmus* (Mammalia: Carnivora) from Hokkaido, Northern Japan. Royal Society Open Science 5.

Valenzuela-Toro, A., N. D. Pyenson, and P. Koch. 2018. How good is the fossil record of pinnipeds? A historiographic evaluation of its biases and modes. Society of Vertebrate Paleontology Program and Abstract Book.

Velez-Juarbe, J. 2017. *Eotaria citrica, sp. nov.,* a new stem otariid from the “Topanga” formation of Southern California. PeerJ 2017:1–25.

Velez-Juarbe, J. 2018. New data on the early odobenid *Neotherium mirum* Kellogg, 1931, and other pinniped remains from the Sharktooth Hill Bonebed, California. Journal of Vertebrate Paleontology 38:1–14.

Wickham, H. 2016. ggplot2: elegant graphics for data analysis. Spring-Verlag, New York, New York.

Wyss, A. R. 1988. Evidence from flipper structure for a single origin of pinnipeds. Nature 334:427–428.

Zelditch, M. L., D. L. Swiderski, and H. D. Sheets. 2004. Geometric morphometrics for biologicals: a primer. Elsevier Academic Press, London, United Kingdom.

Chapter IV

Aiello-Lammens, M.E., Boria, R.A., Radosavljevic, A., Vilela, B. & Anderson, R.P. (2015) spThin: An R package for spatial thinning of species occurrence records for use in ecological niche models. Ecography 38, 541–545. https://doi.org/10.1111/ecog.01132

Alonso-Garcia, M., Sierro, F.J., Kucera, M., Flores, J.A., Cacho, I. & Andersen, N. (2011) Ocean circulation, ice sheet growth and interhemispheric coupling of millennial climate variability during the mid-Pleistocene (ca 800-400ka). Quaternary Science Reviews 30, 3234–3247. https://doi.org/10.1016/j.quascirev.2011.08.005

Amiraux, R., Rontani, J.-F., Armougom, F., Frouin, E., Babin, M., Artigue, L. & Bonin, P. (2021) Bacterial diversity and lipid biomarkers in sea ice and sinking particulate organic material during the melt season in the Canadian Arctic. Elementa: Science of the Anthropocene 9. https://doi.org/10.1525/elementa.2019.040

Anderson, M.J. (2001) A new method for non-parametric multivariate analysis of variance. Austral Ecology 26, 32–46. https://doi.org/10.1046/j.1442-9993.2001.01070.x

Anderson, M.J. (2006) Distance-based tests for homogeneity of multivariate dispersions. Biometrics 62, 245–253. https://doi.org/10.1111/j.1541-0420.2005.00440.x

Anderson, M.J. & Walsh, D.C.I. (2013) PERMANOVA, ANOSIM, and the Mantel test in the face of heterogeneous dispersions: What null hypothesis are you testing? Ecological Monographs 83, 557–574. https://doi.org/10.1890/12-2010.1

Årthun, M., Onarheim, I.H., Dörr, J. & Eldevik, T. (2021) The seasonal and regional transition to an ice-free Arctic. Geophysical Research Letters 48. https://doi.org/10.1029/2020GL090825

Assis, J., Tyberghein, L., Bosch, S., Verbruggen, H., Serrão, E.A. & De Clerck, O. (2018) Bio-ORACLE v2.0: Extending marine data layers for bioclimatic modelling. Global Ecology and Biogeography 27, 277–284. https://doi.org/10.1111/geb.12693

Batchelor, C.L., Margold, M., Krapp, M., Murton, D.K., Dalton, A.S., Gibbard, P.L., Stokes, C.R., Murton, J.B. & Manica, A. (2019) The configuration of Northern Hemisphere ice sheets through the Quaternary. Nature Communications 10, 1–10. https://doi.org/10.1038/s41467-019-11601-2

Beatty, W.S., Jay, C. V., Fischbach, A.S., Grebmeier, J.M., Taylor, R.L., Blanchard, A.L. & Jewett, S.C. (2016) Space use of a dominant Arctic vertebrate: Effects of prey, sea ice, and land on Pacific walrus resource selection. Biological Conservation 203, 25–32. https://doi.org/10.1016/j.biocon.2016.08.035

Berends, C.J., De Boer, B. & Van De Wal, R.S.W. (2021) Reconstructing the evolution of ice sheets, sea level, and atmospheric CO2during the past 3.6 million years. Climate of the Past 17, 361–377. https://doi.org/10.5194/cp-17-361-2021

Bloxam, Q.M.C. & Tonge, S.J. (1995) Amphibians: suitable candidates for breeding-release programmes. Review of Industrial Organization 4, 636–644. https://doi.org/10.1007/BF00222519

Boessenecker, R.W. & Churchill, M. (2021) The surprising evolutionary heritage of the Atlantic walrus as chronicled by the fossil record. INC. https://doi.org/10.1016/b978-0-12-817430-2.00006-6

Bonan, D.B., Lehner, F. & Holland, M.M. (2021) Partitioning uncertainty in projections of Arctic sea ice. Environmental Research Letters 16. https://doi.org/10.1088/1748-9326/abe0ec

Boria, R.A., Olson, L.E., Goodman, S.M. & Anderson, R.P. (2014) Spatial filtering to reduce sampling bias can improve the performance of ecological niche models. Ecological Modelling 275, 73–77. https://doi.org/10.1016/j.ecolmodel.2013.12.012

Borisiak, A.A. (1930) A fossil walrus from the Okhotsk coast. Ezhegodnik Russian Paleontology 8.

Born, E.W., Acquarone, M., Knutsen, L.Ø. & Toudal, L. (2005) Homing behaviour in an Atlantic walrus (Odobenus rosmarus rosmarus). Aquatic Mammals 31, 23–33. https://doi.org/10.1578/am.31.1.2005.23

Born, E.W., Gjertz, I. & Reeves, R.R. (1995) Population assessment of Atlantic walrus (Odobenus rosmarus rosmarus L.).

Bosch, S., Tyberghein, L. & De Clerck, O. (2017) sdmpredictors: an R package for species distribution modelling predictor datasets.

Campagna, C., R. Harcourt, R. Gentry, D. Costa, A. Valenzuela-Toro, M. Sepúlveda, T. Jeanniard-du-Dot, C. Guinet, D. Hocking, T. Park, J. Rule, F. Marx, M. Cassini, M. Kiyota, B. Le Boeuf, C. Bisioli, S. Ryazanov, C. Bonin, V. Franco-Trecu, J. Kingston Sinclair, S. Goldsworthy, I. Charrier, F. Hanke, C. Reichmuth, P. Cook, Z. Schakner, D. Blumstein, E. DeRango, J. Schwarz, C. Llamazares-Martín, E. Palagi, D. Rodríguez, G. Giardino, M. Mandiola, J. Gana, M. De León, J. Bastida, S. Morón, P. Denuncio, R. Bastida, E. Miller, A. Kochnev, A. Trites, E. Crespo, B. L. Chilvers, R. McIntosh, B. Pitcher, R. Kirkwood, F. Elorriaga-Verplancken, K. Acevedo-Whitehouse, T. Norris, A. Gutiérrez-Gutiérrez, M. José Amador-Capitanachi, A. Juárez-Ruiz, J. Sandoval-Sierra, C. Gálvez, X. Moreno-Sánchez, D. Naya, P. Inchausti, M. Riofrío-Lazo, and D. Páez-Rosas. 2021. Ethology and Behavioral Ecology of Otariids and the Odobenid. 667 pp.

Clarke, A. & Peck, L.S. (1991) The physiology of polar marine zooplankton. Polar Research 10, 355–370. https://doi.org/10.3402/polar.v10i2.6752

Davis, E.B., Mcguire, J.L. & Orcutt, J.D. (2014) Ecological niche models of mammalian glacial refugia show consistent bias. Ecography 37, 1133–1138. https://doi.org/10.1111/ecog.01294

Dennis, R.L.H. & Thomas, C.D. (2000) Bias in butterfly distribution maps the influence of hot spots and recorder's home range. Journal of Insect Conservation 4, 73–77.

Diebold, F.X. & Rudebusch, G.D. (2021) Probability assessments of an ice-free Arctic: comparing statistical and climate model projections. Journal of Econometrics. https://doi.org/10.1016/j.jeconom.2020.12.007

Dietl, G.P., Kidwell, S.M., Brenner, M., Burney, D.A., Flessa, K.W., Jackson, S.T. & Koch, P.L. (2015) Conservation paleobiology: leveraging knowledge of the past to inform conservation and restoration. Annual Review of Earth and Planetary Sciences 43, 79–103. https://doi.org/10.1146/annurev-earth-040610-133349

Divoky, G.J., Lukacs, P.M. & Druckenmiller, M.L. (2015) Effects of recent decreases in Arctic sea ice on an ice-associated marine bird. Progress in Oceanography 136, 151–161. https://doi.org/10.1016/j.pocean.2015.05.010

Van Dolah, R.F., Hyland, J.L., Holland, A.F., Rosen, J.S. & Snoots, T.R. (1999) A benthic index of biological integrity for assessing habitat quality in estuaries of the southeastern USA. Marine Environmental Research 48, 269–283. https://doi.org/10.1016/S0141-1136(99)00056-2

Dormann, C.F., Elith, J., Bacher, S., et al. (2013) Collinearity: a review of methods to deal with it and a simulation study evaluating their performance. Ecography 36, 27–46. https://doi.org/10.1111/j.1600-0587.2012.07348.x

Elith, J., Graham, C.H., Anderson, R.P., et al. (2006) Novel methods improve prediction of species' distributions from occurrence data. Ecography 29, 129–151.

Elith, J., Kearney, M. & Phillips, S. (2010) The art of modelling range-shifting species. Methods in Ecology and Evolution 1, 330–342. https://doi.org/10.1111/j.2041-210x.2010.00036.x

Fay, F.H. (1982) Ecology and biology of the Pacific walrus, *Odobenus rosmarus divergens* Illiger. North American Fauna 74, 1–279. https://doi.org/10.3996/nafa.74.0001

Fay, F.H. (1985) *Odobenus rosmarus*. Mammalian Species, 1–7.

Feng, X. & Papeş, M. (2017) Physiological limits in an ecological niche modeling framework: A case study of water temperature and salinity constraints of freshwater bivalves invasive in USA. Ecological Modelling 346, 48–57. https://doi.org/10.1016/j.ecolmodel.2016.11.008

Fischbach, A.S., Monson, D.H., Jay, C. V & Interior, U.S.D. of the (2009) Enumeration of Pacific walrus carcasses on beaches of the Chukchi Sea in Alaska following a mortality event, September 2009. Open-File Report, 10.

Fourcade, Y., Engler, J.O., Rödder, D. & Secondi, J. (2014) Mapping species distributions with MAXENT using a geographically biased sample of presence data: A performance assessment of methods for correcting sampling bias. PLoS ONE 9, 1–13. https://doi.org/10.1371/journal.pone.0097122

García-Roselló, E., Guisande, C., Manjarrés-Hernández, A., et al. (2015) Can we derive macroecological patterns from primary Global Biodiversity Information Facility data? Global Ecology and Biogeography 24, 335–347. https://doi.org/10.1111/geb.12260

Garde, E., Jung-Madsen, S., Ditlevsen, S., Hansen, R.G., Zinglersen, K.B. & Heide-Jørgensen, M.P. (2018) Diving behavior of the Atlantic walrus in high Arctic Greenland and Canada. Journal of Experimental Marine Biology and Ecology 500, 89–99. https://doi.org/10.1016/j.jembe.2017.12.009

Garlich-Miller, J., MacCracken, J.G., Snyder, J., Meehan, R., Myers, M., Wilder, J.M., Lance, E. & Matz, A. (2011) Status review of the Pacific walrus (*Odobenus rosmarus divergens*).

GBIF.org (30 July 2021) GBIF Occurrence Download https://www.gbif.org/occurrence/download/0334982-200613084148143

Gebruk, A., Mikhaylyukova, P., Mardashova, M., Semenova, V., Henry, L.A., Shabalin, N., Narayanaswamy, B.E. & Mokievsky, V. (2021) Integrated study of benthic foraging resources for Atlantic walrus (*Odobenus rosmarus rosmarus*) in the Pechora Sea, south-eastern Barents Sea. Aquatic Conservation: Marine and Freshwater Ecosystems 31, 112–125. https://doi.org/10.1002/aqc.3418

Gjertz, I., Henriksen, G., Øritsland, T. & Wiig, Ø. (1993) Observations of walruses along the Norwegian coast 1967–1992. Polar Research 12, 27–31. https://doi.org/10.3402/polar.v12i1.6700

Glazov, D.M., Shpak, O. V., Kuznetsova, D.M., Solovyev, B.A., Udovik, D.A., Platonov, N.G., Mordvintsev, I.N., Ivanov, D.I. & Rozhnov, V. V. (2013) Observations of the walrus (*Odobenus rosmarus*) in the Barents, Kara, and Laptev seas in 2010-2012. Biology Bulletin 40, 783–789. https://doi.org/10.1134/S1062359013090057

Goertz, C.E.C., Polasek, L., Burek, K., Suydam, R. & Sformo, T. (2017) Demography and pathology of a Pacific walrus (*Odobenus rosmarus divergens*) mass-mortality event at Icy Cape, Alaska, September 2009. Polar Biology 40, 989–996. https://doi.org/10.1007/s00300-016-2023-x

Green, R.H. (1973) Growth and mortality in an Arctic intertidal population of *Macoma balthica* (Pelecypoda, Tellinidae). Journal of the Fisheries Research Board of Canada 30, 1345–1348. https://doi.org/10.1139/f73-215

De Groeve, J., Kusumoto, B., Koene, E., et al. (2022) Global raster dataset on historical coastline positions and shelf sea extents since the Last Glacial Maximum. Global Ecology and Biogeography 31, 2162–2171. https://doi.org/10.1111/geb.13573

Gross, M. (2018) Arctic shipping threatens wildlife. Current Biology 28, R803–R805. https://doi.org/10.1016/j.cub.2018.07.053

Guarino, M.V., Sime, L.C., Schröeder, D., et al. (2020) Sea-ice-free Arctic during the Last Interglacial supports fast future loss. Nature Climate Change 10, 928–932. https://doi.org/10.1038/s41558-020-0865-2

Harington, C.R. (2008) The evolution of Arctic marine mammals. Ecological Applications 18, 23–40. https://doi.org/10.1890/06-0624.1

Hernandez, P.A., Graham, C.H., Master, L.L. & Albert, D.L. (2006) The effect of sample size and species characteristics on performance of different species distribution modeling methods. Ecography 29, 773–785. https://doi.org/10.1111/j.0906-7590.2006.04700.x

Higdon, J.W. & Stewart, D.B. (2018) State of circumpolar walrus (*Odobenus rosmarus*) populations.

Hijmans, R.J. (2020) raster: geographic data analysis and modeling. R package version 3.3-7. https://CRAN.R-project.org/package=raster

Hijmans, A.R.J., Phillips, S., Leathwick, J., Elith, J. & Hijmans, M.R.J. (2017) Package 'dismo.' Circles 9, 1–68.

Hocking, D.P., Park, T., Rule, J.P. & Marx, F.G. (2021) Prey Capture and processing in fur seals, sea lions and the walrus. In: Ethology and Behavioral Ecology of Marine Mammals. (ed. by C. Campagna and R. Harcourt), pp. 101–121, Springer Nature Switzerland AG. https://doi.org/10.1007/978-3-030-59184-7_5

Huntington, H.P., Danielson, S.L., Wiese, F.K., et al. (2020) Evidence suggests potential transformation of the Pacific Arctic ecosystem is underway. Nature Climate Change 10, 342–348. https://doi.org/10.1038/s41558-020-0695-2

Jacobs, P., Lenssen, N., Schmidt, G. & Rohde, R. (2021) The Arctic is now warming four times as fast as the rest of the globe. In: AGU Fall Meeting.

Jahn, A., Kay, J.E., Holland, M.M. & Hall, D.M. (2016) How predictable is the timing of a summer ice-free Arctic? Geophysical Research Letters 43, 9113–9120. https://doi.org/10.1002/2016GL070067

Jarvie, S., Worthy, T.H., Saltré, F., Scofield, R.P., Seddon, P.J. & Cree, A. (2021) Using Holocene fossils to model the future: Distribution of climate suitability for tuatara, the last rhynchocephalian. Journal of Biogeography 48, 1489–1502. https://doi.org/10.1111/jbi.14092

Jay, C. V. & Fischbach, A.S. (2010) Pacific walrus response to Arctic sea ice losses.

Jay, C. V., Fischbach, A.S. & Kochnev, A.A. (2012) Walrus areas of use in the Chukchi Sea during sparse sea ice cover. Marine Ecology Progress Series 468, 1–13. https://doi.org/10.3354/meps10057

Jay, C. V., Marcot, B.G. & Douglas, D.C. (2011) Projected status of the Pacific walrus (*Odobenus rosmarus divergens*) in the twenty-first century. Polar Biology 34, 1065–1084. https://doi.org/10.1007/s00300-011-0967-4

Jay, C. V., Taylor, R.L., Fischbach, A.S., Udevitz, M.S. & Beatty, W.S. (2017) Walrus haul-out and in water activity levels relative to sea ice availability in the Chukchi Sea. Journal of Mammalogy 98, 386–396. https://doi.org/10.1093/jmammal/gyw195

Jefferson, G.T. (1991) A catalogue of late Quaternary vertebrates from California: Part one, nonmarine lower vertebrate and avian taxa. Natural History Museum of Los Angeles County: Technical Reports 5, 60.

Kadmon, R., Farber, O. & Danin, A. (2004) Effect of roadside bias on the accuracy of predictive maps produced by bioclimatic models. Ecological Applications 14, 401–413. https://doi.org/10.1890/02-5364

Kaky, E., Nolan, V., Alatawi, A. & Gilbert, F. (2020) A comparison between Ensemble and MaxEnt species distribution modelling approaches for conservation: a case study with Egyptian medicinal plants. Ecological Informatics 60, 101150. https://doi.org/10.1016/j.ecoinf.2020.101150

Kass, J.M., Muscarella, R., Galante, P.J., Bohl, C.L., Pinilla-Buitrago, G.E., Boria, R.A., Soley-Guardia, M. & Anderson, R.P. (2021) ENMeval 2.0: Redesigned for customizable and reproducible modeling of species' niches and distributions. Methods in Ecology and Evolution 12, 1602–1608. https://doi.org/10.1111/2041-210X.13628

Katz, T.S. & Zellmer, A.J. (2018) Comparison of model selection technique performance in predicting the spread of newly invasive species: a case study with *Batrachochytrium salamandrivorans*. Biological Invasions 20, 2107–2119. https://doi.org/10.1007/s10530-018-1690-7

Keighley, X., Pálsson, S., Einarsson, B.F., Petersen, A., Fernández-Coll, M., Jordan, P., Olsen, M.T. & Malmquist, H.J. (2019) Disappearance of Icelandic walruses coincided with Norse settlement. Molecular Biology and Evolution 36, 2656–2667. https://doi.org/10.1093/molbev/msz196

Kovacs, K.M., Aars, J. & Lydersen, C. (2014) Walruses recovering after 60+ years of protection in Svalbard, Norway. Polar Research 33. https://doi.org/10.3402/polar.v33.26034

Kramer-Schadt, S., Niedballa, J., Pilgrim, J.D., et al. (2013) The importance of correcting for sampling bias in MaxEnt species distribution models. Diversity and Distributions 19, 1366–1379. https://doi.org/10.1111/ddi.12096

Kryukova, N. V., Kruchenkova, E.P. & Ivanov, D.I. (2012) Killer whales (*Orcinus orca*) hunting for walruses (*Odobenus rosmarus divergens*) near Retkyn Spit, Chukotka. Biology Bulletin 39, 768–778. https://doi.org/10.1134/S106235901209004X

Laidre, K.L., Stern, H., Kovacs, K.M., et al. (2015) Arctic marine mammal population status, sea ice habitat loss, and conservation recommendations for the 21st century. Conservation Biology 29, 724–737. https://doi.org/10.1111/cobi.12474

Legendre, P., & Legendre, L. (1998) Numerical Ecology. Elsevier.

Lefebvre, K.A., Fachon, E., Bowers, E.K., et al. (2022) Paralytic shellfish toxins in Alaskan Arctic food webs during the anomalously warm ocean conditions of 2019 and estimated toxin doses to Pacific walruses and bowhead whales. Harmful Algae 114, 102205. https://doi.org/10.1016/j.hal.2022.102205

Lima-Ribeiro, M.S., Moreno, A.K.M., Terribile, L.C., Caten, C.T., Loyola, R., Rangel, T.F. & Diniz-Filho, J.A.F. (2017) Fossil record improves biodiversity risk assessment under future climate change scenarios. Diversity and Distributions 23, 922–933. https://doi.org/10.1111/ddi.12575

Lindqvist, C., Bachmann, L., Andersen, L.W., Born, E.W., Arnason, U., Kovacs, K.M., Lydersen, C., Abramov, A. V. & Wiig, Ø. (2009) The Laptev Sea walrus *Odobenus rosmarus laptevi*: An enigma revisited. Zoologica Scripta 38, 113–127. https://doi.org/10.1111/j.1463-6409.2008.00364.x

Linnaeus, C. (1758) Systema Naturae per Regna Tria Naturae, secundum Classes, Ordines, Genera, Species, cum Characteribus, Differentiis, Synonymis, Locis. Tomus I. Laurentii Salvii, Holmiae, Stockholm, Sweden.

Lisiecki, L.E. & Raymo, M.E. (2005) A Pliocene-Pleistocene stack of 57 globally distributed benthic δ 18O records. Paleoceanography 20, 1–17. https://doi.org/10.1029/2004PA001071

Lowther, A.D., Kovacs, K.M., Griffiths, D. & Lydersen, C. (2015) Identification of motivational state in adult male Atlantic walruses inferred from changes in movement and diving behavior. Marine Mammal Science 31, 1291–1313. https://doi.org/10.1111/mms.12224

Lydersen, C., Chernook, V.I., Glazov, D.M., Trukhanova, I.S. & Kovacs, K.M. (2012) Aerial survey of Atlantic walruses (*Odobenus rosmarus rosmarus*) in the Pechora Sea, August 2011. Polar Biology 35, 1555–1562. https://doi.org/10.1007/s00300-012-1195-2

MacCracken, J.G. (2012) Pacific walrus and climate change: observations and predictions. Ecology and Evolution 2, 2072–2090. https://doi.org/10.1002/ece3.317

Maguire, K.C., Nieto-Lugilde, D., Fitzpatrick, M.C., Williams, J.W. & Blois, J.L. (2015) Modeling species and community responses to past, present, and future episodes of climatic and ecological change. Annual Review of Ecology, Evolution, and Systematics 46, 343–368. https://doi.org/10.1146/annurev-ecolsys-112414-054441

Mäkinen, J. & Vanhatalo, J. (2018) Hierarchical Bayesian model reveals the distributional shifts of Arctic marine mammals. Diversity and Distributions 24, 1381–1394. https://doi.org/10.1111/ddi.12776

McLeod, B.A., Frasier, T.R. & Lucas, Z. (2014) Assessment of the extirpated Maritimes walrus using morphological and ancient DNA analysis. PLoS ONE 9, 1–14. https://doi.org/10.1371/journal.pone.0099569

Meehl, G.A., Chung, C.T.Y., Arblaster, J.M., Holland, M.M. & Bitz, C.M. (2018) Tropical decadal variability and the rate of Arctic sea ice decrease. Geophysical Research Letters 45, 11,326-11,333. https://doi.org/10.1029/2018GL079989

Metcalf, V. & Robards, M. (2008) Sustaining a healthy human-walrus relationship in a dynamic environment: Challenges for comanagement. Ecological Applications 18, 148–156. https://doi.org/10.1890/06-0642.1

Moreno-Amat, E., Mateo, R.G., Nieto-Lugilde, D., Morueta-Holme, N., Svenning, J.C. & García-Amorena, I. (2015) Impact of model complexity on cross-temporal transferability in Maxent species distribution models: An assessment using paleobotanical data. Ecological Modelling 312, 308–317. https://doi.org/10.1016/j.ecolmodel.2015.05.035

Muscarella, R., Galante, P.J., Soley-Guardia, M., Boria, R.A., Kass, J.M., Uriarte, M. & Anderson, R.P. (2014) ENMeval: An R package for conducting spatially independent evaluations and estimating optimal model complexity for Maxent ecological niche models. Methods in Ecology and Evolution 5, 1198–1205. https://doi.org/10.1111/2041-210x.12261

Myers, C.E., Stigall, A.L. & Lieberman, B.S. (2015) PaleoENM: Applying ecological niche modeling to the fossil record. Paleobiology 41, 226–244. https://doi.org/10.1017/pab.2014.19

Naimi, B. (2015) usdm: Uncertainty analysis for species distribution models. R package version 1.1.

Notz, D. & Stroeve, J. (2018) The trajectory towards a seasonally ice-free Arctic Ocean. Current Climate Change Reports 4, 407–416. https://doi.org/10.1007/s40641-018-0113-2

Ocean Biodiversity Information System (30 November 2021) www.iobis.org

Oksanen, A.J., Blanchet, F.G., Friendly, M., et al. (2018) Package 'vegan' , 1–286.

Øren, K., Kovacs, K.M., Yoccoz, N.G. & Lydersen, C. (2018) Assessing site-use and sources of disturbance at walrus haul-outs using monitoring cameras. Polar Biology 41, 1737–1750. https://doi.org/10.1007/s00300-018-2313-6

Osman, M.B., Tierney, J.E., Zhu, J., Tardif, R., Hakim, G.J., King, J. & Poulsen, C.J. (2021) Globally resolved surface temperatures since the Last Glacial Maximum. Nature 599, 239–244. https://doi.org/10.1038/s41586-021-03984-4

Overland, J.E. & Wang, M. (2013) When will the summer Arctic be nearly sea ice free? Geophysical Research Letters 40, 2097–2101. https://doi.org/10.1002/grl.50316

Ovsyanikov, N.G., Menyushina, I.E., and Bezrukov, A.V. (2008) Collection of Scientific Papers from the Marine Mammals of the Holarctic V Conference, Odessa, Ukraine.

Pearson, R.G., Raxworthy, C.J., Nakamura, M. & Townsend Peterson, A. (2007) Predicting species distributions from small numbers of occurrence records: a test case using cryptic geckos in Madagascar. Journal of Biogeography 34, 102–117. https://doi.org/10.1111/j.1365-2699.2006.01594.x

Peters, S.E. & McClennen, M. (2015) The Paleobiology Database application programming interface. Paleobiology 42, 1–7. https://doi.org/10.1017/pab.2015.39

Phillips, S.J., Anderson, R.P., Dudík, M., Schapire, R.E. & Blair, M.E. (2017) Opening the black box: an open-source release of Maxent. Ecography 40, 887–893. https://doi.org/10.1111/ecog.03049

Phillips, S.J., Dudík, M. & Schapire, R.E. (2004) A maximum entropy approach to species distribution modeling. Proceedings, Twenty-First International Conference on Machine Learning, ICML 2004, 655–662. https://doi.org/10.1145/1015330.1015412

Post, E., Bhatt, U.S., Bitz, C.M., Brodie, J.F., Fulton, T.L., Hebblewhite, M., Kerby, J., Kutz, S.J., Stirling, I. & Walker, D.A. (2013) Ecological consequences of sea-ice decline. Science 341, 519–525.

Pourmozaffar, S., Tamadoni Jahromi, S., Rameshi, H., Sadeghi, A., Bagheri, T., Behzadi, S., Gozari, M., Zahedi, M.R. & Abrari Lazarjani, S. (2020) The role of salinity in physiological responses of bivalves. Reviews in Aquaculture 12, 1548–1566. https://doi.org/10.1111/raq.12397

QGIS Development Team. (2022) QGIS Geographic Information System. Open Source Geospatial Foundation Project. http://qgis.osgeo.org

R Core Team. (2021) R: a language and environment for statistical computing, R Foundation for Statistical Computing, Vienna, Austria. http://www.R-project.org/

Radosavljevic, A. & Anderson, R.P. (2014) Making better MAXENT models of species distributions: complexity, overfitting and evaluation. Journal of Biogeography 41, 629–643. https://doi.org/10.1111/jbi.12227

Rantanen, M., Karpechko, A.Y., Lipponen, A., Ruosteenoja, K., Vihma, T., Laaksonen, A., Nordling, K. & Hyvärinen, O. (2021) The Arctic has warmed nearly four times faster than the globe since 1979. Communication 3, 1–10. https://doi.org/10.1038/s43247-022-00498-3

Ray, G.C., Hufford, G.L., Overland, J.E., Krupnik, I., McCormick-Ray, J., Frey, K. & Labunski, E. (2016) Decadal Bering Sea seascape change: consequences for Pacific walruses and indigenous hunters. Ecological Applications 26, 24–41. https://doi.org/10.1890/15-0430

Ray, G.C., McCormick-Ray, J., Berg, P. & Epstein, H.E. (2006) Pacific walrus: benthic bioturbator of Beringia. Journal of Experimental Marine Biology and Ecology 330, 403–419. https://doi.org/10.1016/j.jembe.2005.12.043

Reeves, R. R., B. S. Stewart, and S. Leatherwood. 1992. The Sierra Club Handbook of Seals and Sirenians. Sierra Club Books, San Francisco, California. xvi + 359 pp.

Riahi, K., Rao, S., Krey, V., Cho, C., Chirkov, V., Fischer, G., Kindermann, G., Nakicenovic, N. & Rafaj, P. (2011) RCP 8.5—A scenario of comparatively high greenhouse gas emissions. Climatic Change 109, 33–57. https://doi.org/10.1007/s10584-011-0149-y

Rode, K.D., Regehr, E. V., Douglas, D.C., Durner, G., Derocher, A.E., Thiemann, G.W. & Budge, S.M. (2014) Variation in the response of an Arctic top predator experiencing habitat loss: Feeding and reproductive ecology of two polar bear populations. Global Change Biology 20, 76–88. https://doi.org/10.1111/gcb.12339

Roth, J.A. and Laerm, J. (1980) A late Pleistocene vertebrate assemblage from Edisto Island, South Carolina, USA. Brimleyana 3, 1-30.

Sbrocco, E.J. (2014) Paleo-MARSPEC: gridded ocean climate layers for the mid-Holocene and Last Glacial Maximum. Ecology 95, 1710–1710. https://doi.org/10.1890/14-0443.1

Shin, Y., Min, M.S. & Borzée, A. (2021) Driven to the edge: species distribution modeling of a clawed salamander (Hynobiidae: *Onychodactylus koreanus*) predicts range shifts and drastic decrease of suitable habitats in response to climate change. Ecology and Evolution 11, 14669–14688. https://doi.org/10.1002/ece3.8155

Shoemaker, K.T., Heffelfinger, L.J., Jackson, N.J., Blum, M.E., Wasley, T. & Stewart, K.M. (2018) A machine-learning approach for extending classical wildlife resource selection analyses. Ecology and Evolution 8, 3556–3569. https://doi.org/10.1002/ece3.3936

Simoes, M., Romero-Alvarez, D., Nuñez-Penichet, C., Jiménez, L. & E. Cobos, M. (2020) General theory and good practices in ecological niche modeling: a basic guide. Biodiversity Informatics 15, 67–68. https://doi.org/10.17161/bi.v15i2.13376

Slobodin, S.B. (2010) About walruses in the Sea of Okhotsk (according to historical sources). Bulletin of the Far Eastern Branch of the Russian Academy of Sciences 2, pp. 15-24.

Spencer, A.M., Embry, A.F., Gautier, D.L., Stoupakova, A. V. & Sørensen, K. (2011) Chapter 1: An overview of the petroleum geology of the Arctic. Geological Society Memoir 35, 1–15. https://doi.org/10.1144/M35.1

Svenning, J.C., Fløjgaard, C., Marske, K.A., Nógues-Bravo, D. & Normand, S. (2011) Applications of species distribution modeling to paleobiology. Quaternary Science Reviews 30, 2930–2947. https://doi.org/10.1016/j.quascirev.2011.06.012

Theocharis, D., Pettit, S., Rodrigues, V.S. & Haider, J. (2018) Arctic shipping: A systematic literature review of comparative studies. Journal of Transport Geography 69, 112–128. https://doi.org/10.1016/j.jtrangeo.2018.04.010

Turner, M.G., Calder, W.J., Cumming, G.S., et al. (2020) Climate change, ecosystems and abrupt change: science priorities. Philosophical Transactions of the Royal Society B: Biological Sciences 375. https://doi.org/10.1098/rstb.2019.0105

Tyberghein, L., Verbruggen, H., Pauly, K., Troupin, C., Mineur, F. & De Clerck, O. (2012) Bio-ORACLE: a global environmental dataset for marine species distribution modelling. Global Ecology and Biogeography 21, 272–281. https://doi.org/10.1111/j.1466-8238.2011.00656.x

Udevitz, M.S., Jay, C. V., Taylor, R.L., Fischbach, A.S., Beatty, W.S. & Noren, S.R. (2017) Forecasting consequences of changing sea ice availability for Pacific walruses. Ecosphere 8. https://doi.org/10.1002/ecs2.2014

Udevitz, M.S., Taylor, R.L., Garlich-Miller, J.L., Quakenbush, L.T. & Snyder, J.A. (2013) Potential population-level effects of increased haulout-related mortality of Pacific walrus calves. Polar Biology 36, 291–298. https://doi.org/10.1007/s00300-012-1259-3

Vasilevskii, R.S. (1971) Origin and Ancient Culture of the Koryaks. Institut Istorii, Novosibirsk, Siberia.

Veloz, S.D. (2009) Spatially autocorrelated sampling falsely inflates measures of accuracy for presence-only niche models. Journal of Biogeography 36, 2290–2299. https://doi.org/10.1111/j.1365-2699.2009.02174.x

Verbitsky, M.Y., Crucifix, M. & Volobuev, D.M. (2018) A theory of Pleistocene glacial rhythmicity. Earth System Dynamics 9, 1025–1043. https://doi.org/10.5194/esd-9-1025-2018

van Vuuren, D.P., Edmonds, J., Kainuma, M., et al. (2011) The representative concentration pathways: An overview. Climatic Change 109, 5–31. https://doi.org/10.1007/s10584-011-0148-z

Warren, D.L. & Seifert, S.N. (2011) Ecological niche modeling in Maxent: the importance of model complexity and the performance of model selection criteria. Ecological Applications 21, 335–342. https://doi.org/10.1890/10-1171.1

Wassmann, P., Duarte, C.M., Agustí, S. & Sejr, M.K. (2011) Footprints of climate change in the Arctic marine ecosystem. Global Change Biology 17, 1235–1249. https://doi.org/10.1111/j.1365-2486.2010.02311.x

Werner, I. (1997) Grazing of Arctic under-ice amphipods on sea-ice algae. Marine Ecology Progress Series 160, 93–99. https://doi.org/10.3354/meps160093

Wilson, S.C., Crawford, I., Trukhanova, I., Dmitrieva, L. & Goodman, S.J. (2020) Estimating risk to ice-breeding pinnipeds from shipping in Arctic and sub-Arctic seas. Marine Policy 111, 103694. https://doi.org/10.1016/j.marpol.2019.103694

Winsor, P. & Björk, G. (2000) Polynya activity in the Arctic Ocean from 1958 to 1997. Journal of Geophysical Research: Oceans 105, 8789–8803. https://doi.org/10.1029/1999jc900305

Yletyinen, J. (2019) Arctic climate resilience. Nature Climate Change 9, 805–806. https://doi.org/10.1038/s41558-019-0616-4

Zachos, J.C., Dickens, G.R. & Zeebe, R.E. (2008) An early Cenozoic perspective on greenhouse warming and carbon-cycle dynamics. Nature 451, 279–283. https://doi.org/10.1038/nature06588

Zagrebelny, S.V., and Kochnev, A.A. (2017) Influence of climate change on summer-fall distribution of Pacific walrus in the western Bering Sea: analysis of reasons and consequences. Izvestiya TINRO 190, 3.

Zyryanov, S. V. & Vorontsov, A. V. (2009) Observations of the Atlantic walrus *Odobenus rosmarus rosmarus* in spring of 1997 in the Kara Sea and southeastern part of the Barents Sea. Zoological Journal 78, 1254–1256.

Appendix A

Berta, A., and A. Wyss. 1994. Pinniped phylogeny; pp. 33–56 in T. A. Deméré and A. Berta (eds.), Contributions in Marine Mammal Paleontology Honoring Frank C. Whitmore, Jr.: Proceedings of the San Diego Society of Natural History 29.

Boessenecker RW, Churchill M. 2013. A reevaluation of the morphology, paleoecology, and phylogenetic relationships of the enigmatic walrus *Pelagiarctos*. PLoS ONE 8:e54311.

Boessenecker, R. W., and M. Churchill. 2015. The oldest known fur seal. Biology Letters 11:21040835.

Boessenecker, R. W., and M. Churchill. 2018. The last of the desmatophocid seals: a new species of *Allodesmus* from the upper Miocene of Washington, USA, and a revision of the taxonomy of Desmatophocidae. Zoological Journal of the Linnaean Society XX:1–25.

Deméré, T. A. 1994. The family Odobenidae: a phylogenetic analysis of fossil and living taxa. Proceedings of the San Diego Society of Natural History 29:99–123.

Deméré, T. A., and A. Berta. 2002. The Miocene pinniped *Desmatophoca oregonensis* Condon, 1906 (Mammalia: Carnivora), from the Astoria Formation, Oregon. Smithsonian Contributions to Paleobiology 93:113–147.

Furbish, R. 2015. Something old, something new, something swimming in the blue: an analysis of the pinniped family Desmatophocidae, its phylogenetic position, and swimming mode. Unpublished M.S., San Diego State University, San Diego, California, 75 pp.

Kohno, N. 1996. Miocene pinniped *Allodesmus* (Mammalia: Carnivora); with special reference to the “Mito seal” from Ibaraki Prefecture, Central Japan. Transactions of the Proceedings of the Paleontological Society of Japan 181:388–404.

Kohno, N., H. Koike, and K. Narita. 2007. Outline of fossil marine mammals from the middle Miocene Bessho and Aoki Formations, Nagano Prefecture, Japan. Research Reports of the Shinshushinmachi Fossil Museum 10:1–45.

Tonomori, W.H., H. Sawamura, T. Sato, and N. Kohno. 2018. A new Miocene pinniped *Allodesmus* (Mammalia: Carnivora) from Hokkaido, Northern Japan. Royal Society Open Science 5:172440.

Appendix C

Boessenecker, R.W. and M. Churchill. 2018. The last of the desmatophocid seals: a new species of Allodesmus from the upper Miocene of Washington, USA, and a revision of the taxonomy of Desmatophocidae. Zoological Journal of the Linnean Society XX:1–25. https://doi.org/10.1093/zoolinnean/zlx098/4783131

Poust, A. and R. W. Boessenecker. 2018. Expanding the geographic and geochronologic range of early pinnipeds: new specimens of *Enaliarctos* from Northern California and Oregon. Acta Palaeontologica Polonica 63:25–40. https://doi.org/10.4202/app.00399.2017

Appendix E

Boyce, M. S., P. R. Vernier, S. E. Nielsen, and F. K. A. Schmiegelow. 2002. Evaluating resource selection functions. Ecological Modelling 157:281–300.

Kass, J. M., R. Muscarella, P. J. Galante, C. L. Bohl, G. E. Pinilla-Buitrago, R. A. Boria, M. Soley-Guardia, and R. P. Anderson. 2021. ENMeval 2.0: Redesigned for customizable and reproducible modeling of species' niches and distributions. Methods in Ecology and Evolution 12:1602–1608.